A Biophysical Approach to Sensory Transduction by Vertebrate Hair Cells

---

Thesis by
David Paul Corey
In Partial Fulfillment of the Requirements for the Degree of Doctor of Philosophy

---

California Institute of Technology
Pasadena, California

1980
(Submitted May 27, 1980)

---

for my teachers:

Peter Skiff

Peter Valberg

Ann Stuart

Jim Hudspeth

ACKNOWLEDGEMENT

This thesis is for my teachers, especially those named, who had faith in me when few others did, who gave me support when I needed it, and who taught me more things than I could ever remember.

Many people have my appreciation for helping with this work, and for making my time at Caltech happy and productive. I can name just a few, but thank you all.

Pancho Bezanilla, John Moore, Fred Sigworth and Chuck Stevens taught me about voltage clamps and stuff like that, saving me much time and trouble. Chuck has agreed to continue with it, which delights me no end. Sally Krasne put up with my questions and confusions for a whole term and months more, but I hope she realizes the worlds she opened up for me. Mike Walsh was a veritable textbook on current methods in electronics, and never seemed to mind that I had to do it for myself. David Van Essen read stacks of manuscripts, and will be asked again, for he calmly and firmly points out all the weaknesses of an argument or experiment, and so strengthens the work. Jake even more calmly provided a sterling example of the Right Way to Do Things, and has helped with this work both directly and indirectly for years. Tom Corey did the cover you've all been asking about. I can give you his address when it's your turn. Ruth Anne Eatock managed to forgive my gaucheries to become a delightful colleague, collaborator and friend. John Maunsell, who may never forgive the "Bob," gave me more help and support of all kinds than he will ever let me repay. This work could not have been done without the huge amount of software he developed, to name but one. Dan Margoliash brought an interest and a critical mind to this work through many late night talks, and taught me besides that it was OK to want to be great. (I have since learned there's no chance, but wish Dan the best of luck.) Maurine Packard, professionally and by nature a mother, in the grandest sense, took care of us all in sickness and in health.

Even as graduate students, we are not so different from children. Totally dependent on others for the space and money to live and work, we wish fiercely to be independent. Painfully incompetent in comparison, we seek to establish ourselves as capable scientists. With the support comes a merged identity: the work of the group is inevitably attributed to the advisor, and yet this false attribution is neither a sufficient nor a desired return for years of investment. For both student and teacher, the return must be in the growth. For understanding all this, and for being a friend and a teacher through it all, Jim Hudspeth has my greatest thanks.

Lastly, I must thank Jeanne. If I have made the transition from student to scientist with any modicum of grace, it is due to her support and understanding.

This research was financially supported by NIH grants NS-13154, GM-07616, and GM-02031, by the Ann Peppers, William Randolph Hearst, and Alfred P. Sloan Foundations, and by funds from the Division of Biology of the California Institute of Technology, all of which I gratefully acknowledge. I also appreciate support from the Jean Weigle Memorial Fund, for preparation of this thesis, and particularly thank Connie Katz, for cheerfully and flawlessly crafting the manuscript, against the usual impossible deadlines.

ABSTRACT

An in vitro preparation of the bullfrog sacculus was developed, in which the macular epithelium was arranged as a septum between two chambers. Hair cells are stimulated by moving the overlying otolithic membrane with a glass stimulus probe; the response is recorded as the transepithelial current with the epithelium voltage-clamped. The preparation complements the intracellular studies of individual hair cells under way in this laboratory, and has the advantages of lower electrical noise, higher temporal resolution, greater stability over time, and separate control of solutions bathing apical and basal surfaces of the epithelium. Its major disadvantage is that stimulation and recording methods are somewhat less direct. Four projects were carried out with this preparation:

The generation of the transepithelial "microphonic" current was analyzed in terms of the passive electrical properties of the epithelium and time- and voltage-dependent conductances of the hair cell membrane. The summed receptor currents are modified by the change in membrane potential of hair cells, by a voltage-dependent potassium conductance, and by an adaptive shift of the responsive range of hair bundles. A mathematical model that includes these effects predicts the observed waveform of the microphonic current.

The ionic selectivity of the transduction channel was studied with this preparation and with intracellular voltage-clamping of individual hair cells. The transduction channel is permeable to all alkali cations, to at least some of the divalent alkaline earth metals, and to many small organic cations. The permeability to anions is not clear. The channel constitutes a large, water-filled pore, of at least 0.65 nm diameter, which appears to contain a binding site for permeant organic cations. While a good fit to the current-voltage relation in Na^+ saline can be obtained with a simple model that includes two energy barriers to permeation near the middle of the membrane, the distribution of barriers is not known with any confidence.

The hair cell response saturates if the mechanically sensitive hair bundle is displaced by more than about 0.4 μm. An adaptation, which follows such saturation and had been seen intracellularly, was shown to be an adaptive shift of the responsive range such as to restore the sensitivity. The shape of the response curve is unchanged by adaptation. The adaptation constitutes a relaxation of the link between hair bundle displacement and bias on the transduction element. The position and shape of the response curve is changed by intracellular Ca^{++} and/or pH, and the rate of the shift is increased by increasing the Ca^{++} concentration.

Following a step displacement of the otolithic membrane, the microphonic current approaches a new equilibrium value over several tens of microseconds. The latency of the response is less than 40 μs at 22 °C. The kinetics of the approach to equilibrium are slower at lower temperatures, and depend on the position of the hair bundle. A three-state model for transduction channel gating is presented that supposes that changing the position of the hair bundle directly and continuously changes the free energies of states of the channel. The model can quantitatively predict the observed kinetics of the current.

Table of Contents

		Page
Dedication		ii
Acknowledgement		iii
Abstract		v
Table of Contents		vii
Békésy		viii
Chapter I	**ANALYSIS OF THE MICROPHONIC POTENTIAL RECORDED IN VITRO.**	1
Chapter II	**IONIC SELECTIVITY OF THE TRANSDUCTION CHANNEL**	59
Chapter III	**ADAPTIVE SHIFT OF THE OPERATING CURVE**	96
Chapter IV	**GATING KINETICS OF THE TRANSDUCTION ELEMENT**	127
References		161

We return now to the problem of the high sensitivity of the ear. From a purely physical point of view, it is startling that a displacement whose magnitude is the diameter of an atom can produce enough voltage to trigger a nerve ending. I have no solution for this problem. But since we have seen how, step by step, the anatomical structures in the ear localize the vibration forces in smaller and smaller compartments, it does not seem impossible that the final mechanical transformer is of molecular dimensions.

Georg v. Békésy, 1962

Chapter I

ANALYSIS OF THE MICROPHONIC POTENTIAL RECORDED IN VITRO

PREFACE

In the Fall of 1976, Sandy Shotwell was interested in looking at hair-cell surface morphology with freeze-fracture microscopy, to see if there were detectable changes that occurred with displacements of the hair bundle between the conducting and the nonconducting states. She needed a convenient measure of the electrical activity of the macula, to monitor the state of the macula while it was superfused with fixative. Jim suggested measuring the extracellular 'microphonic' potential, and I helped Sandy develop a two-bath chamber to get a good signal size.

The project never got very far, because the signals recorded with this in vitro microphonic were virtually uninterpretable and became more so as the stimulus and ionic conditions were varied. While Sandy moved on to other things, I spent most of the following three years trying to understand the microphonic. Stimulation, perfusion, and recording techniques were improved, the preparation slowly became understood and so became a useful complement to the concurrent intracellular studies, and many aspects of the microphonic response turned out to be interesting in their own right. The major byproducts are presented in the last three chapters of this thesis: Ionic Selectivity of the Transduction Channel, Adaptive Shift of the Operating Range, and Gating Kinetics of the Transduction Element. The preparation also saved me from microelectrode-pulling for the remainder of my graduate career.

The generation of the in vitro microphonic potential is now largely understood, and our understanding is presented in the following chapter. The paper serves as a foundation for the secondary studies; it also serves to point out the difficulties in interpretation of the microphonic response in any preparation.

INTRODUCTION

Fifty years ago Wever & Bray (1930) recorded from the eighth nerve of cats what they considered to be whole-nerve action potentials in response to acoustic stimuli. These signals duplicated the waveform of the stimulus with good fidelity, over a range of 125 to 4100 Hz. The results were of fundamental importance to sensory physiology, for they challenged the general principle, then becoming well-established (Adrian, 1928), that the frequency of sensory nerve firing is related to the intensity of a stimulus. The following year Adrian (1931) presented evidence contesting the origin of the potentials, and suggested that they were generated within the cochlea by "some kind of microphonic action." In the intervening years it has become clear that these "microphonic potentials" are in fact produced by hair cells in the cochlea, and correspond to extracellular current flow through the impedance of tissue between the recording electrodes. This was first clearly demonstrated by von Békésy (1950, 1951, 1952a, 1952b) and by Tasaki, Davis & Eldredge (1954). Within the scala media of the cochlea, which the apical surfaces of hair cells face, they found a positive standing potential of 60-90 mV. If the basilar membrane was displaced towards scala media, presumably deflecting each hair bundle towards its kinociliary remnant, then this "endocochlear potential" decreased by 10-20 mV; the opposite displacement caused a slight increase. Sinusoidal displacements, delivered either directly or via the normal auditory pathway, produced an oscillatory potential, the "cochlear microphonic." Furthermore, raising the endocochlear potential by passing current increased the amplitude of the microphonic.

In searching for the source of the cochlear microphonic, they positioned a microelectrode at various points within the cochlea. As the electrode was advanced from scala tympani through the basilar membrane, the size of the microphonic potential increased, and then, as the electrode traversed the reticular lamina into scala media, abruptly reversed in sign. Passage of the electrode from scala vestibuli

through Reisner's membrane into scala media produced no such sign reversal. The fluid within scala media was known by this time to have high K^+ and low Na^+ concentrations (Smith, Lowry & Wu, 1954). It was found by Tasaki et al. that the microphonic was severely decremented when a high-K^+ saline replaced the fluid in scala tympani, where it could bathe the hair cells, but that this was not so for scala vestibuli.

Concurrent work on the lateral-line organ of fish revealed a similar localization of potentials (Jielof, Spoor & de Vries, 1952). The potential of the fluid immediately above the hair cells became more negative in response to stimulation, and the sign of the potential change reversed at a point just below the apical surface of the cells.

On the basis of these observations, Davis (1953) proposed a variable-resistance model for the generation of the cochlear microphonic. In this model, the endocochlear potential, represented as a battery, causes a steady current flow across the organ of Corti. The current is modulated by a change in the resistance of the mechanosensitive hair cells; the change in current is seen as a positive or negative potential depending on the positions of the recording electrodes. In the most elaborate of its many restatements (Davis, 1965), the theory specifically establishes as the driving force the potential across the apical hair cell membrane, which is the difference between the (positive) endocochlear and (negative) intracellular potentials. The inclusion of the intracellular potential is particularly important in generalizing the theory to cover other hair cell organs, where there is no standing potential analogous to the endocochlear potential.

Research in subsequent years has served mostly to confirm (Honrubia & Ward, 1969; Furukawa, Ishii & Matsuura, 1972; Corey & Hudspeth, 1979a) or to confuse this general understanding; the current general opinion (Dallos, 1973) holds it to be essentially correct.

In this chapter we undertake an analysis of the microphonic potential recorded from an in vitro preparation of the bullfrog sacculus. The preparation was developed to complement intracellular recording from the same organ (Hudspeth & Corey, 1977); the analysis of the microphonic was undertaken to try to understand the responses we recorded. Our analysis does not significantly contradict that of Davis. Rather, the simplification afforded by spatial homogeneities permits extension of the model to include capacitance and time- and voltage-dependent conductances of the cellular elements. This chapter serves to establish this preparation as one that can provide quantitative information on the process of transduction, and conversely to illustrate the great care required in proper interpretation of microphonic potentials in all preparations.

METHODS

Dissection and mounting

Sacculi of adult bullfrogs (Rana catesbeiana) were exposed by a ventral surgical approach, and removed whole into a dish containing an artificial perilymph (see **Salines:** Normal Perilymph). There the otolithic mass was removed, tissue extraneous to the macula trimmed away, and the nerve severed close to the macula. The macula was transferred with a wide-mouth pipette to the experimental chamber, where it was positioned across a 1-mm hole separating upper and lower baths, and fixed in place with a plastic washer (Text-fig. 1A).

The macula of the bullfrog sacculus is a planar surface comprising hair cells with orientations arranged around 360°. The orientation, defined as the direction from the stereocilia to the kinocilium of a hair bundle, represents the direction of greatest mechanical sensitivity. Hair bundles in the periphery of the macula are directed radially outward; across the striola, the irregular line of reversal, they are directed inward (Text-fig. 1B).

For most experiments the portion of the otolithic membrane nearer the nerve's insertion was lifted off the underlying hair cells with a sharpened tungsten dissecting needle, taking care to avoid damaging the epithelium. An area of otolithic membrane about 200 x 300 μm remained attached to perhaps 300 hair cells at the periphery of the macula. This patch was chosen rather than the central patch used in earlier experiments (Corey & Hudspeth, 1979a) because it encompassed a narrower distribution of hair cell orientations, as judged from mapping of kinocilium positions in scanning electron micrographs and from direct observation with differential-interference-contrast optics of hair cells in living whole maculae.

A thin (25 μm) plastic film with a hole (Handi-Wrap, Dow Chemical, Midland, MI) was then positioned over the macula; the hole size, ranging from 300-700 μm diameter, was chosen so as to expose only the region of hair cells still

Text-fig. 1. A, mounting arrangement for the sacculus. The tissue is positioned across a hole between upper and lower baths, so as to separate them ionically and electrically. The apical surfaces of hair cells (HC) and supporting cells face the upper bath; the basolateral surfaces and the cut nerve (N) face the lower bath. The sacculus is held in place with a 150-μm-thick plastic washer (W) and sealed with silicone vacuum grease. For most experiments the otolithic membrane (OM), to which the mechanosensitive hair bundles are normally attached, is peeled up from all but a patch of hair cells in the peripheral macula. These hair cells are stimulated by moving the overlying otolithic membrane with a glass stimulus probe (SP). A thin (25 μm) plastic film (F) restricts transepithelial current flow to the region of the stimulated patch.

B, map of hair cell orientations in the saccular macula, obtained from scanning electron micrographs and from direct microscopic observation. Hair cells are most sensitive along an axis from the stereocilia to the kinocilium of a bundle (arrows). The arc across which orientations reverse is termed the striola and is shown as a solid line. In most experiments hair cells are left attached to the otolithic membrane only in a peripheral patch (lightly shaded) upon which the stimulus probe is placed (heavily shaded). A displacement of the otolithic membrane from left to right in this figure is defined as positive.

A

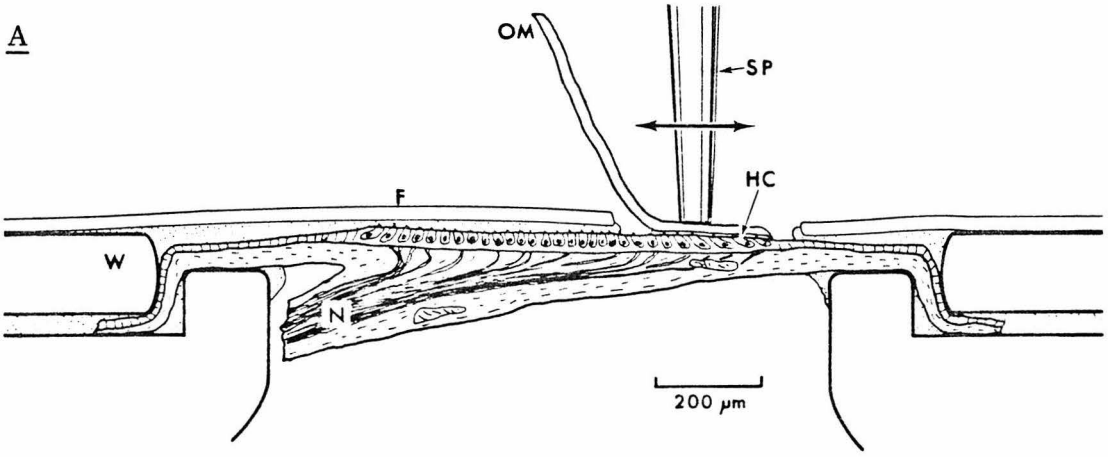

B

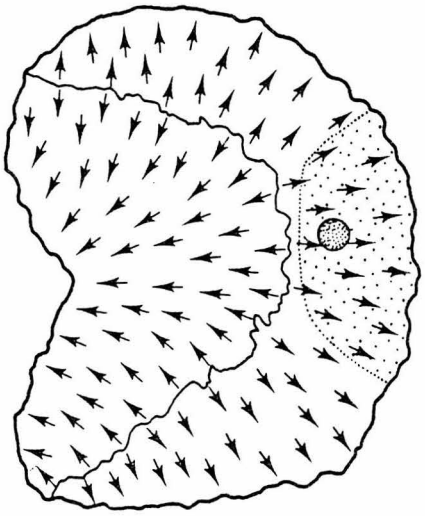

attached to the otolithic membrane. A layer of silicone high-vacuum grease (Dow Corning Corp., Midland, MI) held the film to the macula and prevented current flow across epithelium damaged by the holding washer and across most of the unstimulated macula. The otolithic membrane had a tendency to flop back onto the macula if unrestrained; this was prevented by the sealing film and occasionally by a 3-mm length of human eyelash laid across the edge of the hole.

Perfusion

The upper and lower baths, each with a 0.35-ml volume, were separately perfused with a peristaltic pump, usually at a rate of 1 ml/min. The time required for 99% exchange of fluids is thus less than 2 min, if one assumes uniform mixing, and this was confirmed by measuring the optical density of fluid near the macula when either bath was perfused with a dilute ink solution.

Solution changes in the upper bath normally exerted their full physiological effects within 2 min, that is, within the wash-in time of the bath. Changes in the lower bath, however, often required 5-10 min for their effects to be seen. The morphology of the epithelium appears to create a diffusion barrier between hair cells and the lower bath (see **Part II** below), which would explain this delay.

A thermoelectric temperature control unit maintained the baths within 0.2°C of a desired temperature, as determined by a thermocouple sensor placed in the upper bath 1 mm from the macula.

Salines

The Na^+, Ca^{++} and K^+ concentrations of bullfrog endolymph and perilymph were measured with ion-sensitive microelectrodes. Details of the measurement will be presented in a separate paper (Maunsell, Jacobs & Hudspeth, in preparation). The solutions termed Normal Perilymph and Normal Endolymph (Table 1) duplicate the measured concentrations, and the other solutions are for the most part modifications of these two salines. Solutions used in the top bath are arbitrarily termed

TABLE 1. Ionic composition of saline solutions used in analysis of the microphonic. Values in mM. The table includes small amounts of NaOH or KOH used to titrate the solutions to pH 7.2-7.3

	Normal Endolymph	Na^+ Endolymph	Cs^+ Endolymph	Normal Perilmph	High K^+ Perilymph	TEA Perilymph
Na^+:	2.5	131.7	-	119.3	108.5	119.3
K^+:	124.0	-	1.7	3.6	17.0	3.6
Cs^+:	-	-	130.0	-	-	-
Ca^{++}:	0.26	0.25	0.25	1.36	1.36	1.36
Mg^{++}:	-	-	-	0.68	0.68	0.68
Cl^-:	127.0	132.2	132.2	127.0	129.6	129.0
D-glucose:	3.0	3.0	3.0	3.0	3.0	3.0
HEPES:	5.0	5.0	5.0	5.0	5.0	5.0
TEA:	-	-	-	-	-	2.0

endolymphs; those in the bottom, perilymphs. All solutions were buffered with HEPES and adjusted with NaOH or KOH to pH 7.2-7.3.

Stimulation

The otolithic membrane was moved with a solid glass probe attached to a piezoelectric bimorph element. Details of the construction and calibration of such stimulators have been presented elsewhere (Corey & Hudspeth, 1980a); the particular device used for these experiments is shown in Fig. 7b of that paper. The tip of the probe, ~150 μm in diameter, was ground flat and slightly roughened to engage the otolithic membrane. The probe, oscillating in the horizontal plane, was lowered towards the otolithic membrane until a response was seen; a vertical displacement of 1-3 μm sufficed to bring the response from zero to full-sized. Generally the probe was not moved again for the duration of a 3- to 4-hour experiment.

Stimulation consisted of horizontal displacements of the probe, either sinusoidal tone bursts or step displacements. The rising phase of a "step" displacement was a sigmoidal ramp, complete within 90 μs and with less than 5% ringing following the step (Corey & Hudspeth, 1980a).

The motion of the otolithic membrane in response to horizontal displacement of the probe was measured optically. Clumps of otoconia, 10-20 μm across, remain embedded in the otolithic membrane after removal of the otolithic mass (see Fig. 1 of Corey & Hudspeth, 1979a). Light from a helium-neon laser was focused to a 10 μm spot at the edge of a clump; lateral motion of the embedded clump then modulated the amount of light passing through the epithelium to a photodiode. Briefly, it was found that the otolithic membrane moves as a rigid sheet, and that a step displacement reaches all parts of the sensitive region within 25 μs.

Recording

The potential across the saccular epithelium was measured with chlorided silver electrodes in the top and bottom baths. The high-impedance differential head

stage of the amplifier employed Analogic MP 215 operational amplifiers (the gift of H. J. Weedon of Analogic, Wakefield, MA) for particularly low noise (11 nV/$\sqrt{\text{Hz}}$ equivalent input noise) and high speed (500 kHz bandwidth at all gains). Another pair of electrodes was used to pass current across the epithelium. In the clamp mode, the voltage amplifier became part of a voltage clamp curcuit which held the potential between the two baths at a fixed value, usually 0 mV. The clamp included series-resistance compensation to negate the effects of the series bath resistance; details of the compensation will be given in Chapter IV. A current-to-voltage converter in the current loop provided an output signal corresponding to the clamp current, and it is this signal that is shown as the response in most figures. This epithelial voltage clamp, which measures transepithelial current, should be distinguished from the intracellular voltage clamp used to measure receptor current in single cells (Corey & Hudspeth, 1979b; Chapter II of this thesis).

Stimuli were presented at a rate of one per second and the responses to 5-100 presentations averaged by computer. The figures are tracings from photographic records of the displayed averages.

Terminology

We use a specific terminology for the various recorded signals, both to avoid confusion and to emphasize the similarities to analogous signals in other preparations.

The transepithelial potential is the gross potential measured between the two baths. The microphonic potential is the stimulus-dependent part of it, and thus does not include, for instance, steady diffusion potentials. If the transepithelial potential is clamped to a fixed value, the current necessary is the transepithelial current and the microphonic current is the stimulus-dependent part of it.

In our view, the microphonic potential is not a receptor potential. Rather, the receptor potential is the change in membrane potential of a single cell that leads to the release of transmitter. The receptor current is the current in a single cell

passing through those channels that are opened directly by mechanical stimuli, which we term transduction channels. It is a major—although not unreasonable—assumption throughout this work that the conductance change caused by stimulation corresponds to the gating of several hundred discrete channels, each of which can exist in open or closed states.

The displacement-response curve is the curve relating displacement of the hair bundle and the response it evokes. Usually the response is the microphonic current, but it may also be the receptor potential, or, for instance, the equilibrium probability that a transduction channel is open.

Morphology

For scanning electron microscopy, sacculi were removed from frogs and trimmed of extraneous tissue as for recording, but were then fixed for 60 min at 4°C with 40 mM OsO_4 in 80 mM sodium cacodylate and 10 mM $CaCl_2$ at pH 7.3. Specimens were dehydrated in ethanol, critical-point dried from liquid CO_2 and gold sputter-coated. They were photographed with an Autoscan scanning electron microscope (ETEC Corp., Hayward, CA).

The fixative for transmission electron microscopy was 2% glutaraldehyde in 40 mM sodium phosphate at pH 6.8. After a wash in the phosphate buffer, specimens were postfixed with 1% OsO_4 and then stained with 2 mg/ml tannic acid. They were dehydrated in ethanol and propylene oxide, embedded in Epon, and the sections stained with uranyl acetate and lead citrate before being viewed in a Philips 301 at 80 kV.

The same primary fixation procedure was used for freeze-fracture specimens, which were then equilibrated with 25% glycerol in cacodylate buffer and frozen in Freon-22 cooled to its melting point in liquid N_2. Individual maculae were fractured with a mirror-image specimen holder and replicated with platinum in a Balzers Freeze Etcher. After digestion with sodium hypochlorite, replicas were examined at 80 kV in a Philips 301 electron microscope.

For both transmission and scanning microscopy, shrinkage caused by fixation was estimated by measuring living preparations in vitro while viewing with Nomarski differential-interference-contrast optics at 1000 X.

RESULTS

Part I. Sine-wave analysis

The standing potential across the epithelium was 5-15 mV, endolymph negative, when the baths contained Normal Endolymph and Normal Perilymph. That this corresponds to the diffusion potential across tight junctions selective for K^+ will be shown in Chapter II. The potential change in response to stimulation is the microphonic potential; if the transepithelial potential is clamped to zero, we can measure the microphonic current. A representative response is shown in Text-fig. 2A, where an increase in current passing from upper bath to lower is shown as an upwards deflection. The stimulus here is a tone burst comprising three cycles of a 16.5-Hz, 1.0-μm peak-to-peak sine wave. An upwards deflection represents displacement along the axis of symmetry of the macula and away from the nerve; this displacement, hereafter termed positive, moves hair bundles towards their kinocilia for hair cells in the periphery of the macula, and away from the kinocilia for hair cells in the central macula.

The 2f response

The most conspicuous feature of this response, obtained with the otolithic membrane attached to all hair cells of the macula, is that it has a frequency twice that of the stimulus. This "2f" response was first recognized by de Vries in the fish lateral line, where it was viewed as a full-wave rectification (Jielof et al. 1952). It has since been found in all vertebrate lateral line and otolith organs studied (e.g., Furukawa & Ishii, 1967a; Sand, Ozawa & Hagiwara, 1975; Kroese, van der Zalm & van den Berken, 1980). It is not found, however, in semicircular canals or in mammalian cochleae (de Vries & Bleeker, 1949; Tasaki et al. 1954). The morphological basis for this difference was discovered by Lowenstein & Wersäll (1959), who found that hair cells in skate semicircular canal were of a single orientation, unlike those in lateral line or otolith organs. The generation of the 2f

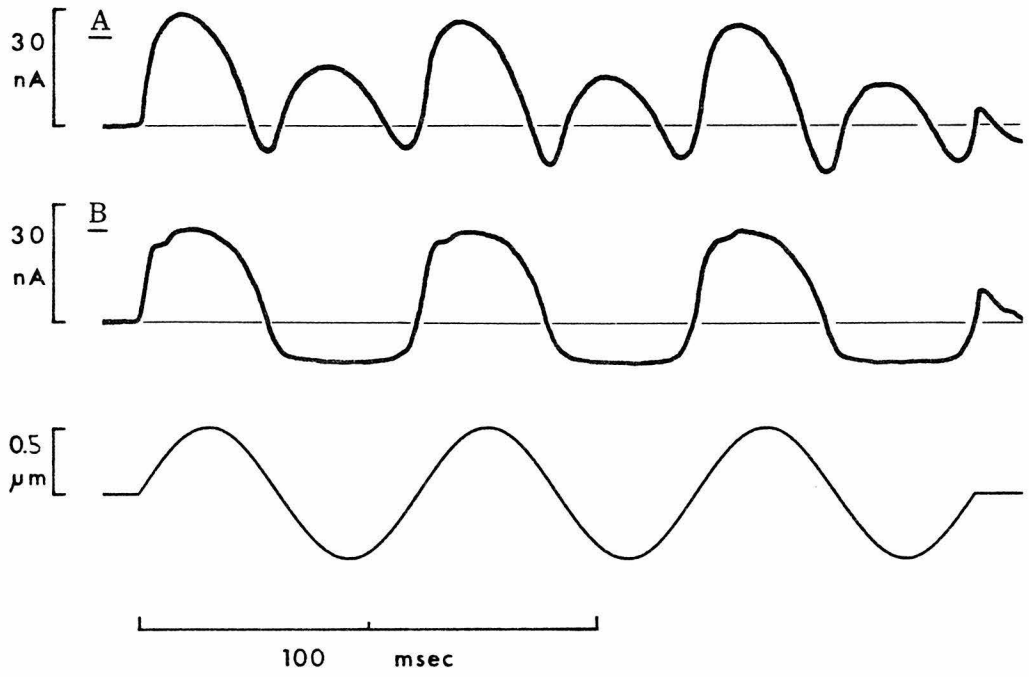

Text-fig. 2. A, microphonic current generated by the whole macula. B, microphonic current generated by a peripheral patch; same preparation as A. For both, current from upper to lower baths, corresponding to current entering the apical hair cell surface, is shown as upwards. The stimulus (bottom trace) is three cycles of a 16.5-Hz sine wave, 1.0-μm peak-to-peak. A positive displacement, from the stereocilia towards the kinocilia of hair bundles in the peripheral patch, is also upwards. Normal Endolymph and Normal Perilymph; 21.5 °C.

response was more explicitly described by Flock & Wersäll (1962): they reasoned that hair cells of opposite orientation, each with a nonlinear (rectifying) displacement-response curve, would sum to produce the double frequency. Their hypothesized nonlinear curve has recently been measured in single hair cells (Hudspeth & Corey, 1977).

This summation of oppositely rectified responses is demonstrated for this preparation simply by decoupling hair cells of one orientation from the otolithic membrane. The response then has the frequency of the stimulus, and shows rectification with negative displacements (Text-fig. 2B).

Angular sensitivity

In Text-fig. 2B, hair cells are stimulated along their most sensitive axis, but sensitivity along other axes may also be measured. A two-dimensional bimorph stimulator (Corey & Hudspeth, 1980a) was used to move the otolithic membrane patch along various axes; the sensitivity to small displacements as a function of angle is shown in Text-fig. 3. The angular sensitivity approximates a cosine relationship, indicating a lack of sensitivity to components of the displacement perpendicular to the best axis. While the sensitivity is abnormally flat for angles near 0°, this is probably a consequence of the slight spread of orientations within the stimulated patch. The cosine relationship has been confirmed, with greater detail, for single hair bundles (Shotwell & Hudspeth, 1980).

Saturation

Besides the rectification with negative displacements, Text-fig. 2 shows a slight saturation for positive displacements. This lack of a linear response to large stimuli has been found for virtually all hair cell organs (e.g., Jielof et al. 1952; Flock, 1965; Furukawa et al. 1972; Dallos, 1973); it is shown in greater detail for this preparation in Text-fig. 4. A fairly sharp saturation occurs with small negative displacements, and a more gradual saturation occurs with positive displacements. A

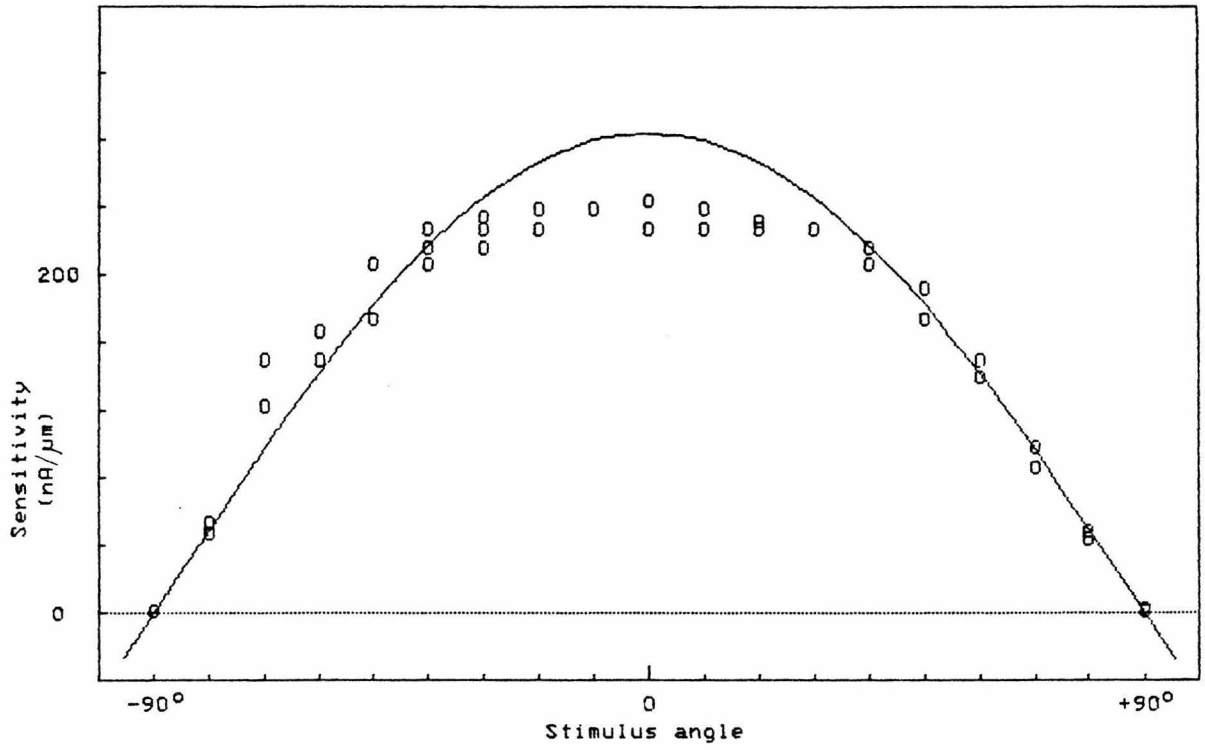

Text-fig. 3. Angular sensitivity of a peripheral patch of macula. The stimulus was a 1.0-μm peak-to-peak, 10-Hz triangle wave. 0° corresponds to the usual positive displacement. The measured response was the microphonic current under voltage clamp, low-pass filtered at 18 Hz; the plotted sensitivity is the maximum slope of the response in nA/μm. The curve is proportional to cos(Θ), arbitrarily scaled to fit the sensitivity for large positive and negative angles. Normal Endolymph and Normal Perilymph; 22.0 °C.

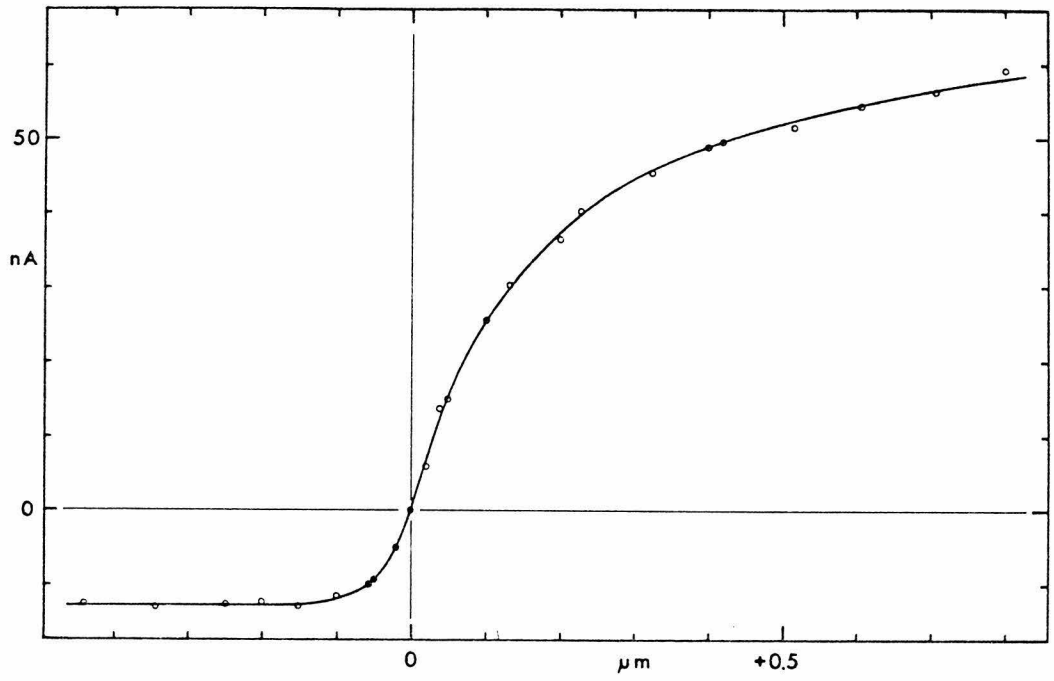

Text-fig. 4. "Instantaneous" displacement-response curve of a peripheral patch. Same preparation as in Text-fig. 2. The stimuli were steps 2 msec in duration and of various amplitudes. The transepithelial current, recorded with the voltage clamp and series resistance compensation, was measured about 50 μsec after the rise of the step, when the current had settled to the new value. The intracellular potential changes negligibly during this time, and so this curve excludes the complications of time- and voltage-dependent conductance changes that are secondary to the intracellular receptor potential. The curve was drawn through the data points by eye. Normal Endolymph and Normal Perilymph; 21.5 °C.

nonlinear transfer curve of this sort acts to generate harmonics in response to sinusoidal stimuli; such harmonics have been measured in mammalian cochlea (Newman, Stevens & Davis, 1937; Hubbard, Mountain & Geisler, 1979). The saturation for large positive and negative displacements generates odd harmonics, while the asymmetry of the saturation generates even harmonics (Dallos, 1973, p. 395).

Frequency dependence

Finally, Text-fig. 2 shows the response reaching a peak before the stimulus has peaked. This phase-lead of the microphonic potential at low frequencies becomes a phase-lag at high frequencies (Text-fig. 5). At either extreme, the amplitude of the response is reduced. The frequency sensitivity of both phase and amplitude can be fitted by treating the sacculus as a bandpass filter, with first-order slopes (6 dB/octave) at both low and high frequencies, and half-power frequencies (-3 dB) at 25 and 220 Hz, respectively. Bandpass filtering of this sort, particularly the high-pass characteristic, has been noted in many other hair cell organs (Jielof et al. 1952; Furukawa & Ishii, 1967b; Kroese et al. 1980).

Step response

A transfer function for the sacculus that can be described in the frequency domain as a first-order bandpass filter should produce a characteristic response when studied in the time domain. Following a step displacement of the otolithic membrane, the response should rise rapidly to a new level, and then relax exponentially to zero with a time constant equal to $1/2\pi f_o$, where f_o is the low-frequency half-power point. The actual behavior of the preparation is shown in Text-fig. 6, where A is the response of the whole macula and B is the response after detaching the otolithic membrane from cells of one orientation.

The responses, particularly B, are not quite as expected. The decline is not a simple exponential, there is an additional bump on the falling phase, and the undershoot following the step is not a simple negative step with relaxation. The

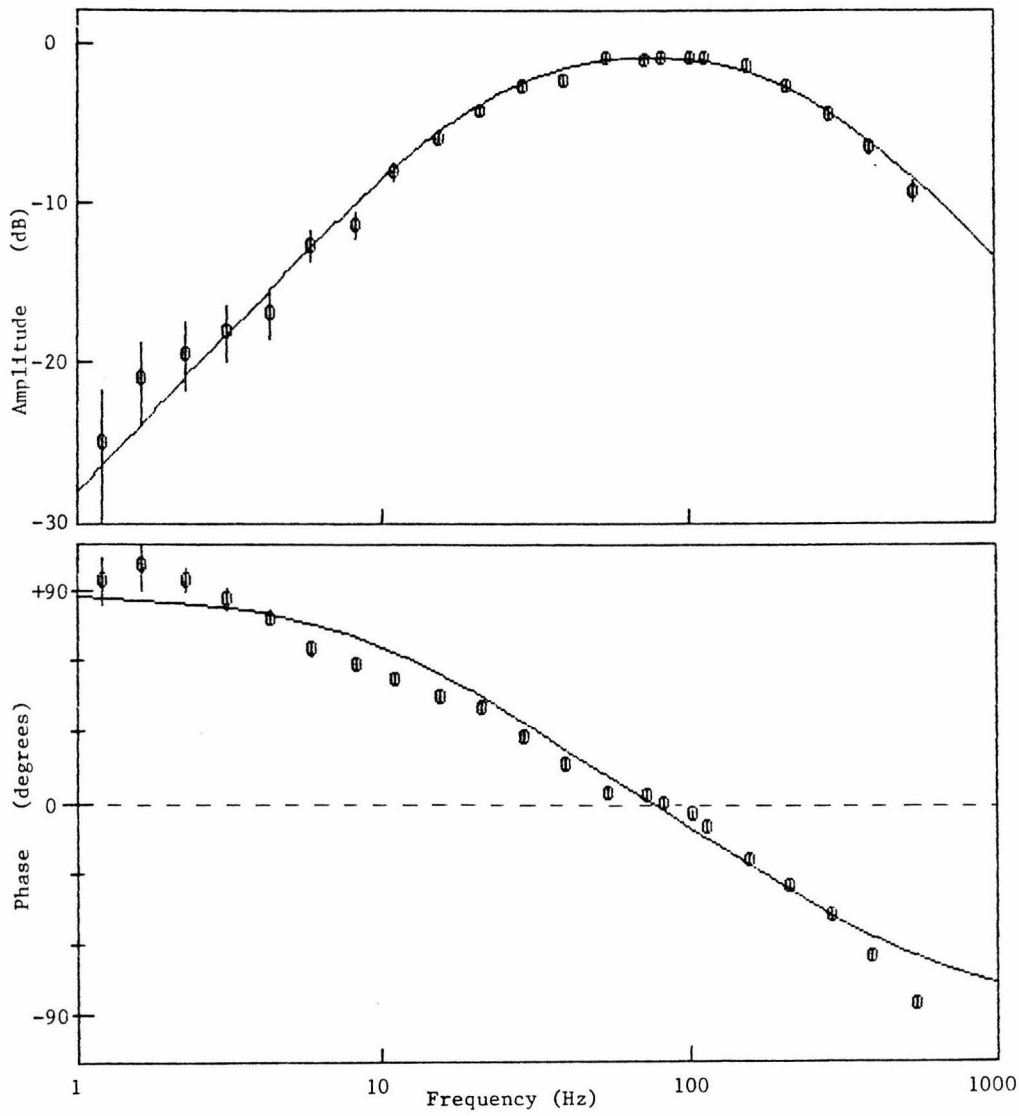

Text-fig. 5. Frequency dependence of the microphonic potential. A 0.3-μm peak-to-peak sine wave was presented to the whole macula. A, amplitude was measured after correcting for the rectification occurring with negative displacements, and is plotted as log(amplitude) on a decibel scale relative to the maximum response (0 db). B, phase was measured as the position of the larger of the two peaks relative to the peak of the sine-wave stimulus; positive phase is a phase lead. The two curves are calculated for a bandpass filter with first-order low- and high-frequency slopes, and half-power frequencies at 25 and 220 Hz respectivley. Normal Endolymph and Normal Perilymph; 22.5 °C.

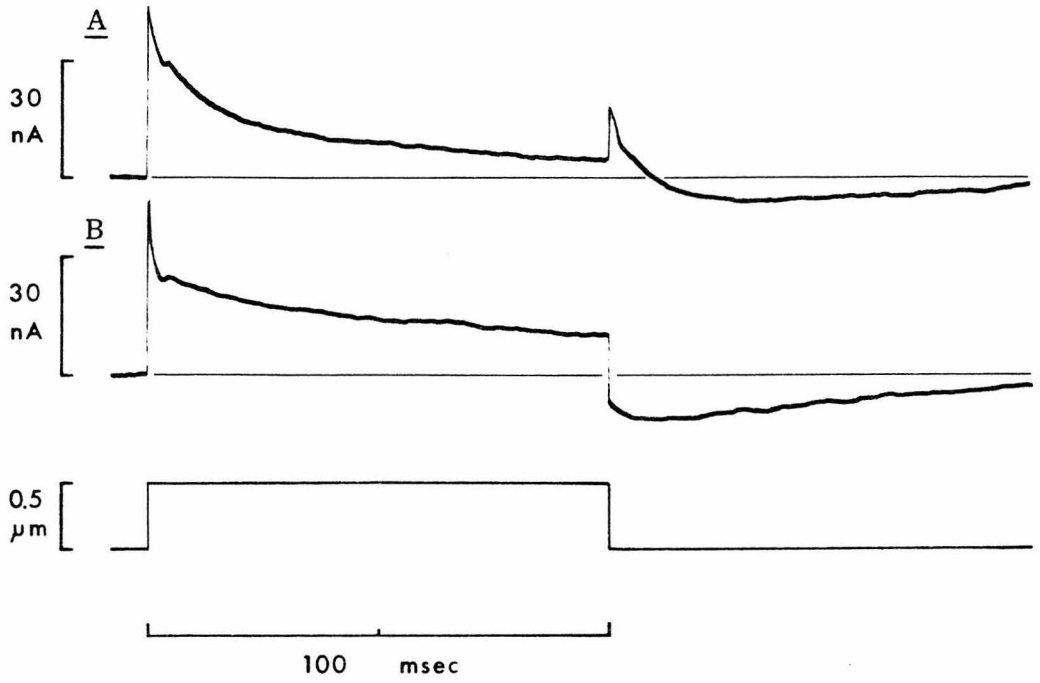

Text-fig. 6. A, microphonic current generated by the whole macula in response to a step displacement stimulus. B, microphonic current generated by a peripheral patch; both A and B are from the same preparation as in Text-fig. 2. The stimulus (bottom trace) is a 100-msec step of 0.5-μm amplitude. Normal Endolymph and Normal Perilymph; 21.5 °C.

responses to sine-wave stimuli do not adequately predict the response to a step; thus a bandpass filter is not a satisfactory description of the transfer function.

It is our contention, rather, that analysis in the frequency domain is not a particularly good way to study organs of the acousticolateralis system, if one is interested in the events associated with transduction in hair cells. The nonlinearities already apparent are not conveniently treated by considering them as harmonic sources. Moreover, the biological processes yet to be elucidated are not likely to be linear, nor memoryless. For the remainder of this paper, our purpose will be to describe the response to a step displacement (Text-fig. 6B) in terms of time- and voltage-dependent cellular processes. It will become apparent, we hope, that this brings one a good deal closer to an understanding of the transduction process.

Part II. Equivalent circuit of the macular epithelium

In order to understand how conductance changes affect the step response, we must first understand current paths in the epithelium. We start by estimating the equivalent circuit of the epithelium from measurements of electron micrographs and from intracellular recording.

Morphology

Plate 1 shows a cross section of the macular epithelium. The epithelium is composed of hair cells and supporting cells, occurring in roughly a 1:2 ratio. The apical (mucosal or luminal) surfaces of hair cells and supporting cells face the endolymph of the sacculus in vivo, or the upper bath of the chamber in vitro. Apical surfaces are ringed with tight junctions (Hudspeth, 1980), which constitute the principal diffusion barrier of the epithelium. Supporting cells extend to the bottom of the epithelium, where their basal surfaces tessellate the bottom (perilymphatic or serosal) side of the epithelium. An extracellular basal lamina extends over the basal surfaces of supporting cells, but it is not thought to be a significant diffusion barrier. Immediately above the basal lamina, the lateral surfaces of supporting cells are very closely apposed, running within about 20 nm of each other over 2 to 5 μm. In this region there are as well numerous and extensive gap junctions between supporting cells (Hudspeth, 1980). The close apposition most likely does constitute a diffusion barrier. As hair cells do not extend to the bottom of the epithelium, their basolateral surfaces are enclosed within a space, here termed the peribasal space, bounded by tight junctions at the top and the close apposition of supporting cells at the bottom. The restricted access to this space is expected to cause the same complications for current flow and for ionic equilibration as do the T-tubule system of skeletal muscle (Standen & Stanfield, 1979), the periaxonal space of squid axon (Taylor, Bezanilla & Rojas, 1980), and the membrane infoldings of pacemaker cells in Aplysia (Eaton, 1972). Below the basal lamina lie myelinated nerve fibers and associated connective

EXPLANATION OF PLATE

Transmission electron micrograph showing a small portion of the macular epithelium. X 4,000.

OM	otolithic membrane
HB	hair bundle
HC	hair cell
SC	supporting cell
PS	peribasal space
BL	basal lamina

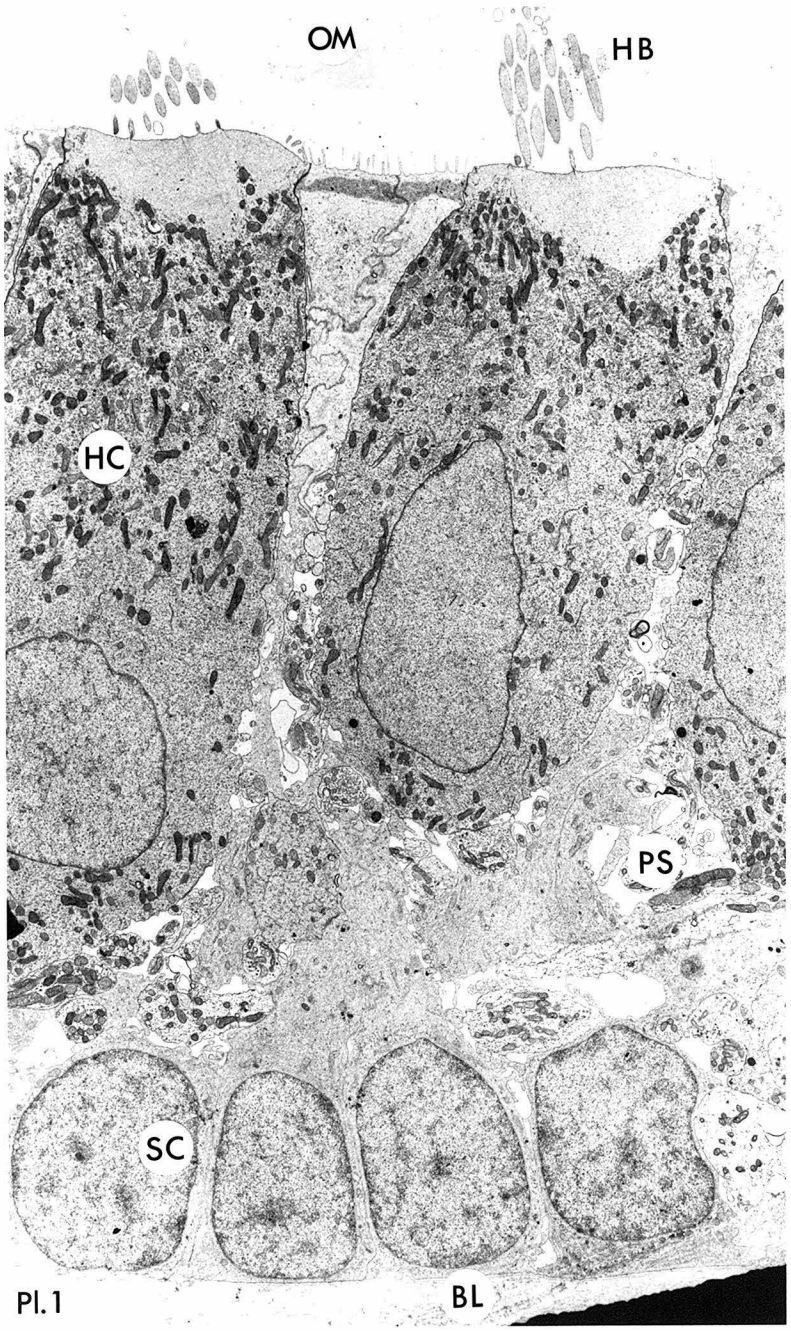

Pl. 1

tissue, which are not expected to present a barrier to diffusion. The otolithic membrane above the epithelium, laced as it is with holes above the hair cells (Corey & Hudspeth, 1979) is similarly not a barrier.

Equivalent circuit

The cellular elements of the epithelium can be reduced to equivalent resistances and capacitances (Text-fig. 7) representing the various cell surfaces and diffusion barriers. To facilitate comparison with other preparations, values are given as for a square centimeter of epithelium (Ωcm^2 or $\mu F/cm^2$), although the entire macula encompasses just 0.0035 cm^2. From the size of the macula, the cell density can be calculated. The 3000 hair cells and 6000 supporting cells in a 0.0035 cm^2 macula equal 8.6×10^5 hair cells/cm^2 and 1.7×10^6 supporting cells/cm^2.

The resistance of the close basal apposition of supporting cells can be calculated from dimensions of the apposition. The density of supporting cells and the serpentine course of the apposition leads to an estimate for a total length of basal boundary of 5200 cm/cm^2. With a width of 20 nm, height of 3 μm, and resistivity (as for saline) of 90 Ωcm^2 at 22°C, this region has a transverse resistance of R_{ca} = 2.6 Ωcm^2.

The series access resistance of the chamber, though not strictly proportional to epithelial area, can at least be normalized to a square centimeter area. With a 0.0035 cm^2 hole in the plastic sealing film, the chamber resistance alone has been measured to be 1850 Ω at 22°C; R_{ch} is thus equivalent to 6.5 Ωcm^2.

The apical surfaces of hair cells average 360 μm^2 in area, most of which is contributed by stereocilia. The calculated length constant for longitudinal current flow in stereocilia is orders of magnitude larger than their length, so stereocilia are isopotential with the rest of the cell: their area is to be included. With the hair cell density, and assuming 1 $\mu F/cm^2$ of cell membrane, this gives C_{ha} = 3.1 $\mu F/cm^2$.

Similarly, the basolateral hair cell area is 2000 μm^2, so C_{hb} = 17.2 $\mu F/cm^2$.

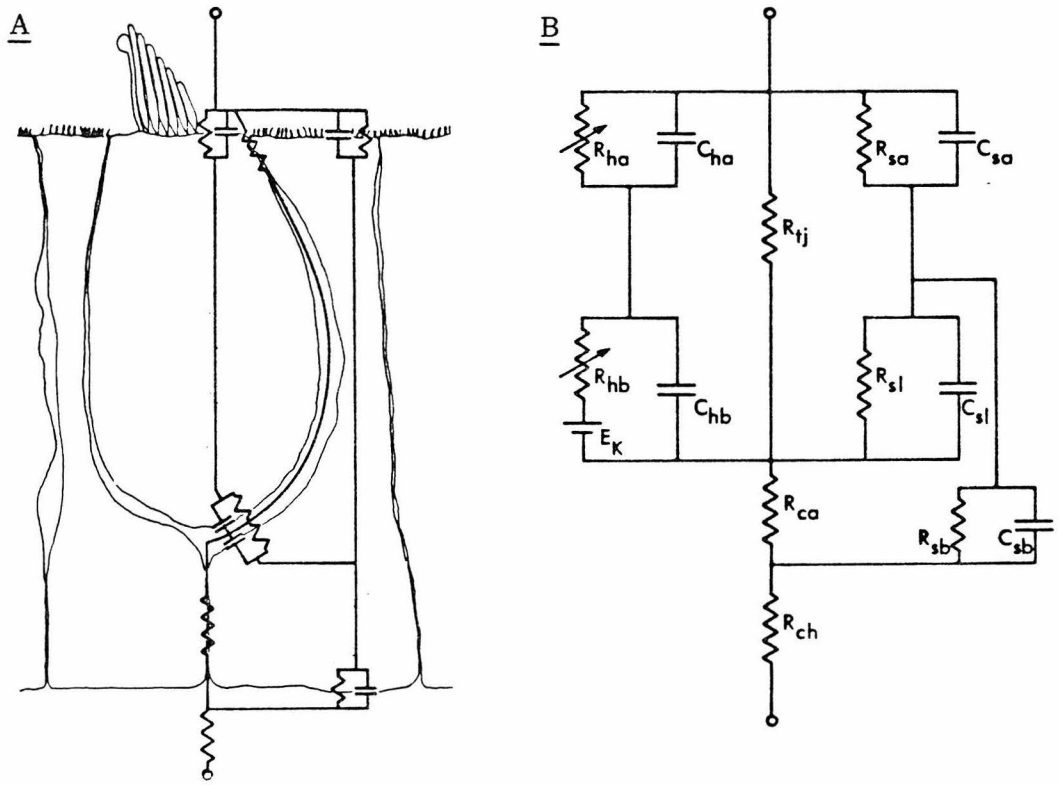

Text-fig. 7. Equivalent circuit of the epithelium. A represents a cross-section of epithelium, and shows only those elements thought to present an impedance to current flow. Superimposed is an electrical schematic representation which includes the resistance and capacitance of cell membranes and resistance of narrow intercellular spaces or junctions. The schematic also includes a resistor representing the series access resistance of the chamber. This corresponds to the resistances of saline between the voltage-measuring electrodes in each bath and the top and bottom faces of the epithelium, but it is shown as a single resistor in series with the bottom face. B, the electrical schematic is redrawn to clarify the circuit; symbols are given for each element. The resistance and capacitance of the basolateral hair-cell surface, R_{hb} and C_{hb}, are in series with the potassium Nernst potential, E_K = -80 mV. Since the reversal potential for both leakage and receptor currents through the apical membrane is $\sim$0 mV, no battery is shown for the apical hair-cell surface. Nor is a battery shown for any of the supporting-cell surfaces: while there is probably a steady current through supporting cells, the modulation of this current by changing hair-cell resistances is negligible.

The apical and basolateral hair cell resistances may be calculated from properties measured with intracellular recording (Corey & Hudspeth, 1979b). The resting input impedance is 300-1000 MΩ, with no electrodes in the cell; 500 MΩ is a reasonable mean value. If the membrane resistivity is equal for apical and basolateral surfaces, we calculate from the relative areas an apical resistance of 3300 MΩ and basolateral resistance of 590 MΩ. In addition, the receptor current with a saturating displacement of the hair bundle is typically 200 pA when the membrane potential is -60 mV. The reversal potential is near 0 mV, so the parallel path through transduction channels of the apical membrane is 300 MΩ. The apical resistance estimate becomes 275 MΩ, at its lowest; from the cell density $R_{na} = 320\ \Omega cm^2$.

Several lines of evidence support the contention that the mechanically activated conductance is in the apical membrane. Intracellular recording from voltage-clamped hair cells reveals a conductance increase with positive bundle displacements (Corey & Hudspeth, 1979b), so the receptor current is inward at the resting potential. The transepithelial voltage clamp shows an increase in current from top to bottom with stimulation (Text-figs. 2 and 6); thus the receptor current must enter the apical hair cell surface. Also, the microphonic current is blocked by removal of permeant ions from the upper bath, but not from the lower bath. Finally, the latency of the response is just 40 μs at room temperature (Corey & Hudspeth, 1979a). A second messenger could not diffuse from the stereocilia to the basolateral membrane in this short time, and there is no morphological evidence for a mechanical linkage to the basolateral surface.

Finally, the transducer channel conductance would cause a change in membrane potential from the resting -65 mV to about -25 mV, except that the delayed rectification limits the depolarization to about -45 mV. As the delayed rectification conductance is in series with the Nernst potential for K^+ of -80 mV (measured from the reversal of tail currents with the intracellular voltage clamp), we

can calculate a net basolateral resistance of 214 MΩ. The lowest value for the hair cell basolateral surface resistance is then 214 MΩ, when the delayed rectification is fully conducting. From the cell density, we get $R_{hb} = 250\ \Omega cm^2$.

The supporting-cell apical surface area is 59% of the epithelial area, measured from freeze-fracture electron micrographs, but the extensive microvilli of supporting cells add a surface area 9.3 times the flat area. Thus $C_{sa} = 6.1\ \mu F/cm^2$.

The basal surface—that surface facing the basal lamina—is smooth and tessellates the bottom side of the epithelium. This gives the trivial result, $C_{sb} = 1.0\ \mu F/cm^2$.

The lateral supporting cell surface is harder to estimate. When the assumption that it is comparable to the hair cell basolateral area, and with the known 1:2 ratio, we estimate $C_{sl} = 35\ \mu F/cm^2$.

The input resistance of supporting cells is unknown, and would be difficult to estimate in any case because of the electrical coupling. We will simply assume a membrane resistivity of $5000\ \Omega cm^2$. With the surface areas estimated above, this gives $R_{sa} = 820\ \Omega cm^2$, $R_{sl} = 140\ \Omega cm^2$, and $R_{sb} = 5000\ \Omega cm^2$.

These estimates are obviously no more than that, and must be checked with more extensive electrophysiology. We have more confidence in some than in others: hair cell resistances and capacitances are probably within 20% of our estimate, but supporting cell resistances may be incorrect by a factor of 2 or more.

Behavior of the equivalent circuit

Applied transepithelial current. The values estimated above can be checked by passing a step of current across the epithelium and measuring the resulting potential. For this rough measurement, several of the circuit elements do not affect the response. The hair cell apical and basal membranes, in series with each other, are together in parallel with the tight junctions. As the series hair-cell resistance is much larger than the tight-junction resistance, the former element is negligible. By

the same reasoning, all the supporting-cell resistance elements are negligible. The supporting cell basal capacitance is much less than the (virtually) parallel lateral capacitance, so we can neglect it also. The resulting circuit, lumping the series/parallel membrane capacitances to form an epithelial capacitance (C_e), is shown in Text-fig. 8A. If the transepithelial current is stepped from 0 to i, we expect a voltage step equal to $i(R_{ch}+R_{ca})$, followed by an exponential charging curve to $i(R_{ch}+R_{ca}+R_{tj})$ with a time constant $R_{tj}C_e$.

The predicted and experimentally measured curves are shown in Text-fig. 8B. The form is generally as expected, but with differences in detail. First, the time constant of the experimental curve is shorter than predicted: 320 μs compared to the predicted 400 μs. In fact, the time constant and the apparent value of R_{tj} are quite variable among preparations, and are inversely correlated with the difficulty of the dissection. This points to a variability in tight-junction integrity, either naturally occurring or experimentally induced.

Second, the charging curve is not purely exponential, but can be described as a sum of exponential curves. Significant deviation from a single time constant is not predicted by either the simplified or the full equivalent circuit. Two other factors, though, might explain it. We have treated the macula as a homogeneous epithelium. If there were a difference between areas, perhaps a spatial variability in tight-junction integrity, then the measured charging curve would be a sum of curves with different time constants. Alternatively, our equivalent circuit might be inadequate in describing diffusion barriers. A close apposition between hair cells and supporting cells would cause a distributed resistance in the peribasal space; this in turn would cause a distributed time constant for charging membrane capacitances. The latter effect has been treated in detail for rabbit urinary bladder epithelium by Clausen, Lewis & Diamond (1979); we will perform a similar complex-impedance analysis for the sacculus to distinguish between these possibilities.

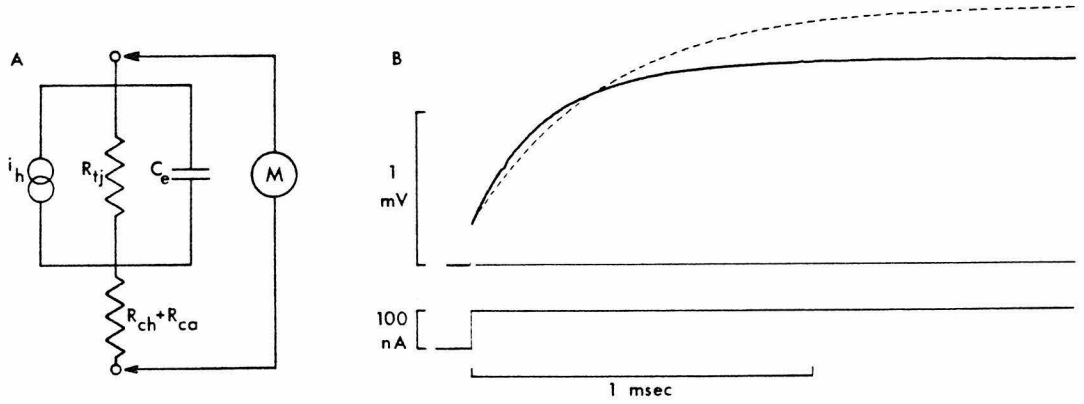

Text-fig. 8. Testing the simplified equivalent circuit. A, the equivalent circuit of Text-fig. 7 is condensed to four elements. The net current flowing from apex to base in hair cells is approximated as a current source i_h with infinite series resistance. The tight-junction resistance, R_{tj}, is much lower than the parallel resistance of supporting and hair cells, and so dominates that branch of the circuit. C_e represents the lumped capacitance of supporting and hair cells. The series access resistance of the chamber, R_{ch}, and the resistance of the close supporting-cell apposition, R_{ca}, are in series and so represented as a single summed element. The generalized meter, M, measures from the upper bath to the lower. It is a voltmeter for the measurement of Text-fig. 8B, but can represent a voltage clamp (essentially an ammeter) or a compensated voltage clamp (an ammeter placed across R_{tj}). B, the voltage across the epithelium is measured in response to an applied transepithelial current step. For both traces, the initial voltage step corresponds to the iR drop across $R_{ca} + R_{ch}$; the subsequent approach to steady state corresponds to the charging of C_e. The solid curve is the experimentally measured curve; the dashed curve is the response of the equivalent circuit in A. The general form of both curves is the same; there is in fact more variation among experimentally measured curves than between these two. The major difference is that the experimental curve does not display a single exponential relaxation. Normal Endolymph and Normal Perilymph; 22.0 °C.

These differences in detail are of little consequence here—although they will become important when looking at very fast phenomena (Chapter IV)—and we will take the model to be essentially correct.

Microphonic potential. The measured potential can now be predicted for the case in which the current source is the summed receptor current rather than external electrodes. If the transducer conductance is suddenly increased, current (i_h) flows in through the apical hair-cell surface, out through the basolateral surface, and back across tight junctions to the upper bath. As the series hair-cell resistance ($R_{ha}+R_{hb}$) is much larger than the tight-junction resistance, the hair cell can be roughly modelled as a current source (Text-fig. 8A). We thereby separate factors governing the generation of the hair-cell current from the effect the current has on the transepithelial potential. Following a step increase in the hair cell current, the microphonic potential shows the same charging curve as was generated by passing current (time constant $T = C_e R_{tj}$), but without the initial step. It reaches a steady-state value of $i_h R_{tj}$ (Text-fig. 9A). This charging of the epithelial capacitance is responsible for the low-pass filter characteristics of Text-fig. 5; the epithelial time constant of that preparation was 725 μsec, equal to $1/2\pi \cdot 220$ Hz.

The hair-cell current does not remain constant following a step, however. As the receptor current depolarizes the hair cell, the driving force decreases and so does the receptor current. The rate of decline is governed by the membrane time constant, $t_h = (C_{ha}+C_{hb})/(1/R_{ha}+1/R_{hb})$, which ranges from 2.5 to 16 msec depending on the membrane conductances that are active. The decrease in the driving force causes the fast decline in the response to a step (Text-fig. 9B); it is partially responsible for the high-pass filtering shown in Text-fig. 5.

Microphonic current. Under voltage-clamp conditions, the top bath is functionally short-circuited to the bottom bath, and we measure the current through this shunt. The clamp thus puts the summed close-apposition and chamber resistances

Text-fig. 9. The microphonic in response to a 0.5-μm step displacement. Motion of the stimulus probe is shown in the bottom two traces. A,B, the microphonic potential measured across the epithelium has an amplitude equal to $i_h R_{tj}$ at long times (B); at short time (A) it shows an exponential charging curve with a time constant $T = C_e R_{tj}$. C,D, the microphonic current measured by voltage clamping across the epithelium is somewhat less than i_h: the series resistance reduces it to $i_h \cdot R_{tj}/(R_{ch} + R_{ca} + R_{tj})$. At short times (C), the recorded current approaches steady state with a time constant (in theory) of $T = C_e/[1/R_{tj} + 1/(R_{ca} + R_{ch})] \simeq C_e/(R_{ca} + R_{ch})$; in practice the finite risetime of the probe and the opening of transduction channels prolong the rise. E,F, the microphonic current measured with a series-resistance-compensated voltage clamp measures all of the hair cell current, i_h. The fast rising phase now directly reflects the opening rate of transduction channels, distorted only by the finite risetime of the probe and the limited speed of the voltage-clamp electronics.

Traces shown are averaged responses to several presentations: 5 for A and B, 30 for C and D, and 100 for E and F. As might be expected, the noise increases with the speed of the recording arrangement. Noise of the microphonic potential, filtered as it is by the epithelial capacitance, is actually dominated by mechanical noise of the stimulus probe ($\curvearrowleft$0.003 μm root-mean-squared). When the epithelium is voltage clamped, thermal current noise of the series resistance becomes more important; with a series-compensated clamp, the clamp electronics dominates.

Normal Endolymph and Normal Periplymph; 22.0 °C.

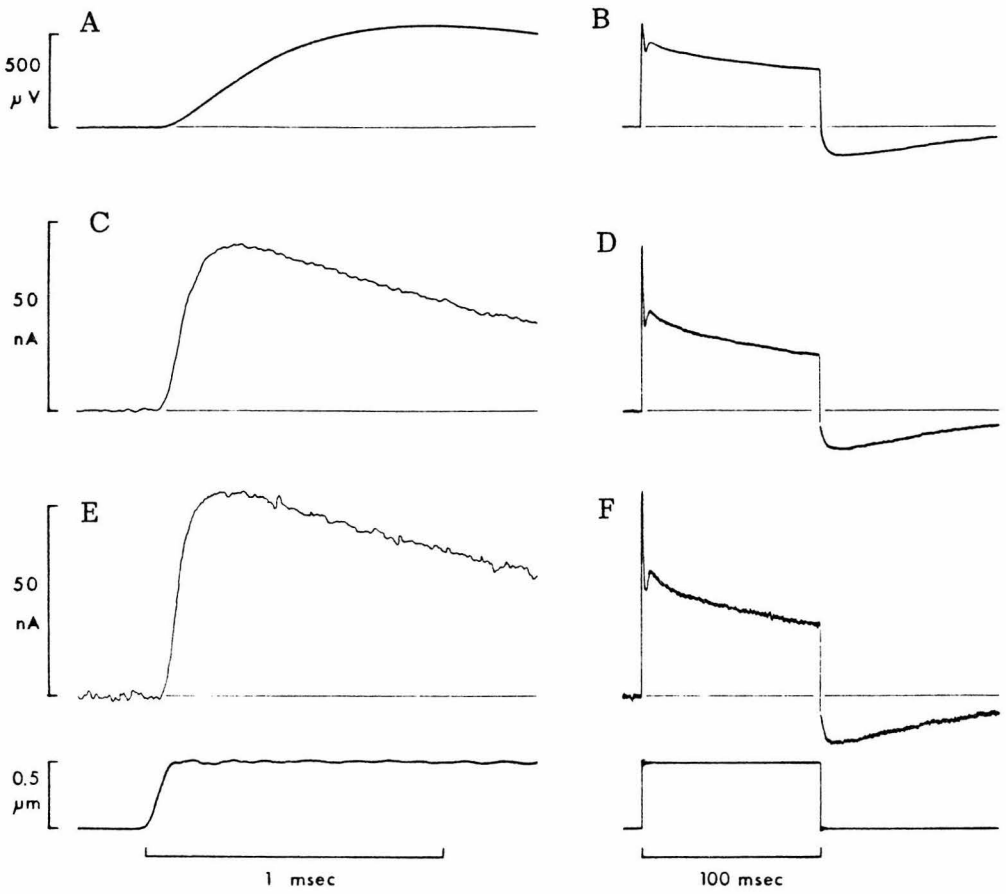
A
B
500
μV
C
D
50
nA
E
F
50
nA
0.5
μm
1 msec
100 msec

($R_{ca} + R_{ch}$) in parallel with the tight junctions (R_{tj}), and consequently reduces the epithelial time constant from 400 μs to about 60 μs (Text-fig. 9C). At short times, as before, all the hair-cell current passes through the epithelial capacitance; none is measured by the clamp. At long times (>>60 μs), the hair-cell current is divided between the two resistive paths. The ratio of currents is equal to the ratio of conductances, so the clamp measures only $R_{tj}/(R_{tj} + R_{ca} + R_{ch}) = 85\%$ of the current through the hair cell. The waveform, however, is essentially identical to that of the microphonic potential (Text-fig. 9D).

Series-resistance compensation. If the value of the series resistance ($R_{ca} + R_{ch}$) is known, the clamp can be constructed to subtract the potential drop caused by current flow across that element. The effect is to clamp directly across R_{tj}. Under these conditions, the time constant of the epithelium is nominally zero (Text-fig. 9E), and the clamp measures all of the hair cell current (Text-fig. 9F).

In this analysis we have partitioned the step response into two temporal domains. For times long compared to the epithelial time constant (>1 msec), the epithelial capacitance is negligible: we see the effects of the changing hair-cell membrane potential and of other slow processes within hair cells. These are the subject of the following part of this paper. For times short compared to the hair-cell time constant (< 1 msec), the driving force for the receptor current is unchanged. The microphonic potential principally shows the charging of the epithelial capacitance; the microphonic current, if measured with a compensated clamp, reflects solely the displacement-sensitivity and time-dependence of the transduction channels. These are the subject of the last paper of this series (Chapter IV of this thesis).

Part III. Dissecting the step response

The equivalent circuit has given us an explanation of one part of the step response: the rapid drop from the initial peak is due to the decrease in driving force as the hair cell depolarizes. This idea may be tested by changing the stimulus amplitude. We expect small displacements to produce a small receptor potential in the hair cell, and consequently to change the driving force very little. The initial drop should be minimal for small displacements; this is shown in Text-fig. 10. The response to a small step has a smooth, slow decline following the fast rise and a nearly symmetrical fall and recovery at the end of the step, actually much like the prediction based on the high-pass filter characteristics.

Similarly, the bump occurring 2-3 msec after the rapid drop is absent in the small-step response, suggesting that this, too, is a function of the voltage change occurring in the hair cell. An obvious candidate is a voltage-sensitive potassium conductance in the basolateral hair cell membrane, which turns on with some delay following a depolarization. A delayed rectification of this sort has been measured with intracellular voltage clamp of single cells (Corey & Hudspeth, 1979b). This conductance may be thought of as causing an increase in outward K^+ current through the basolateral membrane, thereby increasing the measured transepithelial current; alternatively, it may be considered as repolarizing the hair cell membrane, thereby increasing the driving force and so the receptor current. These are equally valid ways of viewing a single phenomenon.

We can attempt to block the purported K^+ conductance with tetraethylammonium ion (TEA); this is shown in Text-fig. 11. With TEA in the lower bath, the initial fast drop simply continues, reaching a (slowly declining) plateau of about 0.4 times the original current. The inference is that the membrane potential during the step is much closer to zero under these conditions: the receptor current has depolarized the cell to perhaps -20 mV, since the delayed rectification which would

Text-fig. 10. Amplitude dependence of the step response. Microphonic current; uncompensated voltage clamp. A, responses to positive displacements of 0.02, 0.05, 0.1, 0.2, 0.5, and 1.0 μm amplitude. The response amplitudes do not change linearly with displacement, as was seen in the displacement-response curve of Text-fig. 4. Moreover, they cannot be superimposed by scaling. The general form is characteristic of all healthy preparations in Normal Endolymph and Normal Perilymph at 22.0 °C; variability occurs in the position of the "bump" (ranging from 2-8 msec after the start of the step), in the slope of the slow decline, and in the amplitude of the undershoot following the end of the step. B, responses to negative displacements of the same amplitudes as in A. The responses show the expected negative saturation, but show also recovery from saturation and a rebound effect following termination of the step. C, probe displacements for A and B.

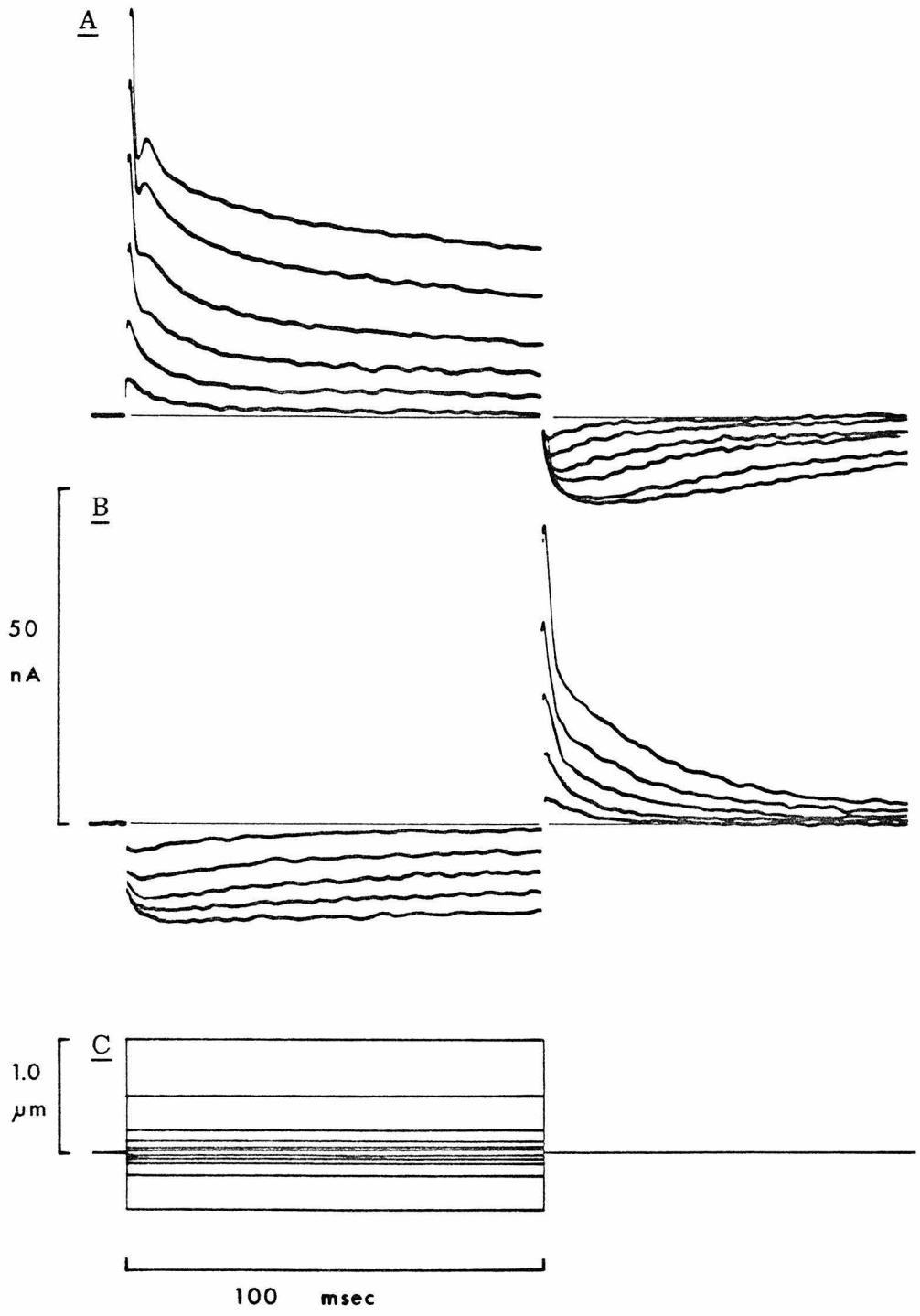
A
B
50
nA
C
1.0
μm
100 msec

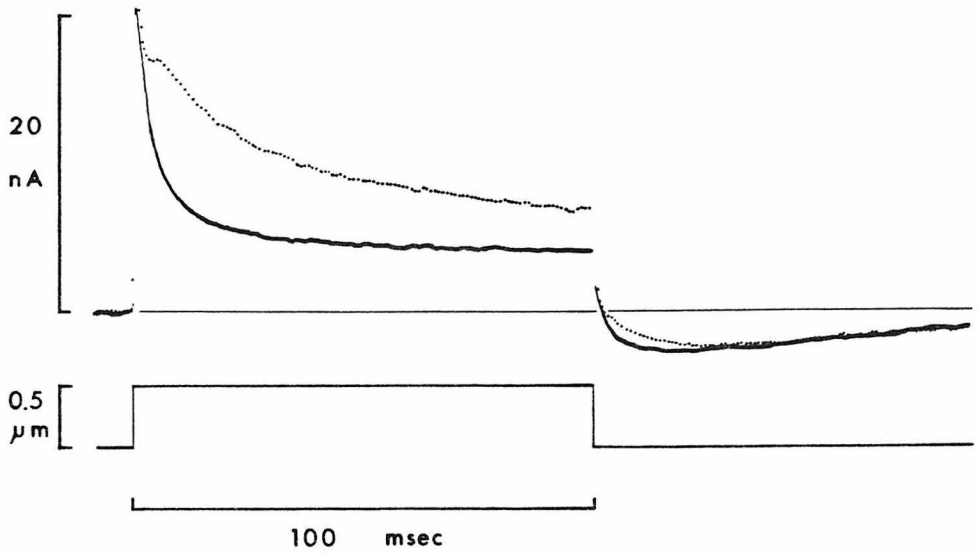

Text-fig. 11. TEA in the lower bath. The control response is shown as a dotted line; the response with TEA as solid. The responses are initially the same, but following the fast drop, where the control shows a bumpiform recovery, the TEA response continues to drop. The effect was fully reversible when Normal Perilymph was washed back.

Microphonic current; uncompensated voltage clamp. Normal Endolymph and Normal Perilymph; TEA Perilymph contained 2 mM tetraethylammonium chloride. 22.0 °C.

normally hold it at -50 mV has been largely blocked. The effect can be duplicated with 3,4-diaminopyridine in the lower bath, or, interestingly, by replacing K^+ with Cs^+ in the upper bath. We have shown that Cs^+ passes readily through the transduction channels (Corey & Hudspeth, 1979b); as it accumulates inside the cell, it apparently blocks K^+ channels from the inside, as it is known to do in squid axon and frog nerve (Bezanilla & Armstrong, 1972; Hille, 1973).

The converse experiment is to hold the hair-cell membrane potential constant. An elevated K^+ concentration in the lower bath should depolarize hair cells. If the resting potential is moved above the activation potential of the delayed (K^+) rectification mechanism, then the rectification should make the input resistance quite small, and the receptor current should cause little change in the membrane potential. In a sense, we are starting with the conditions normally reached after the bump. Now the step response shows none of the fast drop and bump phenomena (Text-fig. 12): there is little change in the driving force, and there is no delayed activation of voltage-dependent conductances. A response waveform of this sort is seen also when the transepithelial resistance is particularly low, presumably because K^+ from the endolymph is leaking through tight junctions to elevate the peribasal K^+ concentration. The response waveform can be restored to normal by substituting a Na^+ endolymph in the upper bath, as Na^+ may leak through but will not depolarize.

Even with a high K^+ concentration in the lower bath, there is a slow decline in the microphonic current. Under these conditions, in which the membrane potential is virtually clamped, it seems this sag could come only from the properties of the transduction channels. One possibility is an inactivation process, whereby channels spontaneously close or are blocked following activation, much like Na^+ channels in nerve. In this case, a further displacement would have no effect: the channels would be closed, and would have to recover from inactivation before reopening. Another possibility is that the displacement of the hair bundle is somehow not communicated

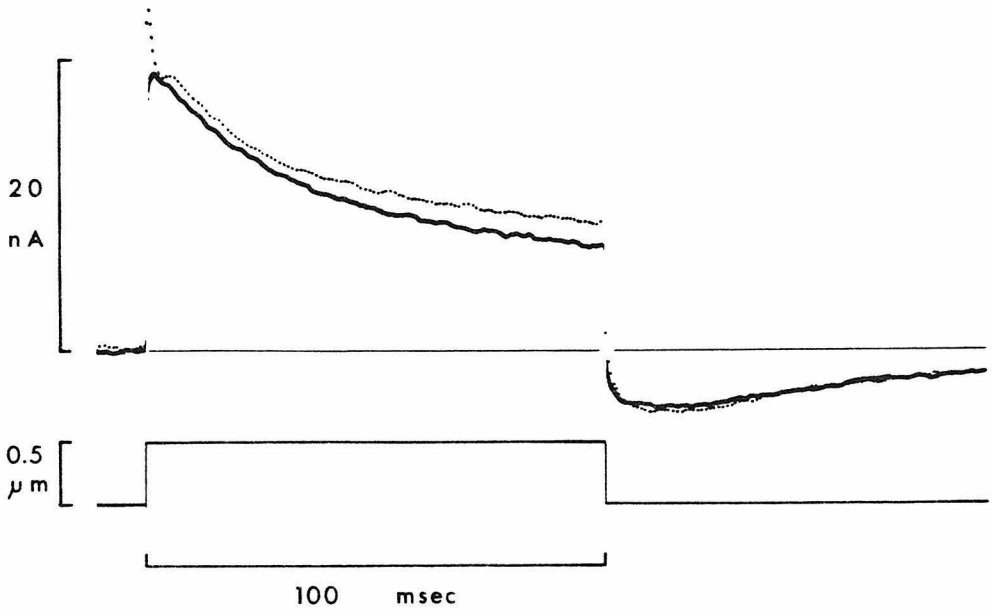

Text-fig. 12. High K^+ in the lower bath. The control response is shown as a dotted line; the response with high K^+ as solid. The initial amplitude is smaller with high K^+, but the response has a smooth decline which nearly matches that of the control in the latter part of the step. The waveform of the undershoot is somewhat sharper with high K^+.

Microphonic current; uncompensated voltage clamp. Normal Endolymph and Normal Perilymph; for High K^+ Perilymph a portion of the Na^+ was substituted with K^+ to bring the K^+ concentration to 17 mM. 22.0 °C.

to the transduction element in a constant manner, that something in the transduction process feeds back to reduce the bias on the transduction elements. If there were so, a further positive displacement of the hair bundles would reopen channels, and would restore the original hair-cell current.

In Text-fig. 13, a saturating positive displacement is applied at various times before and during the step. The membrane potential is held constant with high K^+ in the lower bath. While the microphonic current declines during a maintained step, the current in response to a saturating displacement is nearly unchanged. Similarly, a saturating negative displacement decreases the current to the same level at all times. Thus the total number of activatable channels is unchanged, but the bias on them—how the bundle position is communicated to the transducer—is being reset.

A simple explanation, that the bias reset is merely the otolithic membrane slipping relative to the stimulus probe, was tested by optically monitoring otolithic membrane position (see **METHODS**). The optical signal follows the probe motion, and shows no relaxation during the step. Nor is there slippage between the otolithic membrane and hair bundles: the effect is seen with intracellular recording and direct stimulation of single cells (Chapter III).

The phenomenon is further elucidated with the experiments of Text-fig. 14. Here, as in Text-fig. 4, the instantaneous displacement-response relation is mapped with a series of short steps of different amplitudes. A control series done before a 100-msec step shows the normal displacement-response curve. A series done near the end of the maintained displacement, however, reveals that the curve has shifted along the displacement axis. Following the step, the curve relaxes back to the resting potential (data not shown). Thus channels close during a maintained positive step, not because they are inactivating, but because the displacement-response curve, in a sense, is shifting out from under them.

This shift of the displacement-response curve constitutes an adaptation mechanism for hair cells (and is considered in greater detail in Chapter III).

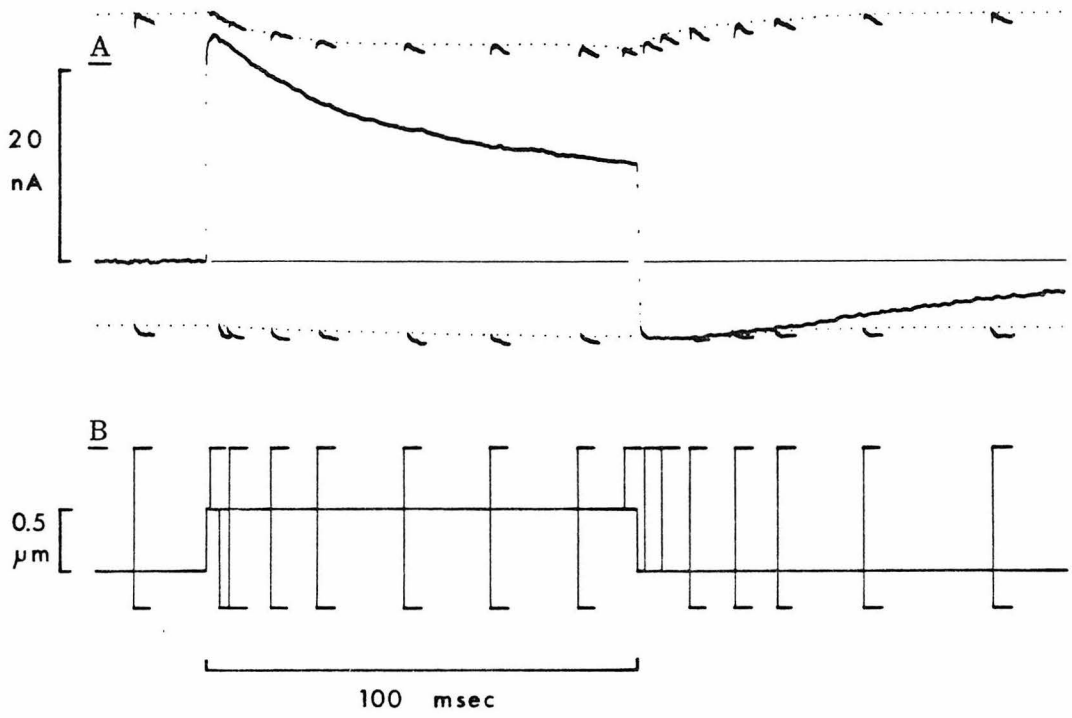

Text-fig. 13. Saturating steps to test the maximum receptor current. B, a normal 0.5-μm, 100-msec step stimulus is presented, but at a given time during the step the probe is further stepped to +1.0 μm or -0.3 μm. These saturating displacements should open or close, respectively, all the available channels. One saturating step is presented with each normal stimulus; the figure is a composite of 48 different presentations. A, the position of the normal response curve within the envelope defined by positive and negative saturations indicates the proportion of channels open. Initially, some 20% of channels are open. The 0.5-μm step raises the proportion to about 90%, but the proportion decreases during the maintained displacement. At the termination of the step, the proportion drops to 0, and then recovers to the initial condition over the next 100 msec or so. Note also that the difference between negative and positive saturation envelopes changes only slightly. The net envelope indicates the maximum current through transduction channels; since the reversal potential for the receptor current is ∿0 mV, the net envelope is proportional to the membrane potential. It changes only slightly during the step when high K^+ is in the lower bath.

Microphonic current; uncompensated voltage clamp. Normal Endolymph and High K^+ Perilymph; 22.0 °C.

Text-fig. 14. Step series to map the displacement-response curve. Same conditions as Text-figs. 12 and 13. B, superimposed on the normal 0.5-μm stimulus are fast test steps of varying amplitude, presented either before or near the end of the stimulus. Again, one test step was presented with each normal stimulus; the figure is a composite of 20 presentations. A, the superimposed response to test steps presented before the normal stimulus shows saturation with large positive steps. Near the end of the maintained step stimulus, however, the same positive steps evoke less current and the negative saturation is more pronounced. C, the displacement-response curves generated in A and B are plotted. Ninety milliseconds after the onset of a 0.5-μm step, the control curve (i) has been shifted along the displacement axis by 0.33 μm (ii); the amplitude is unchanged. Curves drawn by eye with reference to Text-fig. 4.

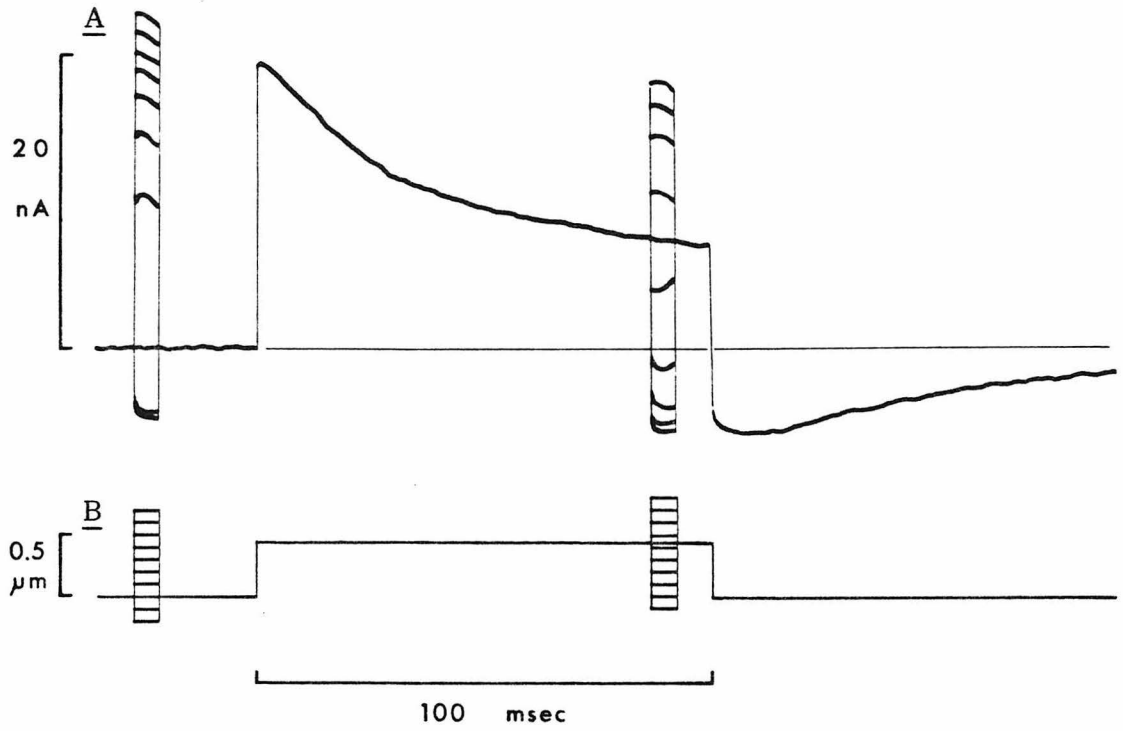
A
20
nA
B
0.5
μm
100 msec

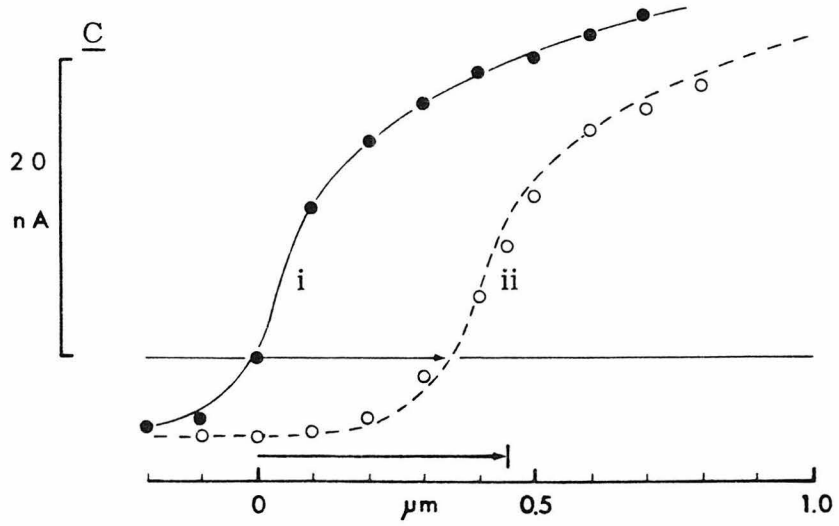
C
20
nA
i
ii
0
μm
0.5
1.0

Following large positive or negative displacements of the hair bundle, which move the bundle out of the responsive range, the adaptive shift acts to move the range to the new bundle position. Hair cells thus maintain a large operating range, but retain high sensitivity to small displacements. For small displacements, the shift acts as a high-pass filter; it is largely responsible for the high-pass filtering and phase lead shown in Text-fig. 5.

It also explains much of the undershoot following the step. At rest, about 20% of the transduction channels are open; the transepithelial current includes this steady component. With a maintained positive displacement, the displacement-response curve shifts to the right. Then, when hair bundles are moved back, the transducer is moved to a portion of the curve where no channels are open: the current becomes less than the resting current. Finally, as the curve relaxes back to the 20% position, the undershoot declines to zero.

Our understanding of these various effects may be summarized with Text-fig. 15, which shows a saturating step experiment like that of Text-fig. 13 but in a normal ionic environment. The figure provides two measures of processes occurring within the hair cells. The difference between positive saturation and negative saturation reflects the maximum possible receptor current and is proportional to the potential across the apical membrane. The position of the response curve within this envelope shows the proportion of channels open, and so continuously indicates the position of the displacement-response curve.

The constriction of the net envelope immediately following the step signals the intracellular depolarization, which occurs concurrently with the initial drop in the microphonic current. The bump in the microphonic current, which we interpret as a basolateral K^+ conductance turning on, is followed by a slight increase in the envelope size—a slight repolarization of the membrane potential. While the envelope is relatively unchanged for the remainder of the step, the microphonic current drops

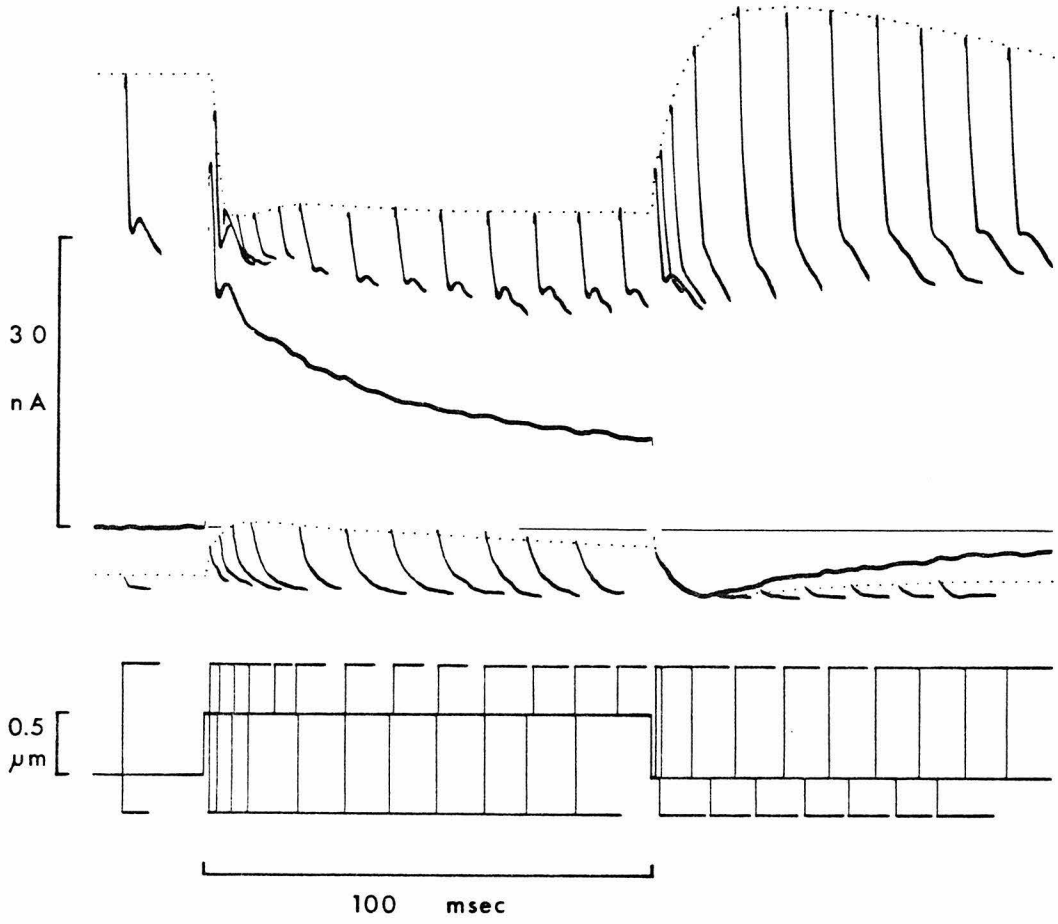

Text-fig. 15. Saturating steps in a normal ionic environment. The stimulus is the same as in Text-fig. 13, but High K^+ Perilymph has been replaced with Normal Perilymph. The net envelope, proportional to the intracellular membrane potential, now shows a large change corresponding to the receptor potential. The shift of the displacement -response curve during the step is still apparent. Microphonic current; uncompensated voltage clamp. Normal Endolymph; 22.0 °c.

steadily as the displacement-response curve shifts. At the offset of the step, the microphonic current drops to meet the lower (negative saturation) envelope: all the transduction channels are closed. The lower envelope and the microphonic current then decline together as the cell membrane capacitance discharges through the slowly-closing K^+ channels. The magnitude of the net envelope increases rapidly, however, with the repolarization: with all channels closed, the hair cell is hyperpolarized beyond the initial resting potential. The membrane potential returns gradually as the displacement-response curve recovers and a portion of the transduction channels reopens.

Part IV. Reconstructing the step response

We have described above several properties of hair cells that are not linear with stimulus displacement or not constant over time, and have presented qualitative evidence to show that these properties can explain the microphonic current response to a step displacement stimulus. Our description would be considerably strengthened if it could be shown that these effects can quantitatively predict the step response. To do this, quantiative relations describing each component were combined, and a solution to the combined expressions was generated by step wise integration with a computer. Quantitative reconstruction does in fact produce most of the characteristic features of the experimental step response.

The instantaneous displacement-response curve is described by an expression of the form

$$P_t = \frac{1}{1 + e^{B}(1 + e^{A})} \qquad \text{where } A = (G_1 + Z_1 D)/RT \text{ and } B = (G_2 + Z_2 D)/RT.$$

P_t is the probability that a transduction channel is open, G_1 is 0.6 kcal/mol, G_2 is 0.3 kcal/mol, Z_1 is 10 kcal/mol-μm, Z_2 is 3 kcal/mol-μm, D is bundle displacement in μm, R and T have their usual thermodynamic meanings and RT = 0.586 kcal/mol. With four free parameters (G_1, G_2, Z_1, Z_2), this expression can be made to fit the experimental curve rather well, but so can a number of other expressions of very different form. The theoretical basis for this particular choice is further discussed in Chapter IV.

The adaptive shift of the displacement-response curve, more detailed measurements of which are presented in the third paper (Chapter III), is not a simple first-order exponential relaxation. It can be roughly fitted, however, by a sum of two exponential decays in time:

$$D = \frac{1}{2} D_o (e^{-t/T_1} + e^{-t/T_2})$$

D_o is the initial bundle displacement at t = 0, D is the effective displacement communicated to the transduction element, T_1 is 15 msec and T_2 is 150 msec. This expression has no theoretical basis, but is the simplest empirical expression that fits our preliminary data. At the termination of the step, D_o is subtracted from D, and each of the two components relaxes to zero with its characteristic time constant.

The membrane capacitance and leakage resistance per area of epithelial surface are given the values calculated in Part II of this paper: apical leakage resistance is 3840 Ωcm^2 and basolateral leakage resistance is 680 Ωcm^2. These are both assumed to be potassium conductances, as in frog nerve (Hille, 1973), so the basolateral leakage is in series with a Nernstian battery of E_K = -80 mV, but the apical leakage has a series battery of $\sim$0 mV. The apical and basolateral capacitances are, respectively, 3.1 $\mu F/cm^2$ and 17.2 $\mu F/cm^2$.

The transduction channels have a resistance when fully activated of 350 Ωcm^2 of epithelium. The reversal potential for the receptor current is $\sim$0 mV (Corey & Hudspeth, 1979b), and the current-voltage relation for the channels is linear over the physiological range (see Chapter II). The current is modulated by the probability that channels are open (the displacement-response curve), thus

$$i_t = P_t G_t V_m \qquad \text{where } G_t = (350\ \Omega cm^2)^{-1}.$$

The delayed rectification is a bit more complex, as both equilibrium values and time course are continuous functions of membrane potential. Two appropriate models are the voltage-sensitive potassium conductance of squid axon (Hodgkin & Huxley, 1952) and that of frog node of Ranvier (data of Dodge, in Hille, 1971). Neither of them, in fact, fits particularly well our preliminary measurements with the intracellular voltage clamp. The hair-cell K^+ conductance appears to have a steeper voltage sensitivity: it turns on over a narrower range of membrane potential than either of the two archetypes. It also shows faster kinetics than the frog node K^+ conductance.

Consequently, we chose expressions of the same general form, but altered parameters to fit our intracellular measurements of K^+ current. The probability of a potassium channel being open is

$$P_K = n^4$$

where n is the probability that a "gating particle" is in state 1, and where two time constants, k_{01} and k_{10}, govern transitions between states 1 and 0:

$$k_{01} = f\, e^{-(G-\delta zF[V_m-V_a])/RT}$$

$$k_{10} = f\, e^{-(G+(1-\delta)zF[V_m-V_a])/RT}.$$

The frequency factor f is taken as $kT/h = 6 \times 10^{12}$ sec^{-1}, G = 14 kcal/mol, $\delta = 0.5$, z = 2.0 electronic charges, V_m is membrane potential, V_a is an "activation potential" at which half the n's are in state 1, and k, T, h, F, and R have their usual thermodynamic meanings. The equilibrium value of P_K is then

$$P_k(\infty) = \left(\frac{k_{01}}{k_{01}+k_{10}}\right)^4$$

The current through voltage-sensitive potassium channels is typically close to a linear function of voltage, and has been modeled as an ohmic resistance in other studies (Hodgkin & Huxley, 1952; Hille, 1971). An ohmic resistance, gated as above, adequately describes the current-voltage relation measured in hair cells (Corey & Hudspeth, 1979b), so we take the voltage-sensitive potassium current to be

$$i_K = P_K G_K (V_m - E_K).$$

G_K is $(20\ \Omega cm^2$ of epithelium$)^{-1}$ and E_K is the potassium Nernst potential of $\sim$-80 mV.

We have some evidence for other membrane conductances in hair cells, and these doubtless contribute to the response. There is a voltage-sensitive Ca^{++} conductance in the basolateral membrane (Hudspeth & Corey, 1977; unpublished results), probably involved with Ca^{++}-dependent transmitter release. The Ca^{++}

influx, more likely than not, modulates a Ca^{++}-activated K^+ conductance (Meech, 1978). An anomalous or inward rectification is activated at membrane potentials more negative than -100 mV (Corey & Hudspeth, 1979b). If this is like other inwardly rectifying conductances, which turn on at less negative potentials when the extracellular K^+ concentration is raised (e.g., Hagiwara & Yoshii, 1979), then it is not significant under normal physiological conditions but will become so with high K^+ in the lower bath.

Nevertheless, these other conductances are not included in the reconstruction, mostly because we have scant quantitative understanding of them, but also because the reconstruction is acceptably close to the experimental results even without their inclusion. We have, incidently, no evidence for voltage-sensitive Na^{++} channels, and we expect that the efferent synapses on hair cells are not active in the in vitro preparation.

The results of this reconstruction are shown in Text-fig. 16. The predicted response waveforms are for the most part identical to the measured responses, with some minor deviations. The initial peak is not so large in the reconstructed waveform as is sometimes measured, suggesting that the real resting potential is more negative (and so the initial current larger) than the model predicts. We might have underestimated a resting basal K^+ conductance, the K^+ concentration might be lower in the peribasal space than in perilymph (possibly maintained lower by supporting cells), or there might be an active electrogenic pump in the hair cell membrane that maintains a high negative resting potential. In Text-fig. 16D, the upper envelope is not quite the same in form as the measured response, for the first few milliseconds after the step. This is most likely due to an inaccuracy in the measured responses because of an insufficient number of steps in that temporal region. The rebound phenomena in that trace, on the other hand, are predicted rather well by the model. Although the model explicitly does not include some conductances of the hair cell membrane, it

seems to describe sufficiently well the major factors that generate the microphonic response to a step stimulus.

Text-fig. 16. Results of the reconstruction. Stimulus and ionic conditions are as for Text-figs. 10, 11, 14, and 15 respectively, with different ionic conditions duplicated by altering the parameters in the computer program that they are supposed to effect. A, responses to steps of -0.5, -0.2, -0.1, -0.05, -0.02, +0.02, +0.05, +0.1, +0.2, +0.5, and +1.0 μm. B, response to a +0.5 μm step. TEA Perilymph is duplicated by setting G_K equal to 1% of its normal value. C, response to a +0.45 μm step, with test steps to various levels before the stimulus step and after 90 msec. High-K^+ Perilymph was duplicated by changing E_K to -50 mV. D, response to a +0.5 μm step, with test steps at various times to +1.0 μm or -0.5 μm.

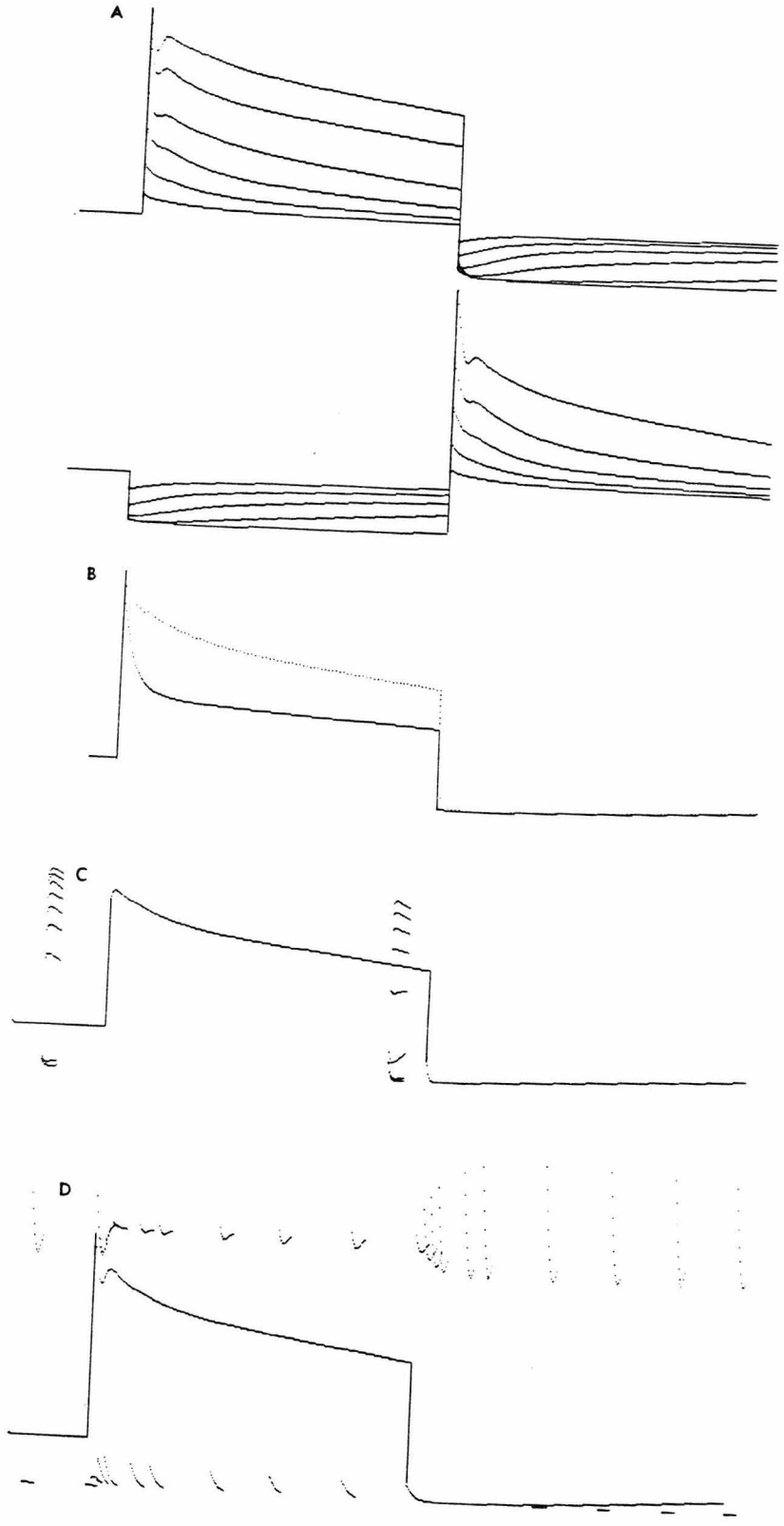
A
B
C
D

DISCUSSION

This analysis has served to clarify some aspects of the microphonic potential observed in other hair cell preparations. The nature of the 2f response to sinusoidal stimuli, while not currently a point of controversy, was at least clearly demonstrated here by decoupling one population of hair cells from the stimulus. The high-pass filter characteristics of the response were shown to be a consequence of the adaptive shift of the displacement-response curve. This permits, for instance, a more direct assessment of the effect of certain drugs on hair cell transduction (Kroese & van den Bercken, 1980). The low-pass characteristics were attributed to the passive electrical time constant of the epithelium, which acts as a first-order filter of the microphonic current. The action of agents or cellular functions that change apical or basal hair cell membrane conductances (e.g., Flock & Russell, 1976) are easier to understand and quantify from their effects on the microphonic responses.

Several characteristics of the response had not previously been reported. The very fast rise of the microphonic current following a step displacement provides a minimum latency for the transduction process and so rules out some hypothesized transduction mechanisms (Chapter IV; Corey & Hudspeth, 1979a). The adaptive shift of the displacement-response curve reveals a fundamental adaptation process occurring in hair cells at the level of transduction (Chapter III; Eatock, Corey & Hudspeth, 1979).

Most important, perhaps, the analysis sufficiently clarifies the generation of the microphonic response so that the preparation may be used as a quantitative tool for further studies on transduction. Alterations in the stereotyped response to a step are well-defined results of certain cellular changes. For instance, elimination of the fast drop and bump in the response to large steps signals depolarization of the hair cell membrane. Increase or decrease in the rate of the slow decline indicates a change in the adaptive mechanism. Agents that affect the number of channels open

at rest change the size of the undershoot and can be studied directly by mapping the instantaneous displacement-response curve. Even when two or more effects occur simultaneously, they can be separated by tailoring the stimulus strength and duration to magnify a particular effect. An approach of this sort will be applied in the following three chapters.

Chapter II

IONIC SELECTIVITY OF THE TRANSDUCTION CHANNEL

PREFACE

One of the most intriguing features of vertebrate hair cells is that, no matter in what organ they occur, they are arranged in epithelia separating two different fluids. While the basal surfaces face a normal, high-Na^+ saline (perilymph), the apical surfaces face a high-K^+ saline (endolymph). There has been a considerable amount of work in various systems on trying to understand how the high-K^+ endolymph is related to sensory transduction. While much of it has been hampered by the difficulty of perfusing small and delicate endolymphatic spaces, the general conclusion has been that K^+ carries the receptor current, but that a modicum of Ca^{++} is required to make it all work.

We were particularly interested in this problem, since our initial intracellular experiments were done with normal high-Na^+ saline on all cell surfaces, and thus with the electrochemical gradient for K^+ near zero. We nonetheless observed receptor potentials that were of respectable size.

With the epithelial preparation it was possible to try many different ions in the upper bath, while the hair cells were kept healthy with normal saline in the lower bath. It soon became clear that almost any small cation could carry the receptor current. While the preparation was good for rapid screening of ions, it did not allow control of membrane potential, so the results could not be very quantitative. We consequently extended the intracellular recording to a two-electrode voltage clamp. In normal high-Na^+ saline, the reversal potential for the receptor current was $\sim$0 mV, which could only come from a channel that had nearly equal K^+ and Na^+ permeabilities. The channel was thus nonspecific, with K^+ carrying the receptor current *in vivo*. These results were published in a *Nature* paper, which is reprinted as Part I of this chapter.

The fortunate coincidence of this work with a course on membrane permeability taught by Sally Krasne at UCLA led us to consider in more detail the

internal structure of the channel. By looking at which ions go through and which do not, and how the current-voltage relation is altered with different permeant ions outside the cell, we should be able to describe the channel in terms of minimum pore dimensions, and the position within the pore of energy barriers to permeation. This work is still in progress; a preliminary account of the current understanding is presented in Part II of this chapter.

Part I. Ionic basis of the receptor potential in a vertebrate hair cell*

D. P. Corey & A. J. Hudspeth

Division of Biology, California Institute of Technology, Pasadena, California 91125

Vertebrate hair cells, the primary receptors of auditory, vestibular and lateral-line organs, occur in epithelia which separate fluids of differing ionic composition. The apical surfaces of hair cells, on which the mechanosensitive hair bundles are situated, face a high-K^+ fluid (termed endolymph in the inner ear); the basolateral surfaces instead contact fluid (perilymph or a related substance) of a composition similar to that of other extracellular fluids (Smith et al. 1954; Russell & Sellick, 1976; Peterson et al. 1978). The universal occurrence of high-K^+ fluid on the apical surfaces of hair cells in vertebrates has been taken as evidence that it is important for the transduction process, in particular that it relates to the ionic specificity (Sellick & Johnston, 1975) of the conductance change (Hudspeth & Corey, 1977) underlying the receptor potential. There is, however, conflicting experimental evidence regarding this specificity. K^+ has generally been thought to carry the receptor current, as replacement of endolymph with perilymph in the guinea pig cochlea abolishes the extracellularly recorded microphonic potential (Konishi et al. 1966). Yet microphonic potentials, as well as intracellular receptor potentials, have been recorded in other preparations when the apical surfaces of the hair cells faced instead a high-Na^+ saline, and thus when the electrochemical gradient for K^+ was near zero (Hudspeth & Corey, 1977; Matsuura et al. 1971). Ca^{++} has also been proposed to carry the receptor current (Sand, 1975), but its concentration is quite low in endolymph (Peterson et al. 1978), particularly that of the mammalian cochlea

---

*Nature, Vol. 281, No. 5733, pp. 675-677, October 25, 1979.

(Bosher & Warren, 1978). We present evidence here that the receptor current in a vertebrate hair cell is carried in vivo by K^+, but that the transduction channel is in fact nonspecific, being permeable to Li^+, Na^+, K^+, Rb^+, Cs^+, Ca^{++}, and at least one small organic cation.

Hair cells were prepared for intracellular recording as described previously (Hudspeth & Corey, 1977; Hudspeth & Jacobs, 1979). Sacculi were removed from adult bullfrogs and their otolithic membranes peeled away after loosening by mild proteolysis (incubation for 60 min with 0.03 mg ml^{-1} subtilopeptidase A, EC 3.4.4.16, at 22 °C). The tissue was positioned in an experimental chamber with standard saline on all cell surfaces and viewed with Nomarski differential interference contrast optics. Individual hair cells were penetrated by two glass microelectrodes, each 100-150 MΩ in resistance, connected to a simple voltage clamp circuit. To stimulate each impaled cell, its hair bundle was deflected with a fine glass probe (0.2 μm tip diameter) inserted horizontally between the kinocilium and the rest of the hair bundle. Probes were moved by an electronically controlled, two-dimensional stimulator, over a distance of 1-2 μm, with a 10-Hz, triangle waveform.

We first measured the current-voltage relationship for unstimulated hair cells (Fig. 1). The input resistance measured with two electrodes was 200-300 MΩ at a holding potential of -60 mV. Because the resistance was higher (200-900 MΩ) if measured with one electrode and an active bridge circuit, much of the apparent membrane conductance at this potential resulted from penetration damage. At membrane potentials more positive than about -50 mV, however, the resistance dropped to 6-7 MΩ. This conductance increase was largely blocked by 1 mM 3,4-diaminopyridine (Kirsch & Narahashi, 1978), and is evidently a voltage-dependent K^+ conductance. Such outward or delayed rectification may explain the rather small receptor potentials seen in some hair cell preparations (Harris et al. 1970; Weiss et al. 1974): because of the change in slope conductance, a receptor current which

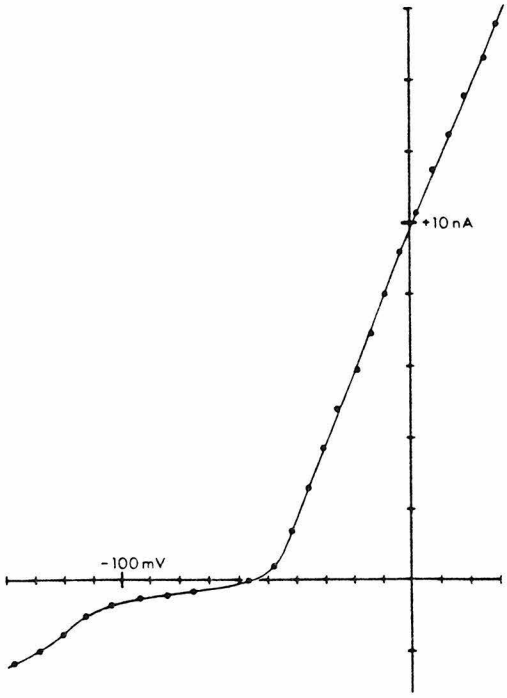

Fig. 1. Current-voltage relationship for a saccular hair cell, measured 50 msec after the start of a voltage step. Inward current is shown as negative. The holding potential was -60 mV. The striking outward rectification which occurs above -50 mV was blocked by 3,4-diaminopyridine and probably corresponds to the delayed rectification of most neurons. Inward or anomalous rectification is evident at potentials below -100 mV.

generates a receptor potential of 20 mV in bullfrog hair cells at a resting potential of -60 mV produces only 0.5 mV at -40 mV. Figure 1 shows an additional conductance increase, an inward or anomalous rectification, at potentials below -100 mV. Such a rectification has been hypothesized to explain certain aspects of electrical behavior of the mammalian cochlea (Hubbard et al. 1977), but has not previously been demonstrated for vertebrate hair cells.

The stimulus-associated current, or receptor current, was measured by presenting periodic mechanical stimuli of saturating amplitude while clamping to various potentials. The receptor current at the holding potential of -60 mV ranged from 45 to 205 pA with a mean of 98 pA ($\pm$37 pA, s.d., n = 28 cells) and with the larger values more representative of healthy cells. Variation in the measured current was caused both by decline in the viability of a cell during prolonged recording and by mechanical drift of the stimulus probe with respect to the responsive range of the hair bundle. The voltage dependence of the receptor current was consequently determined by comparing the receptor current at a test potential to the current at the holding potential immediately before and after the potential step. The receptor current at -60 mV was normalized to 100 pA for each cell, and the receptor current at each test potential then scaled by the same amount. An implicit assumption in this analysis is that the mechanical sensitivity is not also voltage-sensitive, for instance that the responsive range of the hair bundle does not shift as the cell is depolarized.

A representative series of clamp records is shown in Fig. 2a. The receptor current reverses its direction from inward to outward at a membrane potential between -9 and +11 mV. Figure 2b combines normalized data from 24 cells; a linear regression fit to these data indicates a reversal potential of -2 mV. This is not the equilibrium potential for Na^+, K^+, or Ca^{++}, since a standard, 124-mM Na^+ saline solution (Hudspeth & Corey, 1977) faced all cell surfaces during these experiments. It could, however, result from a stimulus-dependent conductance that is nonspecific—that has a limited ability to discriminate among cations.

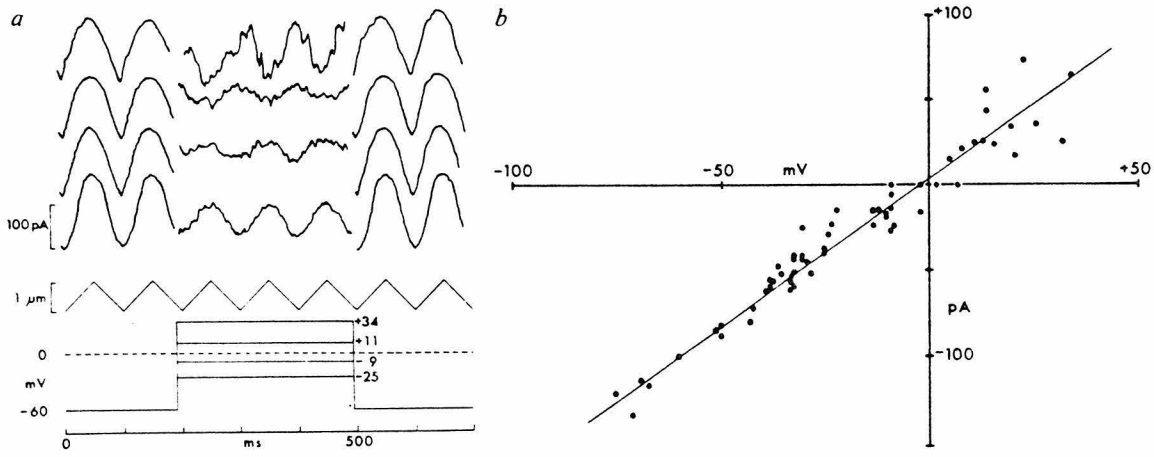

Fig. 2. a, receptor currents at a holding potential of -60 mV and at test potentials of -25, -9, +11, and +34 mV; inward current is shown as negative. The membrane potential was held at -60 mV for 200 msec, clamped to the test potential for 300 msec, and returned to the holding potential. Each trace represents the average of 10 test steps. Ionic currents that were not stimulus-dependent were electronically subtracted before measuring the receptor current. The hair bundle was continuously moved with a 1.1-μm, 10-Hz, triangle-wave stimulus, shown below the current records; downward represents a deflection toward the kinocilium. b, magnitude of the receptor current as a function of membrane potential; normalized data from 24 cells. The line is a linear regression fit to the data (r^2 = 0.97); its zero-current intercept, the reversal potential, is -2 mV. The external fluid was standard, high-Na^+ saline, so that the reversal potential is not the equilibrium potential of Na^+, K^+, or Ca^{++}.

We consequently tested several cations using an in vitro microphonic technique (Corey & Hudspeth, 1979a). The macular epithelium of the sacculus was positioned across a hole between two chambers, so as to separate them ionically and electrically. The potential across the epithelium was monitored with an electrode in each chamber; a second pair of electrodes was used to pass current to clamp the transepithelial potential at zero. Measuring the transepithelial current, rather than the transepithelial potential, avoided variations in response amplitude caused by slow changes in epithelial resistance. Hair cells were stimulated en masse by moving the otolithic membrane, which remained attached to the hair bundles, with a glass probe driven by a piezoelectric element. The stimulus was a saturating step displacement of amplitude 1.5 μm and duration 1 msec. The otolithic membrane can follow this fast stimulus, and the microphonic current turns on and off in much less than this time (Corey & Hudspeth, 1979a). The charging time of the hair cell membrane is much longer, however, so that the intracellular potential should change only slightly during the pulse. The measured current is accordingly dependent on the resting potential and the permeability to the test ion, but not on voltage-sensitive conductances that are secondary to the receptor potential.

The chambers were separately perfused with a test solution on the apical side (130 mM of the relevant monovalent cation, 0.25 mM Ca^{++}, 130 mM Cl^{-}, 3 mM D-glucose, 1 mM HEPES) and an artificial perilymph on the basolateral side (3.63 mM K^{+}, 122 mM Na^{+}, 1.36 mM Ca^{++}, 0.68 mM Mg^{++}, 130 mM Cl^{-}, 3 mM D-glucose, 1 mM HEPES). The apical surfaces of hair cells and supporting cells are bounded by tight junctions, which limit the exchange of ions between the two chambers.

All of the alkali cations supported the microphonic current. The mean relative signal amplitudes from eight experiments were: Li^{+}, 0.9; Na^{+}, 0.9; K^{+}, 1.0; Rb^{+}, 1.0; and Cs^{+}, 1.0. Ammonium ion (NH_4^{+}) was more permeant, with a relative amplitude of 1.3. To establish whether still larger ionic species could traverse the

transduction channel, we bathed the apical surface with test solution containing 130 mM tetramethylammonium ion (TMA). This reduced the microphonic current to 0.2 of its value for 130 mM K^+, suggesting that TMA can pass through the transduction channel, although less readily than the alkali cations. To confirm this observation, TMA was tested on single cells using the intracellular voltage clamp method. The reversal potential, with 130 mM TMA on all cell surfaces, was -25 mV. Assuming that the extracellular TMA activity is roughly the same as the intracellular K^+ activity, this indicates a channel permeability to TMA about 0.4 that of K^+ (Goldman, 1943; Hodgkin & Katz, 1949). The fact that the permeabilities estimated by ionic current and by reversal potential are not equal suggests that TMA partially blocks the transduction channel (Hille, 1975).

The ability of one divalent ion, Ca^{++}, to pass through the transduction channel was also demonstrated by extracellular recording. With 87 mM $CaCl_2$ in the test solution at the apical surface of the hair cell, the microphonic current was 0.3 that produced by 130 mM K^+. Because its concentration in endolymph is very low, Ca^{++} can carry very little of the receptor current in vivo. Ca^{++} does seem, however, to be a necessary cofactor for the response (Hudspeth & Corey, 1977; Sand, 1975): with a 130-mM K^+ saline, the microphonic current was abolished if the Ca^{++} concentration was reduced below about 10 μM. Sr^{++} replaces Ca^{++} in this role, but Mg^{++} and Ba^{++} do not.

Because the transduction channel in frog saccular hair cells is nonspecific, the transduction current in vivo will be carried by cations approximately in proportion to their concentrations in endolymph. K^+, the predominant ion, will normally carry most of the current. The channel is equally permeable to the other alkali cations, however, and moderately permeable to Ca^{++} and to an organic cation, TMA. As the unhydrated diameter of TMA is 0.54 nm, the channel interior must be at least this large. It therefore resembles the nonspecific, acetylcholine-activated channel of the

motor endplate, which has an internal diameter of at least 0.65 nm (Dwyer et al. 1979).

It remains to be seen whether the transduction channels of all vertebrate hair cells are comparably nonspecific. The fact that Na^+ can support transduction in the goldfish sacculus (Matsuura et al. 1971) suggests that the channels in this organ are also nonspecific. The argument that ions other than K^+ cannot carry transduction current in the mammalian cochlea rests on the observation that substitution of Na^+ for K^+ in cochlear endolymph gradually but irreversibly blocks the response (Konishi et al. 1966). This might, however, reflect secondary effects of Na^+ accumulation on hair cells, such as the metabolic work required to pump this ion out of cells, rather than an inability of Na^+ to carry receptor current into cochlear hair cells. Inasmuch as the hair cells of the lower vertebrates share with those of the cochlea a transduction process operating in high-K^+ fluid, mediated by stereocilia (Hudspeth & Jacobs, 1979), and capable of great speed (Corey & Hudspeth, 1979a), it seems likely that the transduction channel of cochlear hair cells is also nonspecific in its ionic selectivity.

Part II. The structure of the channel

The problems of how ions pass through biological membranes, and how membranes can be selectively permeable to different ions, have been studied for nearly a hundred years (see discusson in Hille, 1975). It is now becoming clear that most ion paths through biological membranes are by way of proteinaceous pores, which provide a polar environment to ease the transition from extracellular water through lipid to intracellular water. Interactions between an ion and the channel, and between an ion and water, are complex: only in the last ten years has our understanding progressed to the point of adequately describing ion flux through some of the simpler biological channels. Some of the more difficult problems, for instance the interactions among ions passing through a channel, are still not adequately understood.

Difficulties are compounded by problems in separating ion permeation through a channel and gating of the channel. The voltage-dependent gating of Na^+ channels, for instance, confuses the study of voltage-dependent ion fluxes; the voltage sensitivity of agonist binding causes similar problems with postsynaptic channels.

For this reason, the transduction channel in vertebrate hair cells is an attractive system for studying ion permeation. Its gating appears to be purely mechanical, activated only by displacement of the hair bundle. The gating is fast as well, occurring at room temperature within 100 μs of a displacement. Thus at all potentials the current through the transduction channel is easily separated from current through other channels, simply by measuring the change in membrane current produced by deflection of the bundle. The channel is also not particularly complex. Like the acetylcholine receptor (AChR) channel at the neuromuscular junction, the hair-cell transduction channel has a large, water-filled pore, and is only moderately selective among small cations. Finally, the geometry of hair cells is favorable, in

that different channel species appear to be segregated between apical and basolateral surfaces, which can have different ionic environments. There are some problems of course with studying hair cells, not least of which is their small size and the consequent difficulty of voltage clamping them.

The problem of ion permeation through the transduction channel is approached here with two types of experiments. One is to find the largest ion species that can pass through the channel, which sets a lower limit for the size of the pore, and thereby suggests the degree of hydration of ions passing through the channel. The other is to measure the voltage dependence of the receptor current. The current-voltage relation is dependent on, and can be used to infer, the positions within the channel of energy barriers to permeation.

The size of the pore

The selectivity of the channel was first investigated with the epithelial preparation. The lower bath was perfused with a normal perilymphatic saline, and the upper bath was perfused with a saline containing the test ion (Table 1). The stimulus was a mechanical displacement to -0.5 μm lasting 1 msec, followed by a step to +1.0 μm for another msec. The difference in current between these two saturating positions was taken as proportional to the current through a single channel. As long as the resting potentials did not change with different apical solutions, the difference was proportional to single channel conductance at a fixed potential.

The results are shown in Fig. 3, which plots measured microphonic current vs. the unhydrated diameter of the ion. The current is plotted relative to the current with K^+ in the upper bath, a control that preceded and followed each test solution. The diameter is either twice the crystal radius, or is measured as the diameter of the smallest cylinder that can contain a Corey-Pauling-Koltun model of the ion.

The alkali cations are nearly equally permeant, having relative currents within 10% of each other. Ammonium ion is 30% more permeant, which is similar to

TABLE 1. Ionic composition of saline solutions used in determining ionic selectivity. Values in mM. The values include small amounts of NaOH or KOH used to titrate the solutions to pH 7.2-7.3. X+ and X++ each indicate one of a number of monovalent or divalent test ions

	for intracellular recording		for microphonic recording			
	Normal Saline	X+ Saline	Normal Endolymph	X+ Endolymph	X++ Endolymph	Normal Perilymph
X+:	-	120.0	-	130.0	-	-
Na^+:	117.4	-	2.5	-	-	119.3
K^+:	3.6	1.7	124.0	0.3	0.3	3.6
X++:	-	-	-	-	87.0	-
Ca^{++}:	4.0	4.0	0.26	0.25	-	1.36
Mg^{++}:	-	-	-	-	-	0.68
Cl^-:	129.0	129.7	127.0	131.0	174.6	127.0
D-glucose:	2.8	2.8	3.0	3.0	3.0	3.0
HEPES:	5.0	5.0	5.0	1.0	1.0	5.0

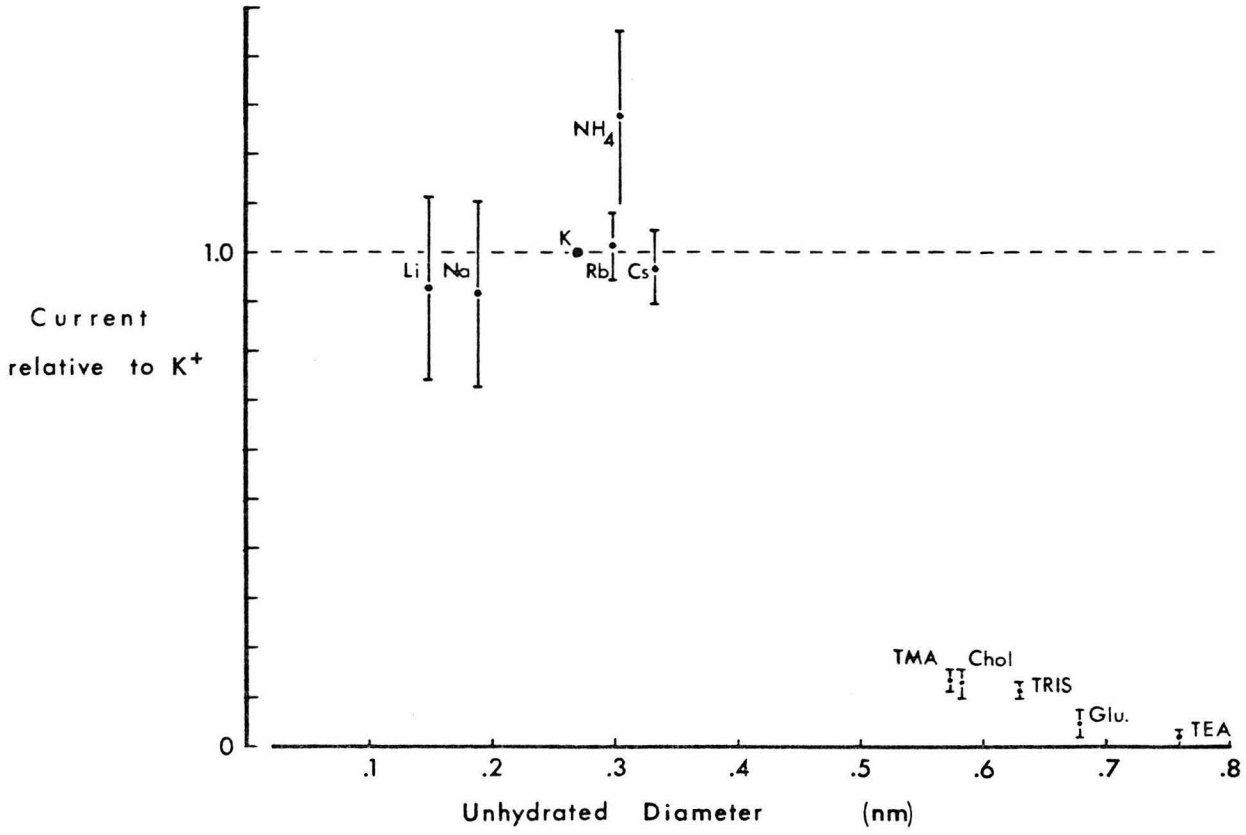

Fig. 3. Permeability of some monovalent cations, relative to K^+. The microphonic current recorded with 130 mM of a test cation in the upper bath is plotted relative to that with 130 mM K^+. The lower bath contained Normal Perilymph for all tests. The unhydrated diameter is twice the crystal radius for the alkali cations, and was measured from CPK models for the organic cations.

its behavior with the AChR channel. Isotonic concentrations of divalent cations (87 mM) also support the microphonic current: not shown in Fig. 3 are Mg^{++} (14% of the K^+ current; 0.13 nm), Ca^{++} (28%; 0.20 nm), and Sr^{++} (48%; 0.22 nm). While the current measured with divalent cations cannot be compared to those with monovalents for a number of reasons, there are distinct trends within each group. For both, the smaller ions (e.g., Mg^{++} and Li^+) carry less current than the larger ones. As the smaller ions have a larger hydrated radius, this suggests that the channel may select largely on the basis of hydrated size. Hydration energies are typically 50-90 kcal/mol; even if only partial dehydration were required for ion passage through the channel, one would expect the energy difference to lead to more than an order of magnitude difference in permeances, rather than the 10% observed.

Another measure of pore size is obtained with small organic cations: the largest ion that carries a detectable current sets a lower limit. With tetramethylammonium ion (TMA; 0.58 nm) in the upper bath (Fig. 3), the microphonic current is 15% that with K^+; choline (13%; 0.58 nm) and TRIS (12%; 0.63 nm) carry about the same current, while piperazine (21%; 0.60 nm) carries a bit more. On the other hand, tetraethylammonium ion (TEA; 0.76 nm) produces a microphonic current that is not significantly different from zero. The largest apparently permeant ion is glucosamine (5%; 0.68 nm), but the permeance of this ion must remain tentative, as the measured current includes an approximate correction for KOH used in buffering the solution.

Thus the cutoff seems to be about 0.65 nm diameter, which is the same as has been measured for the AChR channel (Dwyer et al. 1979). Like the AChR channel, the transduction channel appears to be a large, water-filled pore.

The channel does not discriminate solely on the basis of size, however. Ethanolamine (0.44 nm) and methylamine (0.34 nm) both produce microphonic currents less than 10% that of K^+. If mixed half-and-half with potassium, moreover, the relative currents are considerably less than the 50% expected from the potassium

alone. Thus ethanolamine and methylamine appear to be blocking the channel in the process of passing through, and this suggests an interaction on the basis of more than size. Specifically, they may be binding to an anionic site within the channel. If there were such a site, it would act to exclude passage of anions. Nevertheless, we have no direct evidence for a cationic specificity of the transduction channel.

There are some problems with quantitative interpretation of these experiments. One is simply that the tight junctions are not perfectly tight. A steady diffusion of Na^+ across these junctions from the peribasal space might maintain a significant Na^+ concentration at the apical hair cell surface, and would lead to artifactually high estimates for permeability to organic cations. We suspect that this is not a problem, because the upper bath is large and well-perfused, and the perforated otolithic membrane allows good access of fluids in the upper bath to the apical surface.

On the other hand, diffusion in the other direction may well be a problem. As we saw earlier (Chapter I), if the tight-junction resistance is low, K^+ diffusion from endolymph to the peribasal space is sufficient to depolarize hair cells. Most K^+ channels are moderately permeant to Rb^+ and Cs^+ as well, and these ions would be expected to have qualitatively the same effect. Moreover, the amount of diffusion through tight junctions depends on the ion species (Fig. 4), so the magnitude of the effect is hard to predict. We previously described how voltage-dependent K^+ conductances in the hair-cell membrane influence the waveform of the step response (Chapter I); this understanding in turn provides us with a monitor for changes in membrane potential. In fact, the waveforms of the step response are nearly identical when Li^+, Na^+, K^+, Rb^+, and Cs^+ are in the upper bath, provided that the apparent tight-junction resistance is high. Thus the hair-cell resting potentials with these different ions are probably very similar, and the relative permeabilities measured with the epithelial preparation are reasonably accurate.

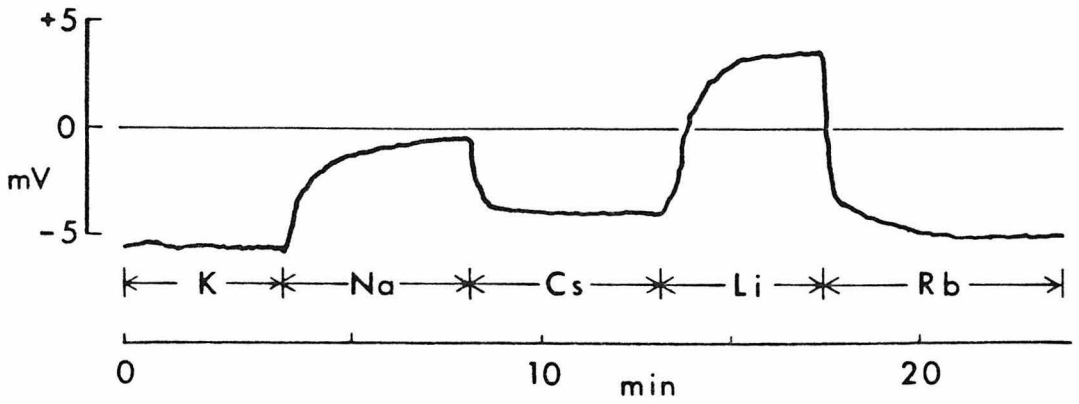

Fig. 4. Ionic selectivity of tight junctions. The transepithelial potential was recorded as a function of time, as the upper bath was perfused with various monovalent cations. The lower bath contained Normal Perilymph, and the epithelium was unclamped and unstimulated. Upwards deflection corresponds to a more positive endosaccular potential; it results from a greater cation flux from bottom to top than top to bottom, and so indicates a less permeant cation in the upper bath. Since the tight junctions dominate the transepithelial resistance, the differences in transepithelial potentials with different cations must reflect a selectivity of the junctional conductance. The order of selectivity is K > Rb > Cs > Na > Li, which is the same as that for bullfrog gallbladder epithelium (Moreno & Diamond, 1975). The magnitude of the potential difference is somewhat less than that for gallbladder, which is to be expected, as the saccular macula is a leakier epithelium.

A more precise measure of permeability is obtained by determining the reversal potential for the receptor current with different ions on each side of the transduction channels. For this measurement, individual hair cells were voltage-clamped with a two-electrode clamp. Hair bundles were stimulated directly with a probe inserted between the kinocilium and the adjacent stereocilia (Fig. 5), and the receptor current was measured as the change in clamp current elicited by a saturating displacement of the bundle.

As discussed in Part I, the reversal potential with Normal Saline (117.4 Na^+, 3.6 K^+; Table 1) on all cell surfaces is near zero. The cytoplasm almost certainly has high K^+ and low Na^+ concentrations, and we concluded that the permeability for Na^+ is near that for K^+.

At this point, it is worth taking a moment to discuss what is meant by 'permeability.' With the Goldman-Hodgkin-Katz (GHK) equation for ion permeation (Goldman, 1943; Hodgkin & Katz, 1949), the current through a channel is proportional to the permeability (P_i) of the channel to an ion and to the concentration (C_i) of the ion. With different ions (n and k) on each side of a membrane, the current is zero at a reversal potential of

$$V_r = \frac{RT}{zF} \ln \frac{C_n P_n}{C_k P_k}$$

where the permeability $$P_i = \frac{\beta \mu RT}{z F}.$$

R, T, z, F are as usual, β is a partition coefficient into the membrane, and μ is a mobility related to the diffusion constant. Similarly, for the single-barrier model (e.g., Corey, 1979) the current is proportional to the product of concentration and permeability, the expression for reversal potential is the same, but the permeability is

$$P_i \propto e^{-G_i/RT}$$

where G_i is the height of the energy barrier to permeation seen by ion i. Other

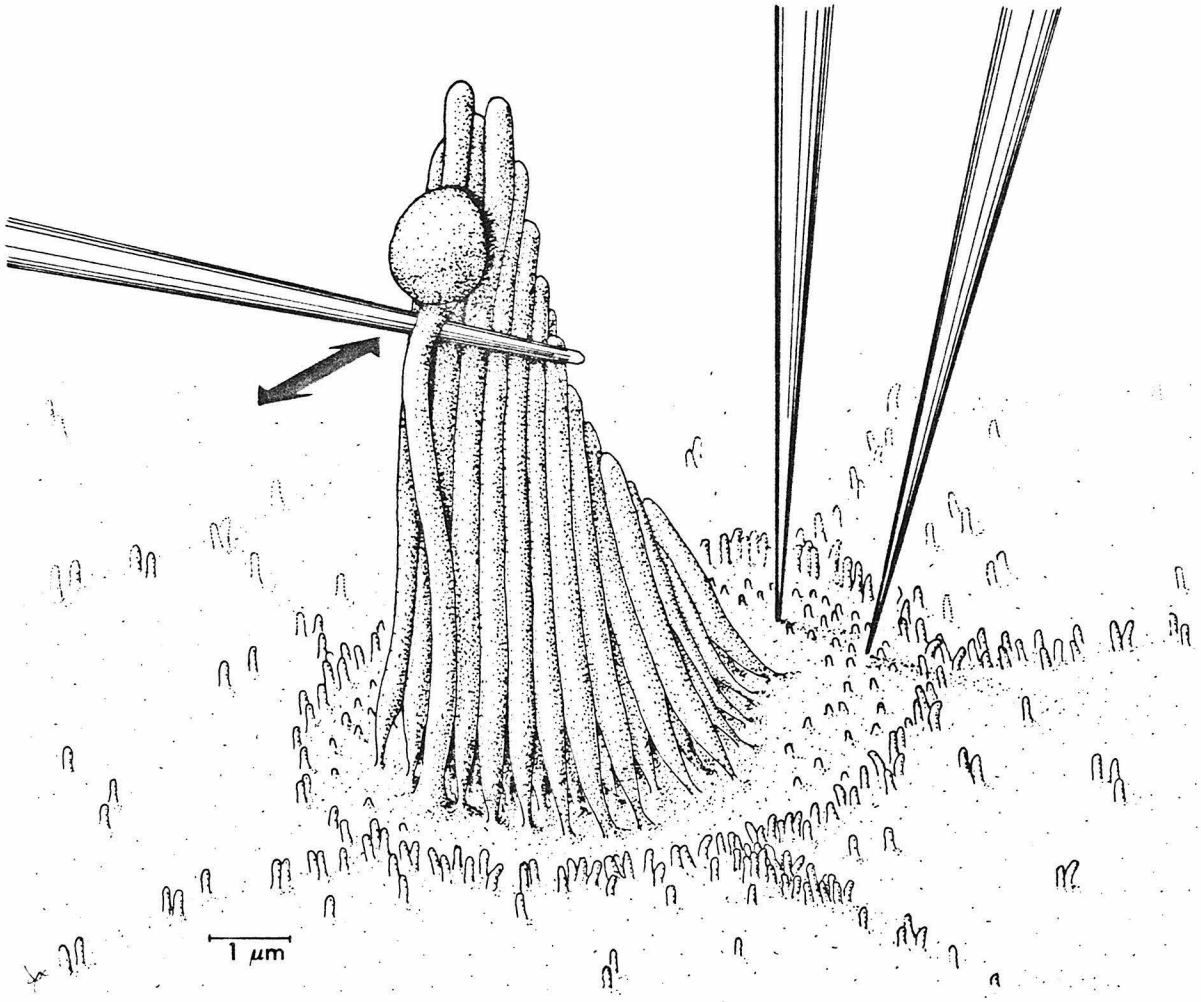

Fig. 5. Schematic of the intracellular voltage-clamp arrangement. The apical surfaces of one hair cell and several supporting cells are shown; the boundary of the hair cell surface is identifiable by a greater density of microvilli. Two glass microelectrodes, one for measuring potential and the other for passing current, penetrate the apical hair cell surface on the edge opposite the kinocilium. A blunt-tipped stimulus probe is laterally inserted between the kinocilium and the adjacent stereocilia, and moved in the horizontal plane as indicated by the arrow. The bulb of the kinocilium is attached to the adjacent stereocilia with filamentous strands, so displacement of the probe can move the bundle to saturation in both directions.

formulations that assume independence of ion movement give a similar result, but calculate the permeability in other ways. These formulations imply that permeability can be measured either by measuring the change in current with concentration, at a fixed potential, or by measuring the reversal potential at a fixed concentration.

In practice, the two approaches often give very different values for permeability. One reason is that for most theories of permeation, permeability is a function of potential (the GHK is an exception). Thus the permeability determined by measuring current is different from that determined by changing the potential to measure the reversal potential. Another, more significant, problem concerns the assumption of ion independence. If, for instance, an ion resides within a channel for some time while passing through, then this closes the channel to passage by other ions and reduces the measured current. Ion fluxes are then not independent; the ion is said to be a partial blocker. Ionic interaction is significant even for a simple channel like the AChR channel (Lewis & Stevens, 1979); it presumably is as well for the transduction channel. While ionic interaction reduces measured currents, the reversal potential (in the simpler models) is unaffected. One has greater faith, then, in permeabilities calculated from the intracellular reversal potential than from the epithelial microphonic current.

The most reliable value for reversal potential with Normal Saline on the outside is $+4\pm3$ mV (N=22). (This is higher than our published value of -2 ± 4 mV, because the earlier measurements did not include a correction for slow electrode drift.) The implication is that the product of concentration and permeability for Na^+ is $e^{4mV/25.4mV} = 1.17$ times that for the intracellular K^+. Of course the intracellular K^+ concentration is not known, and there is no correction for the extracellular Ca^{++}. Thus quantitative comparison among permeant ions must be made by comparing the different reversal potentials measured with each ion on the outside.

Only two alkali cations, Li^+ and Na^+, have been measured in this way to date. The reversal potential with Na^+ saline was 0 ± 4 mV (N=13); with Li^+ it was $+5\pm5$ mV (N=5). The scatter is a significant problem; it occurs primarily among cells, and not among measurements from an individual cell. It is illustrated by noting the difference between the measured reversal potential for Na^+ saline (0 mV) and the measured reversal potential for Normal Saline (4 mV) which is virtually identical to Na^+ saline. The difference can only be experimental variation. At best, these measurements confirm that the permeabilities for Li^+ and Na^+ are within about 25% of each other.

The reversal potential is more useful in detecting the partial blocking effect of moderately permeant cations. Measured by microphonic current, TMA had a permeability relative to K^+ of 15%. Measured intracellularly, the average receptor current at -60 mV was again only 23% that of Na^+. But the reversal potential with TMA saline is -11 ± 4 mV (N=9), indicating a permeability 55% that of Na^+. Similarly, carbamylcholine (0.59 nm diam.) carried a receptor current that was 22% of the K^+ control, but its reversal potential of -15 ± 5 mV (N=8) indicates a relative permeability of 47%. Quite clearly, TMA and carbamylcholine pass through the channel, and the results from the epithelial preparation are not artifacts of leakage. They are also clearly acting as partial blockers. We will return to the matter of blockage in considering the shape of the pore.

The interior of the pore

While reversal potential experiments give a reasonably convincing lower limit for the dimensions of the pore, they provide little insight into the physical-chemical processes that limit ion passage through the channel. Biological channels are more than simple holes: permeation must involve specific interactions between an ion and the channel and between an ion and water. The contemporary theoretical approach is to assume that an ion experiences a variation in electrochemical potential

as it passes through a channel. The potential depends on factors such as the energy of stripping a hydration shell in order to pass by 'tight spots,' the energy of binding to sites within the channel, and the difference in electrical potential caused by the voltage across the membrane. Each combination of ion and channel has a potential profile, expressing the electrochemical potential as a function of the position of the ion along the pore.

There are two mathematical ways of treating passage along the potential profile. The Nernst-Planck theory is a continuous diffusion theory; it integrates an exponential function of the chemical potential to get the permeability (see, for example, Lauger & Neumcke, 1975). The Goldman-Hodgkin-Katz equation is a simple example of the Nernst-Planck formulation in which a single-valued chemical potential is assumed. The other mathematical approach to permeation is reaction-rate theory (Eyring et al. 1949), which simplifies the potential profile to consider only the rate-limiting peaks and significant wells, and calculates the flux from the rate of transitions over the peaks. It is mathematically more tractable than the Nernst-Planck theory and is rapidly becoming the preferred approach. The expressions for a simple two-barrier model are developed in the Appendix to this chapter. Both approaches can predict the current through the channel as a function of membrane potential, and both can predict effects such as interaction between ions and voltage-sensitive blockage of channels.

In practice, of course, the electrochemical potential profile is not known; instead, the behavior of the channel is used to infer a profile. The ultimate goal is to correlate the structures of channels, when they become known, with the apparent electrochemical profiles, as they become sufficiently detailed. In the meantime, the barrier model provides a useful conceptual framework for studying ion permeation; specific channel models, although only inferred, are nevertheless of predictive value.

The experimental data with which we begin to infer a channel structure are shown in Fig. 6, which plots receptor current as a function of voltage (the I-V relation). The data were measured as in Fig. 2a, but over a wider range of membrane potentials. As in Fig. 2b, the receptor currents at various test potentials were measured relative to receptor currents at the holding potential of -60 mV; these were in turn normalized to -100 pA. The line through the data was calculated for two barriers of equal height, positioned at 24% and 71% of the (electrical) distance through the membrane, from outside to inside. While a channel model comprising these two barriers provides an adequate explanation for the data, a number of other explanations must be considered.

The shape of the I-V relation might reflect a voltage-dependent activation of channels, rather than the I-V relation of fully-activated channels. This possibility is partially tested by looking at the effect of membrane potential on the displacement-response curve. In Fig. 7, the membrane potential is changed by 160 mV, but the proportional change in the receptor current with displacement is not significantly changed. If there is a voltage sensitivity to channel activation, it is not part of the mechanical sensitivity, but occurs in series with the mechanical activation. The receptor current also does not show a time dependence, at least over the 100 msec between peaks, so that any voltage-sensitive activation occurs on the order of a few tens of milliseconds. We think such activation is unlikely, but cannot rule it out.

The I-V relation of Fig. 6 is a combination of two I-V relations: that for Na^+ entering the cell and that for K^+ leaving the cell. The inward current is primarily determined by the outer barrier in the Na^+/channel profile, and the outward current by the inner barrier in the K^+/channel profile. Until an I-V relation can be measured with a single species on both sides of the channel, we must invoke the lack of selectivity among alkali cations and assume that the profiles are nearly the same for all alkali cations.

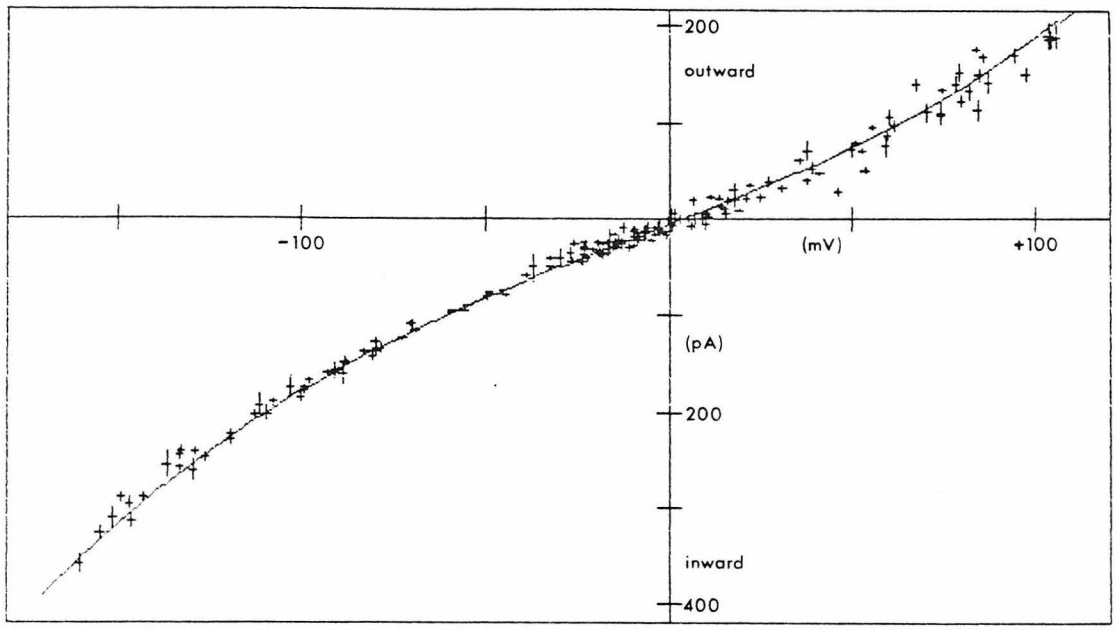

Fig. 6. I-V relation for the transduction channel in Normal Saline. Receptor current is measured as the change in membrane current with supersaturating displacements of the hair bundle, and normalized so that the receptor current at the holding potential of -60 mV is -100 pA. The responses of 8 to 20 presentations of each trial voltage were digitally averaged, and 5 to 9 peak-to-peak current values measured for each trial. The data are plotted as the average $\pm$1.5 x S.E. of these values. Shown are 174 trials from 63 cells. The smooth line through the data was calculated from a model with two barriers and no well. Barriers were of equal height and spaced at .24 and .71 of the electrical distance through the membrane from the outside. Equally good fits, judged by eye, were obtained with the outer barrier lower by 0.5 kcal/mol, and the barriers positioned more towards the outer edge of the membrane, or with the inner barrier lower by 0.5 kcal/mol and the barriers towards the inner edge. This application of the model assumes that Na^+ and K^+ see the same barriers, and that the difference in height between them is the same.

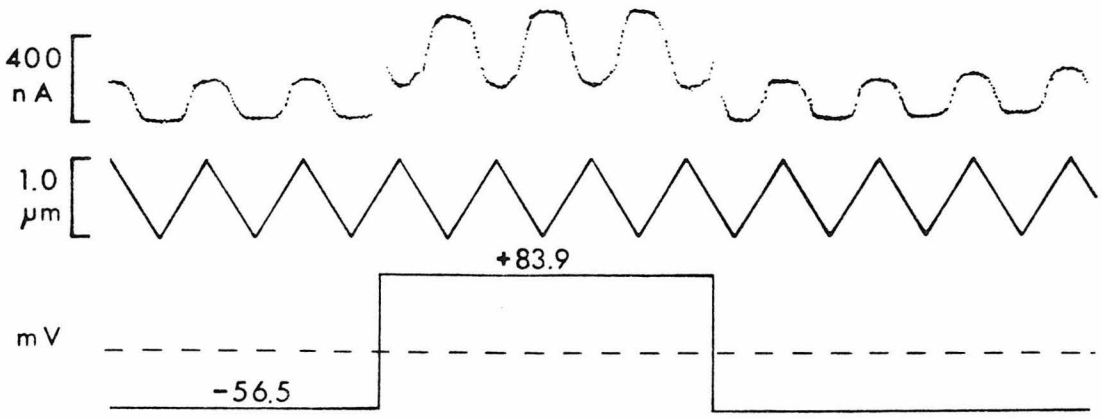

Fig. 7. Voltage insensitivity of the displacement-response curve. The membrane current (top) is shown vs. time, as the bundle is swept linearly through the operating range by the triangle-wave stimulus (middle). The current thereby shows the displacement-response curve, twice in each cycle of the stimulus. The shape of the displacement-response curve does not change perceptibly when the membrane potential is changed from -57 mV to +84 mV (bottom), but the response polarity reverses when the membrane potential is above the reversal potential.

The calculated curve of Fig. 6 is not a unique fit; in fact, a range of barrier models provides a good fit by eye. The characteristics common to good fits are that the barrier heights do not differ by more than 0.5 kcal/mol, and that the positions of outer and inner barriers range from .20 and .65 to .26 and .80. (The outer barrier is better defined, since it regulates the inward current for which we have more data.) For all acceptable fits, the barrier density is more towards the middle of the pore than its edges, and more towards the outer edge than the inner.

The two-barrier model developed in Appendix A neglects the effects of membrane surface charge. The negative charge on most biological membranes produces a negative surface potential of as much as 100 mV, a potential that is not measurable by microelectrodes but that is felt by ions near the membrane. The negative surface potential has two physical effects: it changes the real voltage drop experienced by proteins and ions within the membrane, and it causes accumulation of cations (and depletion of anions) near the membrane surface. Ion concentrations are increased 10-fold for each -58 mV of surface potential for monovalent cations, and 100-fold for divalent cations. These physical effects in turn have two effects on the I-V relation: the current is increased at all potentials, increasing the overall conductivity of the channel, and the increase is greater for inward current, causing an inward rectification. The only way to detect a negative surface charge in practice is to screen some of the charge by increasing the divalent cation concentration, and then to see whether the effects of the concentration change are quantitatively consistent with a reasonable value for surface charge. We have not done this, because lowering Ca^{++} concentration makes hair cells difficult to penetrate, and because Ca^{++} has other effects on transduction that are not yet quantifiable. If there were a negative surface charge, the barrier model would have to be modified by a constant scaling factor (which the plot already incorporates) and by raising the barrier heights. For a surface potential of V_s volts, equivalent to an energy

difference of $\kappa z F V_s$ kcal/mol, a barrier at position δ must be increased by

$$G = (1-\delta)\kappa z F V_s.$$

If the surface potential were -50 mV, for instance, the outer barrier of the model of Fig. 6 ($\delta = .24$) would be increased by 0.88 kcal/mol and the inner barrier ($\delta = .71$) by 0.33 kcal/mol, to maintain a good fit.

The model developed in Appendix A neglects ionic interaction. Some small organic cations quite clearly act as partial blockers; the alkali cations might also, to a lesser extent. If the block were relieved at large positive or negative potentials, then the I-V relation would curve supralinearly at the extremes as the number of free channels increased. Appendix B extends the two-barrier model to include a binding site (a potential-energy well) between the barriers, and different potential profiles for two different ionic species. A peculiar feature of the extended model is that, for the barrier positions of Fig. 6, the I-V relation is virtually unaffected by inclusion of a well in the middle of the pore ($\delta_2 = 0.5$). The currents decrease uniformly as the channel is blocked, but the I-V shape does not change. However, addition of a well can make other barrier models produce that same I-V relation, whether the barriers are positioned towards the edges of the membrane or towards the middle! The extended theory does allow a good fit to the I-V relation for TMA on the outside. The barriers for TMA are raised by 0.35 kcal/mol to fit the reversal potential, a well of -4.4 kcal/mol is included to model the partial blockage, and the well is positioned at $\delta = .26$ to fit the shape of the I-V relation. The extended model thereby accounts for the I-V relation with Na^+, Li^+, or TMA on the outside. It is not too surprising that the model fits these data well, since it has 12 free parameters (energy and positions for two barriers and a well, for two ions). We are left, in fact, with a theory which is powerful enough to describe reversal potentials, current-voltage relations, and the partial blocking effect seen with some ions, yet so versatile that we have virtually no confidence in a model that fits the data.

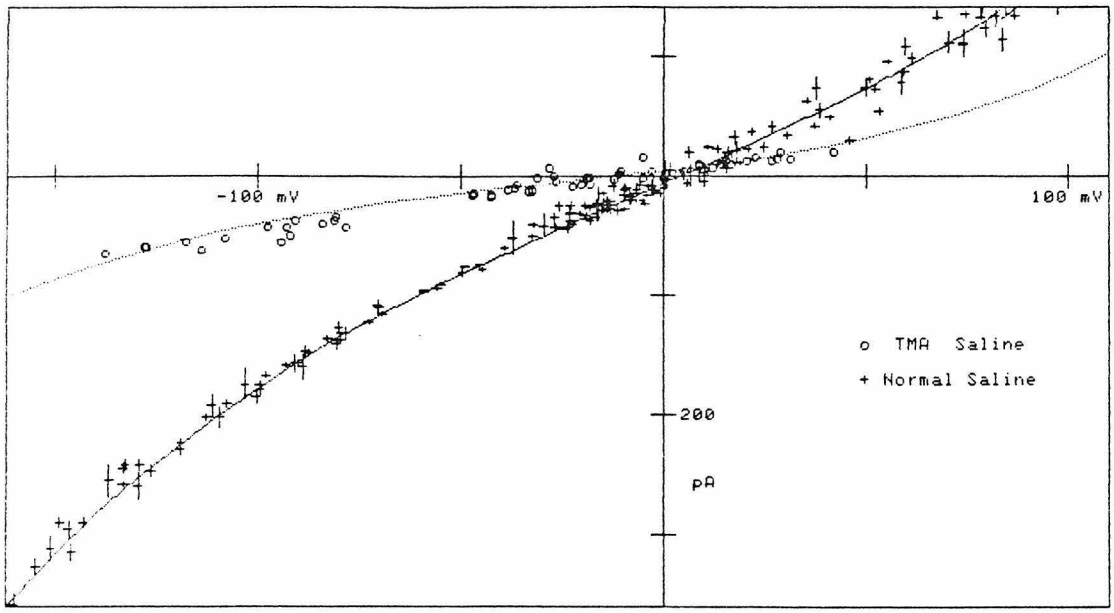

Fig. 8. I-V relations for the transduction channel in Normal Saline and in TMA saline. The data with Normal Saline are reproduced from Fig. 6, along with the calculated curve. The TMA data are fitted by supposing that TMA sees the same barriers as K^+ and Na^+, except that they are 0.35 kcal/mol higher for TMA, and that TMA also sees a well of -4.4 kcal/mol at a position just inside of the outer barrier.

SUMMARY

The transduction channel of vertebrate hair cells is permeable to all alkali cations, to at least some of the divalent alkaline earth metals, and to many small organic cations. The permeability to anions is not clear. The channel constitutes a large, water-filled pore, of at least 0.65 nm diameter, which appears to contain a binding site for permeant organic cations. The distribution of energy barriers within the pore is not known with any confidence.

Certain ambiguities in interpretation of the existing data can be resolved by additional experiments:

Reducing the concentration of permeant ions tests for ionic interaction. Specifically, the shape of the I-V relation when part of the Na^+ in Normal Saline is replaced with sucrose would indicate whether alkali cations also see a well of significant depth within the pore. If there is no well, the two-barrier model of Fig. 6 assumes considerably more credibility.

The existence of surface charge is tested by altering cation concentrations in the saline. Increasing Ca^{++} concentration should reduce the receptor current (which it does, in fact, in the epithelial preparation), and should alter the I-V relation to become more outwardly rectifying. From these changes, the magnitude of the surface charge should be estimable; once known, it can be included in the model.

The equivalence of the potential profiles for the alkali cations is tested by measuring each I-V relation with the same ion on both sides of the membrane. For the moment, this can only be done for K^+, and the experiment requires a two-electrode intracellular voltage clamp with apical and basal surfaces separately superfused. Other methods may soon become available that would make the experiment technically less formidable.

Measurement of single-channel conductance through fluctuation analysis tests for the hypothetical voltage-dependent activation of channels. If the I-V re-

lation for single-channel conductance is the same as that for total receptor current, there is no such activation. The noise level of the clamp electrodes is not low enough to do this experiment.

Finally, we must test the major assumption of this work: that the conductance change results from the opening of discrete membrane channels. Direct observation of unitary channel currents would provide the most convincing confirmation.

APPENDIX TO CHAPTER II

A. Without ionic interaction

The mathematics for a two-barrier, single-site model are developed here. While such a model allows for ionic interaction and voltage-sensitive blockage, I will assume initially that the probability of the site being occupied is negligible, and thus that ion fluxes are independent.

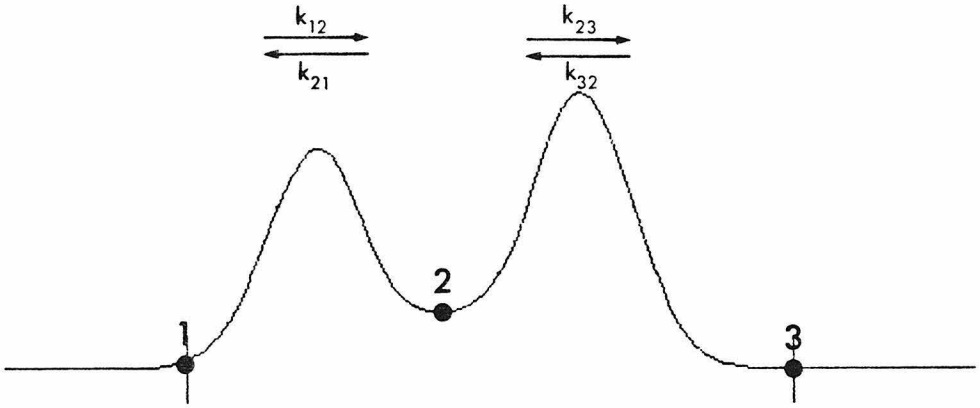

Four rate constants describe the ionic fluxes with this model: k_{12}, k_{21}, k_{23}, and k_{32}. The flux from 1 to 2 depends on the rate constant k_{12} and the number of ions in state 1, N_1:

$$J = N_1 k_{12}$$

The net fluxes are $$J_{12} = N_1 k_{12} - N_2 k_{21}$$

$$J_{23} = N_2 k_{23} - N_3 k_{32}.$$

At steady state, the channels are neither accumulating ions nor being depleted, so the fluxes are equal:

$$J_{12} = J_{23}$$

and this permits the solution

$$J_{13} = \frac{k_{12}k_{23}N_1 - k_{21}k_{32}N_3}{k_{23} + k_{21}} \quad .$$

The N's are numbers of ions in states 1 and 3, but these states are just the outside and inside solutions. The N's are replaced by a "surface concentration," in units of #/area; with an estimate of channels/area, this gives flux/area. As channels/area is rarely known, the conversion in fact simply adds a scaling factor, c:

$$N_1 = cC_1$$

where C_1 is the activity of the ion at the membrane surface.

The flux J_{13} is in ions/sec, which is related to electrical current by

$$I = \frac{-zF}{N_A} J_{13}$$

where z is the ionic charge, F is the Faraday, and N_A is Avogadro's Number. The sign is inverted to maintain the convention of positive (outward) current for a positive intracellular potential, V_m. So

$$I = \frac{-zFc}{N_A} \left[\frac{k_{12}k_{23}D_1 - k_{21}k_{32}C_3}{k_{23} + k_{21}}\right]. \qquad (1a)$$

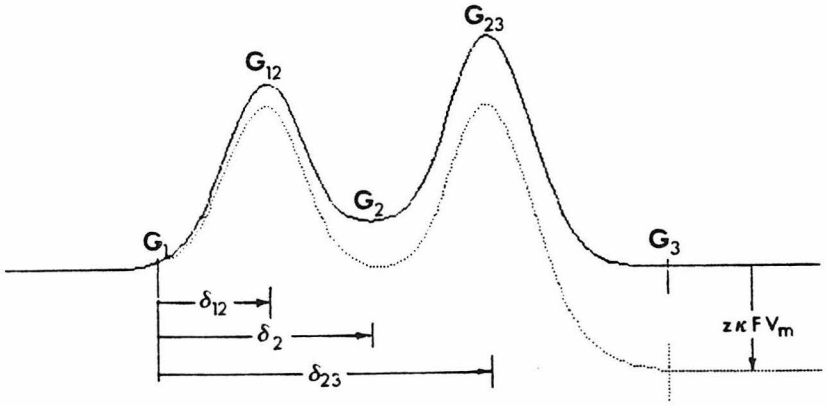

Each rate constant k_{ij} for transition over a barrier depends exponentially on the energy difference between the barrier height and the site:

$$k_{ij} = f\, e^{-(G_{ij} - G_i)/RT} \tag{1b}$$

where G_{ij} is the electrochemical potential at the peak of the barrier, G_i is the electrochemical potential of the ion at the site i, f is equal to or slightly less than $kT/h = 6 \times 10^{12}$ sec^{-1}, and R and T have their usual thermodynamic meanings so that RT = 0.586 kcal/mol at 22°C. If an electrical potential V_m exists across the membrane, then the energy of the ion in the field is added to the energies of barriers and sites:

$$G = z\kappa FV$$

where z is the ionic charge, F is the Faraday, κ converts from joules/mol to kcal/mol and is equal to 2.39×10^{-4} kcal/J, and V is the proportion of the membrane potential V_m felt by an ion at a site. The position of the site in the membrane is given by δ, where δ represents a unitless electrical distance from outside to inside which varies from 0 to 1.0. Only if the potential drops linearly across the membrane—if the field is constant—is δ directly proportional to physical distance.

Thus

$$V = \delta V_m$$

and

$$\Delta G = \delta z\kappa FV_m$$

so

$$G_{ij} = G_{ij} + \delta_{ij}\, z\kappa FV_m \tag{1c}$$

These three equations (1a,b,c) then describe transmembrane current as a function of membrane potential. They can be combined, if $G_1 = 0$, to give

$$I = \frac{-zFc}{N_A}\left[\frac{C_1 - C_3\, e^{\kappa zFV_m/RT}}{e^{G_{12}/RT} + e^{G_{23}/RT}}\right]$$

where, again

$$G_{ij} = G_{ij} + \delta_{ij}\, z\kappa FV_m$$

B. With ionic interaction

The derivation of Appendix A made use of certain simplifications that occur when channels are always empty. This situation occurs when there is not a high affinity of some ion for a site in the channel, which is equivalent to saying that there is not a deep well in the potential profile for that ion. The theory can be extended to include a finite residence time, by supposing that an ion at a site in the channel closes that channel to other ions. It does not assume, however, that other ions can induce the resident ion to leave the channel, and so is not of a class of "knock-on" permeation theories. The mathematics is a simplification of that of Lewis & Stevens (1979) which in turn is an extension of that of Woodhull (1973).

Again, four rate constants describe flux of an ionic species through a channel. Here, however, the rate constants differ in form to express the difference between a concentration-dependent flux into the channel, and a simple probability for leaving the channel:

$$k_{12} = [k]_0 f_2 \, e^{-(G'_{12} - G'_1)/RT}$$

$$k_{32} = [k]_i f_2 \, e^{-(G'_{23} - G'_3)/RT}$$

$$k_{21} = f_1 \, e^{-(G'_{12} - G'_2)/RT}$$

$$k_{23} = f_1 \, e^{-(G'_{23} - G'_2)/RT}$$

where each $G'_{ij} = G_{ij} + \delta_{ij} z\kappa F V_m$.

$[k]_i$ and $[k]_0$ are concentrations of ion k outside (state 1) and inside (state 3) the membrane, $f_1 = 6 \times 10^{12}$ sec^{-1} and $f_2 = 1 \times 10^{11}$ sec^{-1} molar^{-1}. A duplicate set of equations describes fluxes of an ion n with rate constants n_{12}, n_{32}, n_{21} and n_{23}. The valencies of ions k and n are assumed to be equal.

At any time, there is a probability P_0 that a channel is empty, a probability P_k that it has an ion k at state 2, and a probability P_n that it has an ion n at state 2.

Then

$$P_0 + P_k + P_n = 1.$$

At steady state, we can also write

$$P_0(k_{12} + k_{32}) = P_k(k_{21} + k_{23})$$

and

$$P_0(n_{12} + n_{32}) = P_n(n_{21} + n_{23}),$$

and these can be solved to get

$$P_0 = \frac{1}{1 + \left(\frac{k_{12} + k_{32}}{k_{21} + k_{23}}\right) + \left(\frac{n_{12} + n_{32}}{n_{21} + n_{23}}\right)}.$$

The net flux of all ions is

$$J = k_{12}P_0 - k_{21}P_k + n_{12}P_0 - n_{21}P_n$$

and the current is

$$I = -zFJ$$

so

$$I = zF\,\frac{k_{12}-k_{21}\left[\frac{k_{12}+k_{32}}{k_{21}+k_{23}}\right] + n_{12}-n_{21}\left[\frac{n_{12}+n_{32}}{n_{21}+n_{23}}\right]}{1 + \left[\frac{k_{12}+k_{32}}{k_{21}+k_{23}}\right] + \left[\frac{n_{12}+n_{23}}{n_{21}+n_{23}}\right]},$$

with the k's and n's defined as above.

There are several qualitative results of this expression that are of interest. First, it gives the same results as the expression of Appendix A when the well is not deep, and this in practice means not deeper than about -2 kcal/mol. Second, when the barriers are of equal height, the rate-limiting transition for inward current is normally 1 → 2. When the well is made deep, the transition 2 → 3 becomes rate-limiting. Similarly, for outward current 3 → 2 is normally rate-limiting but 2 → 1 becomes rate-limiting with a deep well. If the voltage dependence of 1 → 2 is the

same as that of 2 → 3, and if the voltage dependence of 3 → 2 is the same as that of 2 → 1, then the shape of the current-voltage relation does not change when the well is made deeper: the current simply decreases in magnitude. This condition is met when the well is in the middle of the channel ($\delta_2 = 0.5$) and the barriers are half a membrane-width apart ($\delta_{23} - \delta_{12} = 0.5$). Third, if the δ's = 0.5 condition is not met, then the shape is radically changed when a well is added. The general rule is again that the transitions 2 → 1 and 2 → 3 become rate-limiting, instead of 1 → 2 and 3 → 2. A well in the middle can make the sublinear I-V relation for barriers near the edges look like the supralinear I-V relation for barriers near the middle, and vice versa; an asymmetrically placed well can make barriers near the outer edge look like barriers near the inner edge. Finally, this expression for current has 12 free parameters. If a fit to experimenal data is to be taken seriously, then the data must come from a wide range of experimental conditions, with variations in both concentrations and membrane potential.

Chapter III

ADAPTIVE SHIFT OF THE OPERATING CURVE

PREFACE

The adaptive shift of the operating curve was seen, but not recognized as such, in our earliest intracellular experiments. The probe, or the cell—it was not clear which—would drift out of range and had to be repositioned. By the time that I understood the epithelial preparation well enough to know that the decline in the microphonic current following a step displacement was not artifact, Jim had realized that the operating range of a single hair cell shifted if its hair bundle was displaced and held. The adaptation that I saw, which I thought was a Ca^{++}-dependent inactivation, was faster and so was called 'fast adaptation;' the drift seen with intracellular experiments was termed 'slow adaptation.' When I finally did the appropriate experiment (mapping the instantaneous displacement-response curve) and found that fast inactivation was really an adaptive shift, it became clear that the two phenomena reflected the same process examined over different temporal ranges.

The epithelial preparation was the better one for studying effects of temperature and of divalent cations: the two baths permitted different saline solutions on the apical and basal surfaces, and the better noise and temporal resolution enabled measurement of the instantaneous displacement-response curve. Nevertheless, quantitatively plotting the adaptive shift of curves is extremely tedious, as it requires hundreds of stimulus presentations to get the timecourse of the shift with a single step stimulus. Ruth Anne Eatock worked together with me on all the experiments in which the shift was quantitatively measured, and is presently studying the adaptive shift with intracellular recording.

INTRODUCTION

The eye can detect differences in light intensity over a range of 10^9. The sensitivity of the ear spans an amplitude range of 10^7. Yet for most sensory modalities, we are relatively insensitive to the absolute value of the stimulus, compared to our extraordinary perception of changes: at rest we do not feel the clothes on our skin, but easily detect the landing of an insect thereon.

While the notion that sensory systems adapt to maintained stimuli is very old, the localization of at least part of the adaptation to sensory receptors is more recent, and dates from the advent of sufficiently sensitive recording techniques. Adrian (1928), having shown that the intensity of a sensory stimulus was coded by the frequency of nerve firing, further noted a gradual decline in the firing rate during a steady stimulus. The phenomenon differed in timecourse among various receptors, including muscle spindles, light touch and pain receptors, and photoreceptors, but was similar in character among these receptors, and in each case approximately duplicated the decline in perception of the stimulus.

The particular mechanisms of sensory adaptation are as varied as the stimuli to which the receptors are tuned. Adaptation can occur by attenuation of a physical stimulus before it reaches the receptor per se: constriction of the pupil of the eye, contraction of the tensor tympani and stapedius muscles in the ear, and migration of pigment granules in some invertebrate photoreceptors are examples. In photoreceptors, bright lights reduce the probability of a quantum capture by bleaching visual pigment; even when pigment bleaching is negligible, other adaptation mechanisms reduce the response to each quantum capture (Dowling, 1963; Dodge et al. 1968; Baylor et al. 1979). The reduction is caused by increased cytoplasmic calcium concentration in Limulus (Lisman & Brown, 1972; Brown et al. 1977), in squid (Pinto & Brown, 1977), and probably in most other invertebrate photoreceptors. In the vertebrates, however, photoreceptor adaptation is probably not mediated by Ca^{++}

(Bastian & Fain, 1979), but is caused by or at least correlated with a drop in cGMP levels (Hubbell & Bownds, 1979; Kilbride & Ebrey, 1979). There are also adaptive processes that occur after the generation of the receptor potential in photoreceptors, and before the initiation of spikes in ganglion cells (Baylor & Fettiplace, 1977). These may reflect synaptic fatigue or time-dependent conductances in bipolar and ganglion cells.

Adaptation in some other sensory receptors is not so well understood. Olfactory receptors in the salamander adapt over seconds to maintained concentrations of odourants (Getchell & Shepherd, 1978), but the adaptation could occur at the membrane receptor site, as a consequence of membrane conductance changes, or in spike initiation.

Mechanoreceptors display a similar redundancy in adaptive mechanisms. In Pacinian corpuscles, for instance, displacement is transferred to the sensory ending by fluid-filled lamellae. Lamellae relax within milliseconds following a displacement, causing a rapid decline in the receptor potential. The receptor potential is considerably prolonged if the lamellae are removed and the ending stimulated directly, but then a fatigue in spike initiation becomes apparent which dominates the adaptation (Mendelson & Lowenstein, 1964). Crayfish stretch receptors occur as two types: slow and fast adapting. The receptor potential for both shows a decline following stretch which corresponds to mechanical relaxation of the muscle. In fact, the receptor potential for both is identical; the difference in adaptation rates occurs in an additional adaptation in spike initiation (Nakajima & Onodera, 1969).

In some mechanoreceptors, adaptation occurs that cannot be clearly ascribed to mechanical relaxation or to spike initiation. The reptilian short-capsule muscle spindle adapts rapidly following a maintained stretch. High-speed microcinematography fails to demonstrate the relaxation of any structures around the sensory nerve endings, and the spike generation mechanism shows no decline with

steady applied currents. It may be that ion conductances in the cell membrane cause a decline in the receptor potential, or perhaps there is mechanical relaxation at a scale below that resolvable with light microscopy. At some scale, of course, cellular mechanics is not separable from the chemistry of structural proteins.

The vertebrate hair cell, the most elaborate of the mechanoreceptors, also shows a decline in its receptor potential following maintained displacements of the hair bundle. As we shall show in this chapter, the decline acts like a mechanical relaxation, in that the operating or displacement-response curve shifts uniformly along the displacement axis with time. However, the relaxation occurs wholly within the hair cell, somewhere between displacement of the stereocilia and the communication of that bias to the transduction element. Moreover, the rate is sensitive to the intracellular Ca^{++} concentration. The adaptive shift in hair cells thus has both mechanical and biochemical characteristics. Like the transduction process itself, it appears to occur at a level where the mechanics and the biochemistry are not separable.

METHODS

Preparation

The epithelial preparation was used for the great majority of experiments, and in all of these the otolithic membrane was peeled back to leave a single homogeneous patch of cells in the periphery of the macula. For one experiment, single cells were stimulated while their membrane potentials were held constant with a two-electrode voltage clamp.

Solutions

Either Normal Perilymph or High-K^+ Perilymph was used with the epithelial preparation. The upper bath contained Normal Endolymph or contained a K^+ Endolymph with varied divalent cation concentration and with K^+ concentration varied to maintain a constant ionic strength. The size of the microphonic response was somewhat diminished with higher Ca^{++} concentrations (2-10 mM) in the endolymph; this could be a result of the reduced K^+, a partial blocking action of Ca^{++}, or screening of surface charge.

Terminology

Operating curve is synonymous with displacement-response curve, but is used here for historical reasons. The operating range is the extent, in micrometers of hair bundle displacement, of the sensitive (nonsaturated) region of the operating curve.

Recording and stimulation

The epithelial and intracellular recording methods were as previously described. All records from the epithelial preparation show microphonic current with an uncompensated voltage clamp.

Stimuli with the epithelial preparation usually consisted of an adapting step of 100 msec duration and 0.5 μm amplitude and a test step to another level between about -0.5 and +1.0 μm, occurring at some time during the adapting step. A set of

test steps to various levels was used to map the operating range at a point in time, to generate an 'instantaneous' operating curve. Only one test step occurred with each adapting step, so a set is a composite of many adapting and test step pairs, presented at a rate of 1/sec. While tedious and subject to slow drift in the response, this is the most reliable way to measure the shift in the operating curve during maintained displacement. The waveform in response to a single step displacement can give a qualitative indication of the rate of shift, but it includes time-dependent changes not related to the adaptive shift, and it is not, in any case, linear with the position of the operating curve.

Fitting of operating curves

Averaged responses to test steps were photographed from an oscilloscope during the experiment; later, the amplitudes were measured from film and plotted vs. displacement to produce instantaneous operating curves for various times during the adapting step. A master curve, generated with 16 test steps, was fitted to the instantaneous operating curve by linear translation and compression. Vertical compression—along the current axis—allowed for the change in driving force during the stimulus step; vertical shift allowed for the change in baseline. These two operations were not needed when the membrane potential was held nearly constant with high-K^+ in the lower bath. The horizontal shift—along the displacement axis—then indicated the shift of the operating curve. No horizontal expansion or compression was needed; that it was not is one of the principal findings of this study.

RESULTS

When the membrane potential of hair cells in the epithelial preparation is held nearly constant with high K^+ in the lower bath, the microphonic response to a step displacement shows a sag or decline following the initial peak (Fig. 1). It was argued in Chapter I that this resulted from a shift of the operating curve, such that the bias on the transduction element relaxes during the step. In Part I, this argument is examined in more detail; Part II describes the properties of the adaptive shift.

Part I. Location of the adaptive feedback

The experimental stimulus that is applied to the saccular macula is displacement of the stimulus probe. The measured response is the transepithelial current. The observation is that the response declines during a maintained stimulus step; this can be described most generally as a negative feedback occurring somewhere between the stimulus and the response. There are a number of sequential steps between stimulus and response that could effect the negative feedback by affecting a preceding step and that are not directly measured. Understanding the adaptation is begun by localizing the process within this chain of steps.

The stimulus probe displacement causes a displacement of the otolithic membrane, by means of a simple frictional coupling. The otolithic membrane in turn moves the hair bundles; filamentous attachments constitute the linkage from the otolithic membrane to the bulb of the kinocilium, and from the bulb to the mechanosensitive stereocilia. Displacement of the hair bundle is somehow communicated to the transduction element as a bias that tends to open or close channels. The nature of the bias is not understood, nor is its communication to the transduction element, and these may themselves comprise several steps. Bias on the transduction element opens channels; the mechanism is not clear, but is investigated in Chapter IV. Once channels open, various ions (mostly K^+) carry current into the cell. This causes a

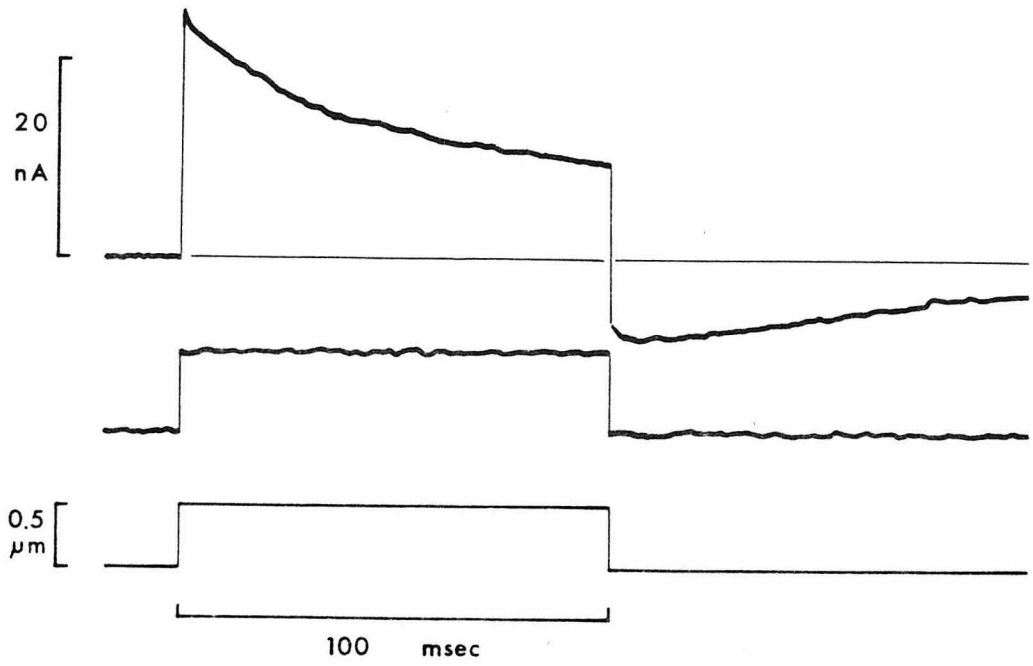

Fig. 1. Decline in the microphonic current following a step displacement of the otolithic membrane. The membrane potential of hair cells is held nearly constant with high-K^+ perilymph, but the microphonic current (top) declines following the step. The decline does not result from slippage of the otolithic membrane, since an optical measure of otolithic membrane displacement shows no decline (middle) during the maintained displacement of the stimulus probe (bottom). High-K^+ Perilymph and Normal (0.25 Ca^{++}) Endolymph; 21.3 °C.

transepithelial current and an intracellular receptor potential, either of which we can measure. These steps are summarized below:

Stimulus probe displacement
↓
Otolithic membrane displacement
↓
Hair bundle displacement
↓
Bias on transduction element
↓
Opening of channels
↓
Ion entry
↓
Transepithelial current/Receptor potential

To study the first link, the otolithic membrane displacement was measured optically by focusing a bright light source on one of the 10-20 μm clumps of otoconia that remain embedded in the membrane after dissection. Motion of the clump changed the amount of light passing on to a photocell; the photocurrent thus indicated the otolithic membrane motion at that clump. The optical signal was abolished if the moving stimulus probe was lifted a few microns off the otolithic membrane, or was reversed in sign if the light was focused on the other side of the clump. Figure 1 shows that the optical signal did not decline following a step stimulus. Thus the position of the otolithic membrane does not relax following the step displacement, and the affected linkage occurs after the motion of the otolithic membrane.

It is not possible to measure motion of hair bundles with this arrangement, and so with the epithelial preparation we cannot rule out a relaxation of the filamentous bonds to the kinocilium. However, the same phenomenon has been studied with intracellular recording and direct stimulation of single hair bundles, by R. A. Eatock and A. J. Hudspeth. Following a maintained displacement of as much as 4 μm, the receptor potential declines, although the bundle can clearly be seen to maintain its displaced position. Thus the affected linkage is after the hair bundle displacement.

We presented in Chapter I, and reproduce here as Fig. 2, evidence that the decline in the response current reflects a shift of the operating curve along the displacement axis. The decline does not reflect an inactivation of the sort that voltage-sensitive Na^+ and K^+ channels experience, since a further displacement of the bundle restores the current. Instead, the instantaneous operating curve mapped during a maintained displacement shows a lateral shift with almost no change in shape. That is to say, the relation between transducer bias and probability of channel opening is unchanged, except that the curve is shifted along the bias axis. Thus the affected linkage occurs before bias on the transduction element, and so must be that between hair bundle displacement and the bias on the transduction element.

The adaptive shift occurs with the epithelial preparation if the membrane potential is held nearly constant with high K^+ in the lower bath (Fig. 1). It also occurs with stimulation of single cells that are voltage-clamped with intracellular microelectrodes (Fig. 3). Thus the element feeding back is not the change in membrane potential, or a subsequent function of membrane potential.

We will present evidence below that the position of the operating curve is a function of intracellular Ca^{++} concentration: the curve is shifted to the right with higher Ca^{++}. The rate of the adaptive shift is also a function of Ca^{++} concentration in the endolymph. A reasonable hypothesis is that Ca^{++} enters the cell when channels open, and once inside, causes the shift of the operating curve. It has been shown (Chapter II) that Ca^{++} can pass through the transduction channel, so that no special route need be hypothesized. The dependence of the rate on Ca^{++} concentration in the upper bath would result simply from Ca^{++} entering faster when there is more of it outside the cell. The return of the operating curve to normal following the stimulus step would then reflect the sequestration of Ca^{++} or its removal by an active pump. With this hypothesis, the feedback element would be ion entry following channel opening, or ion sequestration following channel closing.

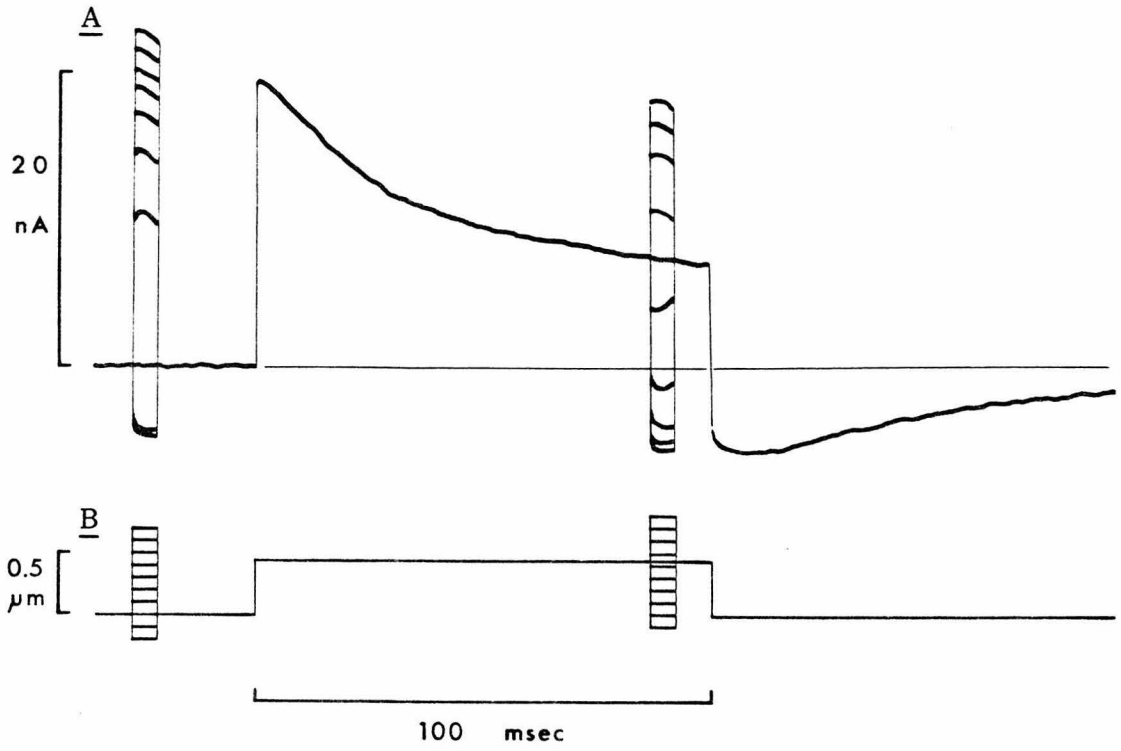

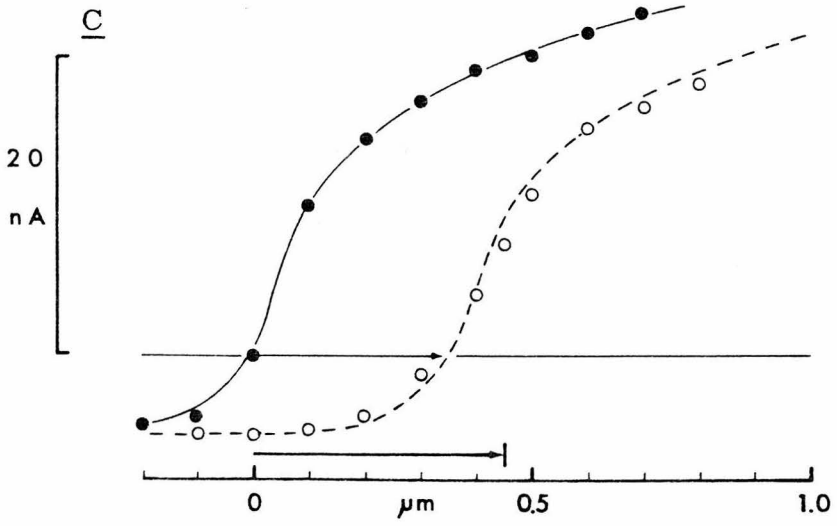

Fig. 2. Adaptive shift of the operating curve. A, the operating curve is mapped with a set of test steps before the stimulus step (B), and 90 msec after onset of the step. C, the microphonic response is plotted vs. displacement for each set: ●, before the step, o, after 90 msec. Within 90 msec the curve has shifted by 0.33 μm, or 73% of the way to the new bundle position. High-K^+ Perilymph and K^+/1.0 Ca^{++} Endolymph; 21.9 °C.

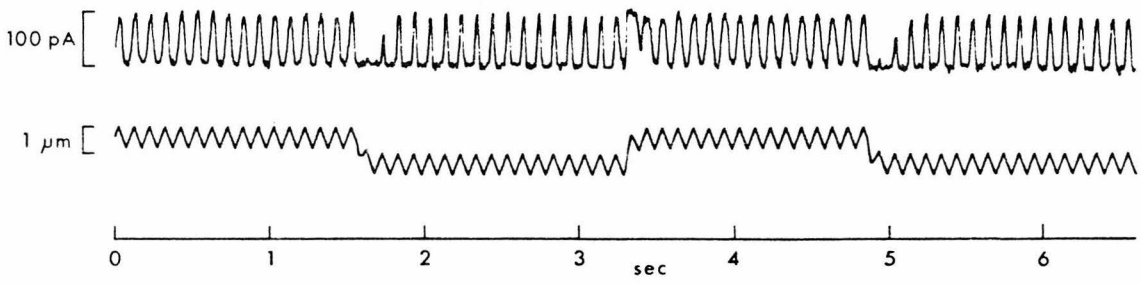

Fig. 3. Adaptation in a single, voltage-clamped cell. The triangle wave stimulus sweeps linearly through the operating range twice each cycle, and so the response defines the operating curve. Top trace, the receptor current with the membrane potential clamped at -60 mV; upward represents current entering the cell. Bottom trace, displacement of the stimulus probe; upward is towards the kinocilium. When the probe is stepped in the positive (upward) direction, the response to the superimposed triangle wave saturates, but then returns in one to three hundred milliseconds. When the step is terminated, the response saturates in the negative direction, but again returns with time. Direct observation of the hair bundle shows no slippage relative to the stimulus probe. Normal (4 mM Ca^{++}) Saline at 23 °C.

The hypothesis has not been tested directly; to do so most convincingly would require a fast, partial, channel blockade, which would decrease the rate of Ca^{++} entry but leave enough current to monitor the adaptation. Instead, it was tested indirectly by considering the step preceding ion entry.

The adaptive shift occurs for both directions of displacement. A large negative step closes all the channels and decreases the transepithelial current. During the maintained step, however, the curve shifts to the left, channels reopen and the current returns. When the step is terminated, there is a surge of current—the rebound effect seen in Fig. 13 of Section I. The amount of rebound indicates the amount of adaptation that occurred during the negative step. Figure 4 shows adaptive rebounds for three negative steps, of amplitudes -0.2 μm, -0.4 μm and -0.8 μm. Both of the larger steps are sufficient to close all channels. The figure shows, however, a larger adaptive rebound for the -0.8 μm step. The observation has been repeated with many preparations, stimulus durations, and Ca^{++} concentrations. It is an important experiment, for the only reasonable interpretation is that the feedback element precedes channel opening or closing. The adaptation cannot be a direct consequence of Ca^{++} entry during a positive displacement, or of its sequestration during a negative displacement.

We conclude that bias on the transduction element feeds back to affect the linkage from hair bundle to transduction element. Because these elements are not well-defined, the conclusion is rather general; it would include mechanisms such as a Ca^{++}-dependent slippage of the transduction element along a linkage element.

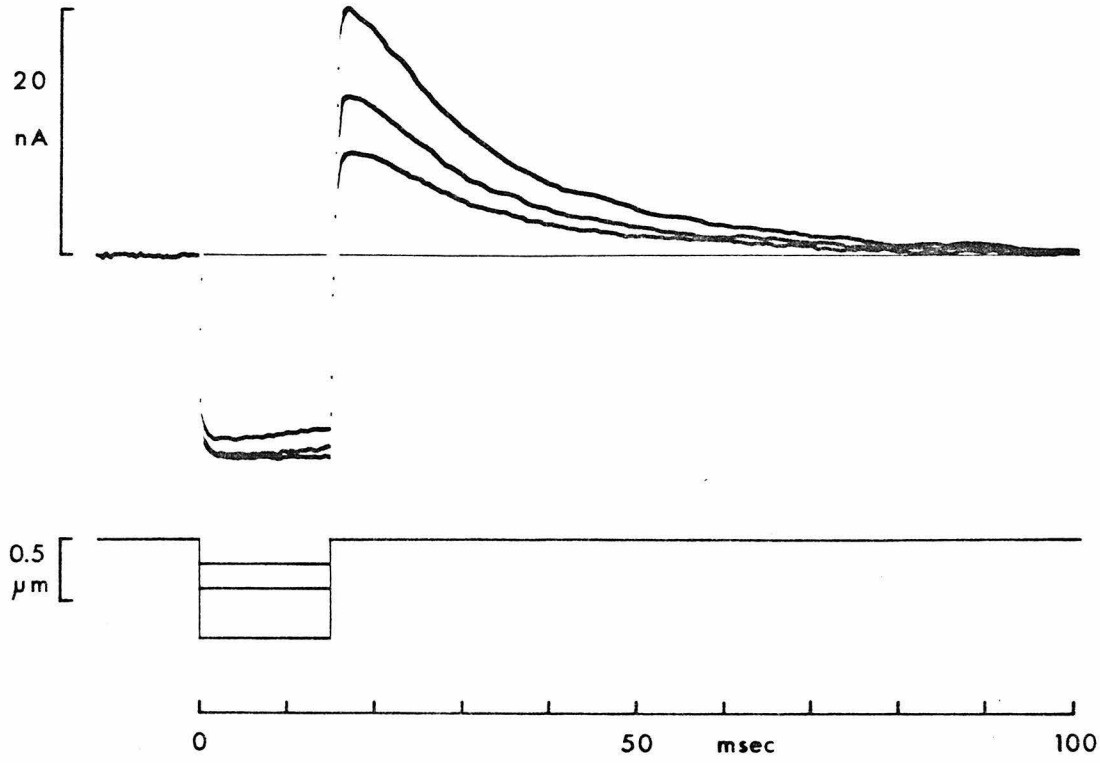

Fig. 4. Adaptive shift with saturating negative steps. Three 20-msec step stimuli are presented, to -0.2 μm, -0.4 μm and -0.8 μm (bottom). Both of the larger steps are sufficient to saturate the transduction in the negative direction, but the largest step causes more adaptation, as judged from the amplitude of the adaptive rebound (top-most trace). Normal Perilymph and K^+/1.0 Ca^{++} Endolymph; 21.5 °C.

Part II. Properties of the adaptive shift, and the effect(s) of calcium

In order to understand the physical mechanism of the adaptive shift, we begin by cataloging some of its characteristics. These cannot provide an explanation, but can point towards some reasonable mechanisms.

The shift is not a simple exponential decay to a new position. Positive stimulus steps to three different levels all evoke a fast shift on the order of 10-20 msec, followed by a slower creep on the order of 100-200 msec, towards the new bundle position (Fig. 5). The adaptation measured with stimulation and recording of single cells sometimes is not complete in many seconds (R. A. Eatock, personal communication). It is not clear whether this timecourse is a basic property of the adaptive shift, or whether the multiple rates measured with the epithelial preparation in fact reflect a summation of single but different rates in different cells.

The rate of the positive shift is slightly greater than the rate of the negative shift. Thus adaptive shifts that act to turn off channels after positive displacements occur more rapidly than shifts that act to turn on channels after negative displacements. For a symmetrical, repetitive stimulus, the net result is to shift the curve to the right—to turn off channels. This effect is shown in Fig. 6 for a sine-wave stimulus. It is clearly of functional significance, for it permits hair cells to adapt to strong oscillatory stimuli.

The rate of the shift is greater at higher temperatures. Although this effect has not been studied in detail, the rate measured from the shift of the instantaneous operating curves has a Q_{10} between 2 and 3. The temperature dependence is illustrated qualitatively by Fig. 7, which shows responses to small displacements with a high-K^+ perilymph. Under these conditions the step response most closely reflects the timecourse of the shift.

The position of the operating curve is a function of Ca^{++} concentration. Even without stimulation, the operating curve can be shifted to the right by

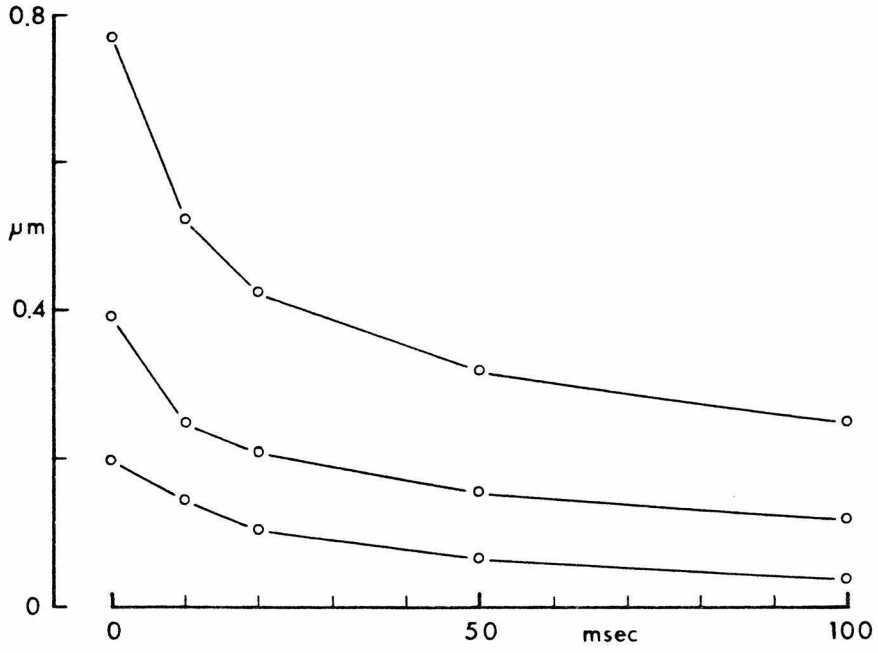

Fig. 5. Timecourse of the adaptive shift, measured from instantaneous operating curves. The displacement axis is the difference between the instantaneous position of the operating curve and the probe displacement, and so corresponds to the effective stimulus to the transduction element. An initial step to +0.77 μm causes an instantaneous bias of 0.77 μm, which declines as the operating curve shifts to the new bundle position. Other steps, to +0.36 μm and +0.20 μm, cause adaptive shifts with the same timecourse, which is not a simple exponential but which can be fitted with a sum of exponentials. Normal Perilymph and Normal (0.25 Ca^{++}) Endolymph; 23.9 °C.

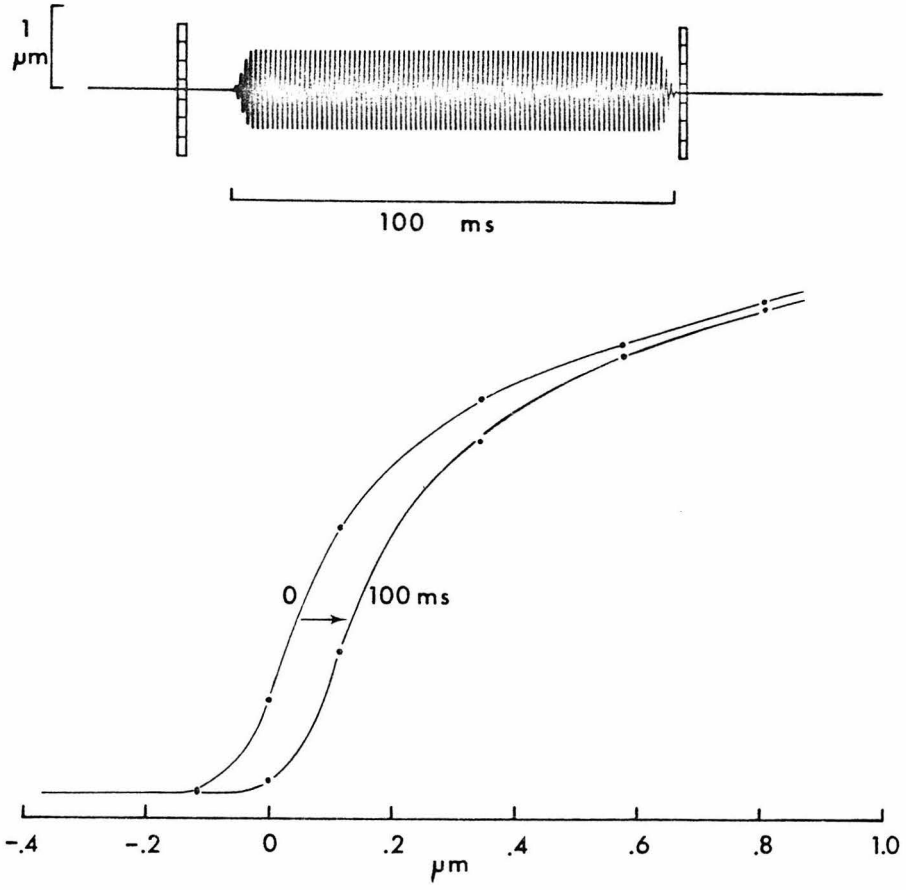

Fig. 6. Adaptive shift in response to a symmetrical stimulus. The instantaneous operating curve is measured before and after a 100-msec tone burst; after the tone burst the curve has shifted to the right, in the direction to decrease the receptor current. The tone applied to the stimulus probe is a large (1.0 μm peak-to-peak) but symmetrical sine wave, so the stimulus has no net displacement. The shift occurs because the rate of adaptation in the positive direction is greater than that in the negative direction. Normal Perilymph and Normal (0.25 Ca^{++}) Endolymph; 20.6 °C.

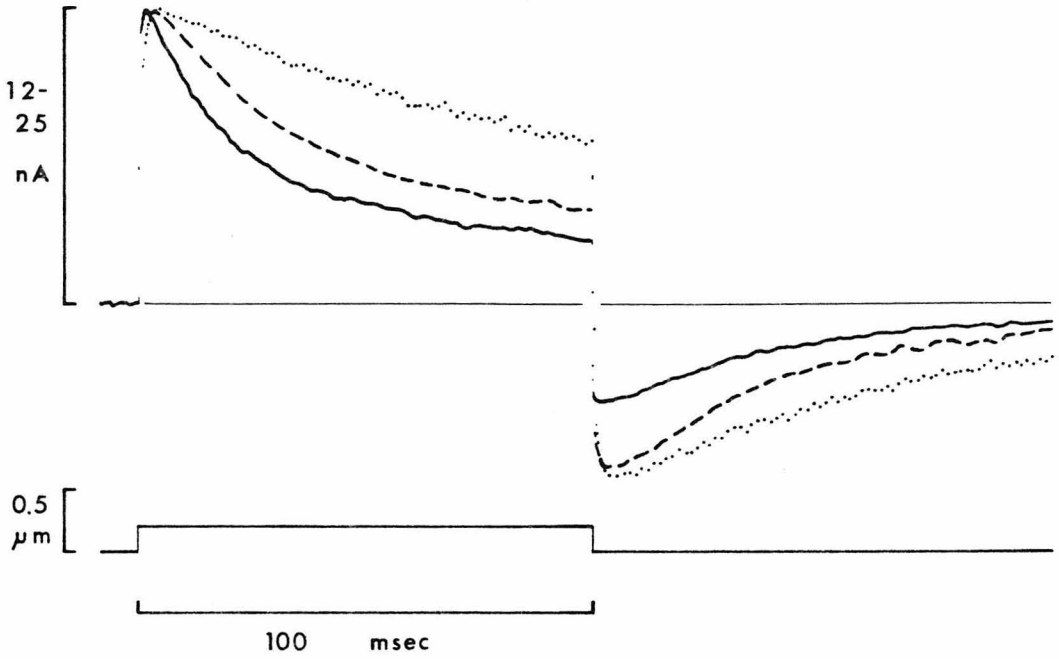

Fig. 7. Temperature dependence of the rate of adaptation. The membrane potential of hair cells is held nearly constant with high-K^+ perilymph to eliminate other time-dependent effects. Stimuli are 0.2-μm steps, which are within the approximately linear region of the operating curve, so that the decline in current mimics the timecourse of the adaptive shift. Microphonic currents are smaller at lower temperatures because of the Q_{10} of ion permeation (about 1.3), but for comparison these records have been normalized to the same peak value. The adaptive shift is most rapid at 25 °C (——), slower at 15 °C (----), and slowest at 5 °C (····). High-K^+ Perilymph and K^+/1.0 Ca^{++} Endolymph.

increasing the Ca^{++} concentration in the upper bath (Fig. 8). The effect is not strong: the shift is no more than +0.1 μm for each order of magnitude increase in Ca^{++} concentration. But it is rapid and very reproducible. These large changes in extracellular Ca^{++} concentration may cause much smaller changes in intracellular free Ca^{++}. As the site of action of Ca^{++} is probably intracellular (see below), the Ca^{++} effect within the cell might be quite large. The effect is not duplicated by Sr^{++} or Mg^{++}: replacement of Ca^{++} in endolymph with Sr^{++} or Mg^{++} shifts the curve towards its position with lower Ca^{++} concentrations.

The rate of the shift is also a function of Ca^{++} concentration. The dependence is shown qualitatively in Fig. 9, and has been confirmed qualitatively by measuring the shifts of instantaneous operating curves. Increasing the Ca^{++} concentration in the upper bath increases the rate of the adaptive shift by 3- to 5-fold for each order of magnitude increase in Ca^{++}. This effect is also not duplicated by Sr^{++}: adding Sr^{++} to an endolymph containing Ca^{++} actually decreases the adaptation rate. Sr^{++} presumably displaces Ca^{++} from its site of action, although the data are not sufficient to demonstrate competitive inhibition.

The action of Ca^{++} on the position of the operating curve probably occurs within the hair cell. Perfusion of the lower bath with a perilymph containing 0.2 mM dinitrophenol (DNP) shifts the operating curve to the right over a period of tens of minutes (Fig. 10). During this time the upper bath is continously perfused with normal endolymph: the apical Ca^{++} concentration is unchanged. Our supposition is that DNP, an uncoupler of oxidative phosphorylation, blocks metabolically-dependent Ca^{++} extrusion and sequestration, and/or causes mitochondria to unload Ca^{++}. Either mechanism could increase the intracellular free Ca^{++} concentration and would explain the change in position of the operating curve if the site of Ca^{++} action were within the cell. It is interesting that the rate of the adaptive shift is not significantly changed by DNP, which suggests that these two effects of Ca^{++} may be quite separate.

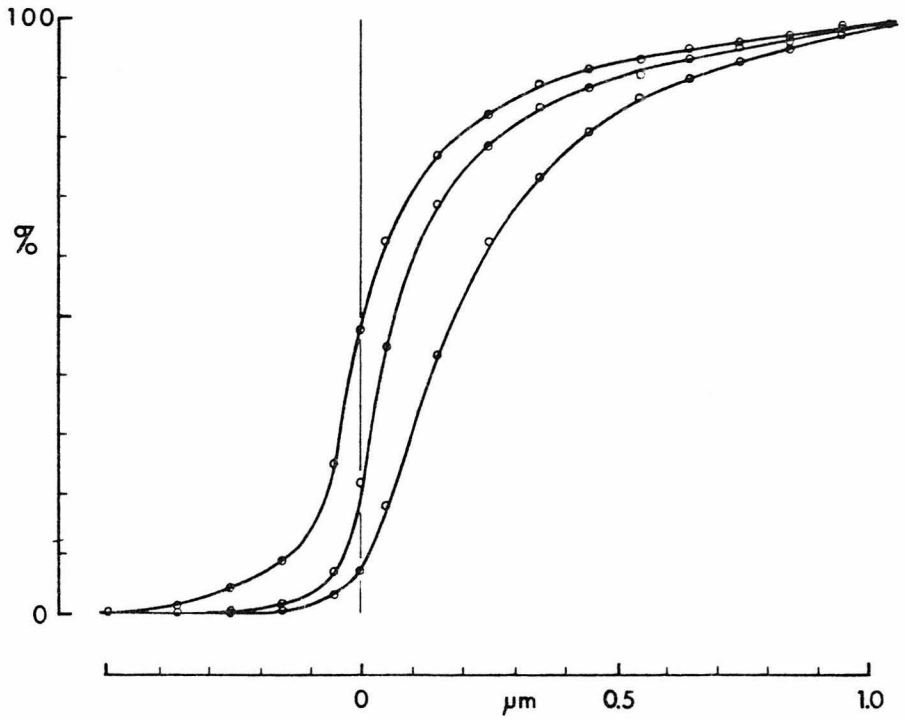

Fig. 8. Ca^{++}-dependent shift of the operating curve at rest. The instantaneous operating curve at rest is mapped with a set of 16 test steps, with different Ca^{++} concentrations in the upper bath. The curve farthest to the right is obtained with 10 mM Ca^{++}, that farthest to the left with 0.1 mM Ca^{++}, and that in the middle with 1.0 mM Ca^{++}. The microphonic currents are smaller by 30-50% in the highest-Ca^{++} saline (10 mM); for comparison peak currents were normalized to the value with 0.1 mM Ca^{++}, and the currents at negative saturation were aligned. In addition, the shape of the curve changes as the Ca^{++} concentration is increased, becoming more linear and assuming a sharper corner at the negative saturation. High-K^{+} Perilymph and K^{+}/x Ca^{++} Endolymph; 21.5 °C.

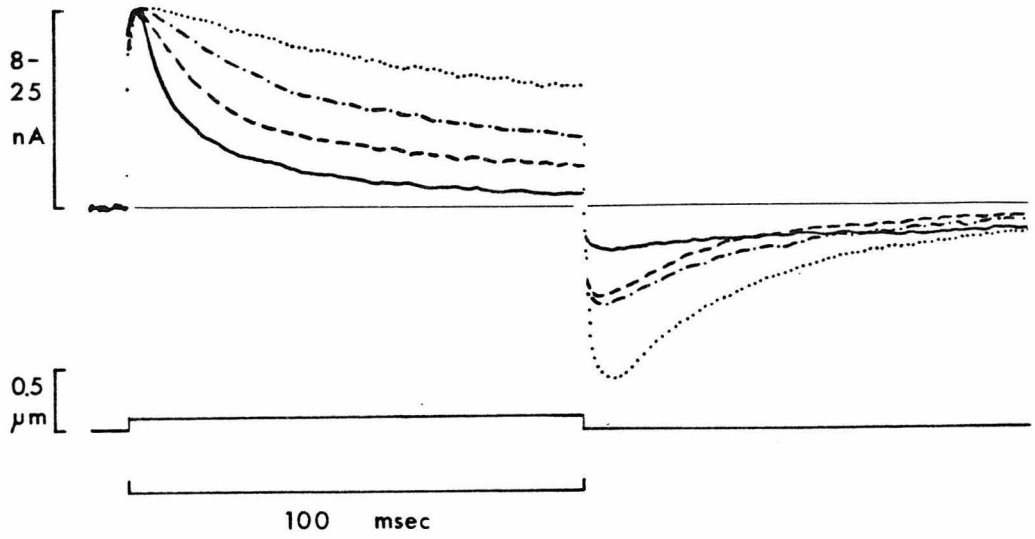

Fig. 9. Ca^{++} dependence of the rate of adaptation. High-K^{+} perilymph and small (0.1 μm) stimuli are used, as for Fig. 7. Endolymphs with different Ca^{++} concentrations are used and currents normalized as for Fig. 8. The adaptation is most rapid with 10 mM Ca^{++} (——), slower with 1.0 mM Ca^{++} (----), and slowest with 0.1 mM Ca^{++} (····). Sr^{++} added to a 1.0 mM Ca^{++} endolymph decreases the rate of adaptation (-·-·-), suggesting that it competes with Ca^{++} for an active site. Same conditions as in Fig. 8.

Fig. 10. Effect of DNP on the position and adaptive shift of the operating curve. The operating curve is mapped with 16 test steps and the response plotted vs. displacement (left). The timecourse of the response to a 100-msec, +0.5-μm step is shown at right. Perilymph is High-K^+ Perilymph to reduce voltage-dependent changes, so the decline in the microphonic current following the step is a qualitative measure of the adaptive shift. Operating curves and step responses are shown for the control before DNP (0 min), and for 16, 26, and 34 min after adding 0.2 mM DNP to the perilymph. The operating curve clearly changes following addition of DNP: fewer of the transduction channels are open at rest, and the shape changes to become more linear and less displacement-sensitive. The rate of adaptation is not significantly changed: at any given time during the step response, the apparent position of the curve, calculated from the microphonic current at that time and from the operating curve, is the same for all four traces. The change in shape of the step response is wholly attributable to the change in shape of the operating curve. Normal (0.25 mM Ca^{++}) Endolymph; 21.9 °C.

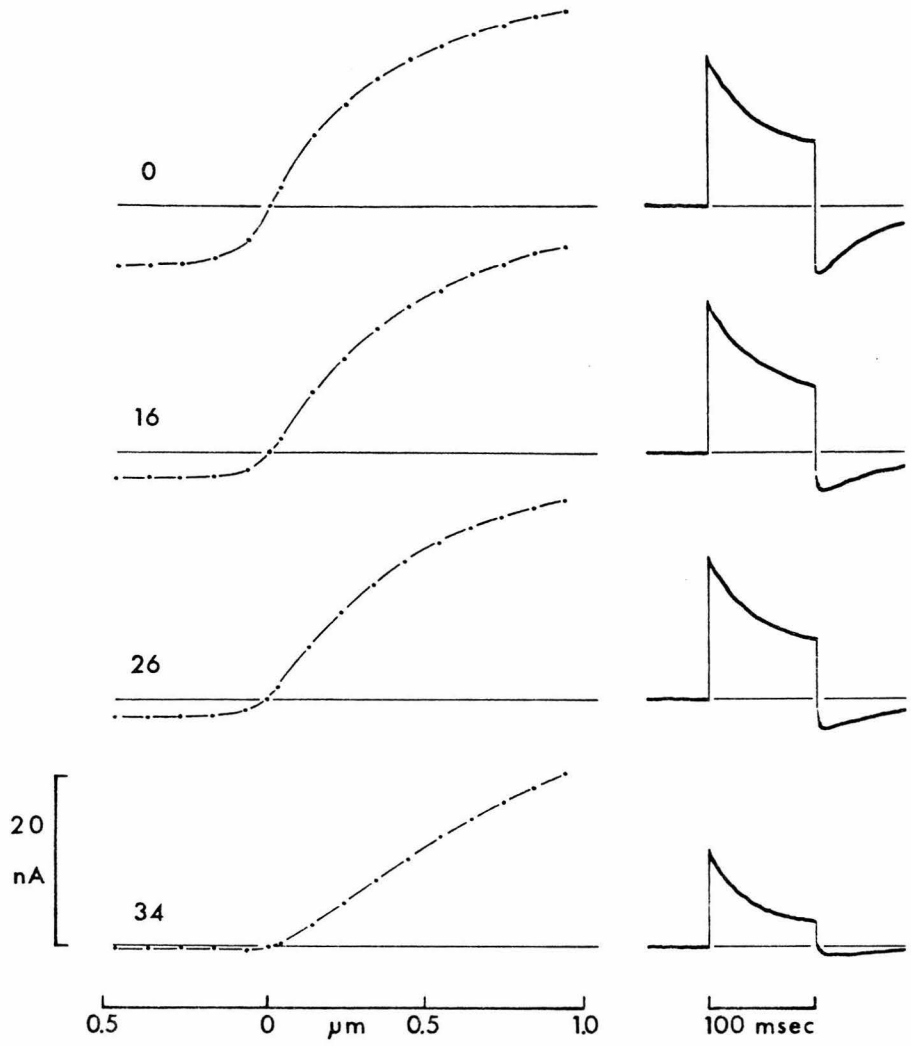
0
16
26
34
20
nA
0.5
0
μm
0.5
1.0
100 msec

The action of lowered Ca^{++} concentration on the resting position of the operating curve and on the rate of the adaptive shift is duplicated by ammonium ion (NH_4^+). Replacement of K^+ in endolymph with NH_4^+ shifts the operating curve to the left, and decreases the rate of adaptation (Fig. 11). The Ca^{++} concentration in endolymph is unchanged. Furthermore, the effect of NH_4^+ occurs over 5-10 min, far longer than the wash-in time of the upper bath. As NH_4^+ passes readily through the transduction channel (Corey & Hudspeth, 1979b) and presumably accumulates inside the hair cells, it seems most likely that NH_4^+ changes the intracellular Ca^{++} concentration and that the effect of Ca^{++} is intracellular.

The actions of Ca^{++} on the resting position of the operating curve, and on the rate of the adaptive shift, are separate effects. When NH_4^+ is subsequently removed from the upper bath and replaced with a K^+ endolymph, the rate of adaptation returns over several minutes to its original value in K^+ endolymph. The operating curve, however, rebounds to a position further to the right than its original position, and then relaxes to the starting position over the next few minutes (Fig. 11). The phenomenon is reminiscent of the "ammonia-rebound" effect, often used to change intracellular pH in other preparations (Boron & De Weer, 1976; Aickin & Thomas, 1977; Umbach, 1979). When extracellular NH_4^+ is increased in these preparations, there is a rapid transmembrane flux of NH_3, which is hydrated within the cells to form NH_4^+ and OH^-. The intracellular pH increases. During the subsequent equilibration the pH returns to normal, although this is a slow process occurring over tens of minutes. Upon removal of NH_4^+ from the extracellular medium, intracellular NH_4^+ dissociates to NH_3 and H^+, and NH_3 leaves the cell, decreasing the intracellular pH to below normal. As intracellular pH and free Ca^{++} concentration are linked in many of the cells that have been studied (Meech & Thomas, 1977; Lea & Ashley, 1978; Baker & Honerjäger, 1978), the rebound in the resting position of the operating curve observed here may well be a secondary effect

Fig. 11. Effects of NH_4^+ endolymph on the position and adaptive shift of the operating curve. A, same stimuli and salines as in Fig. 10. Operating curves and step responses are shown for K^+ endolymph (0 min), after a short equilibration in NH_4^+ endolymph (8.8 min), shortly after returning to K^+ endolymph (11.0 min), and after a short equilibration in K^+ endolymph (18.2 min). While NH_4^+ increases the microphonic current in the first few minutes, the current declines by 8.8 min to less than that with K^+ and then recovers to normal after 10 min in K^+ endolymph. Ca^{++} concentration in endolymph (0.25 μM) is not changed. 21.5 °C.

B, the resting position of the curve and the rate of adaptation are plotted vs. time. The position of the operating curve (middle trace) is plotted as the percentage of channels open at rest, a somewhat qualitative but sensitive measure of the curve position. The rate of adaptation (top trace) is estimated by measuring the microphonic current 40 msec after the step, calculating the shift at that point by converting the current to apparent displacement, and then calculating the initial rate of the shift in μm/sec. Both are approximate measures, but suffice to show changes. The NH_4^+ concentration is shown in the bottom trace, which is derived from the measured exchange time of the upper bath. The concentration ranges from 0 mM (down) to 130 mM (up). Neither the resting position of the curve nor the rate of adaptation returns exactly to its starting position over the time of this experiment, but does so over the following 15-30 min.

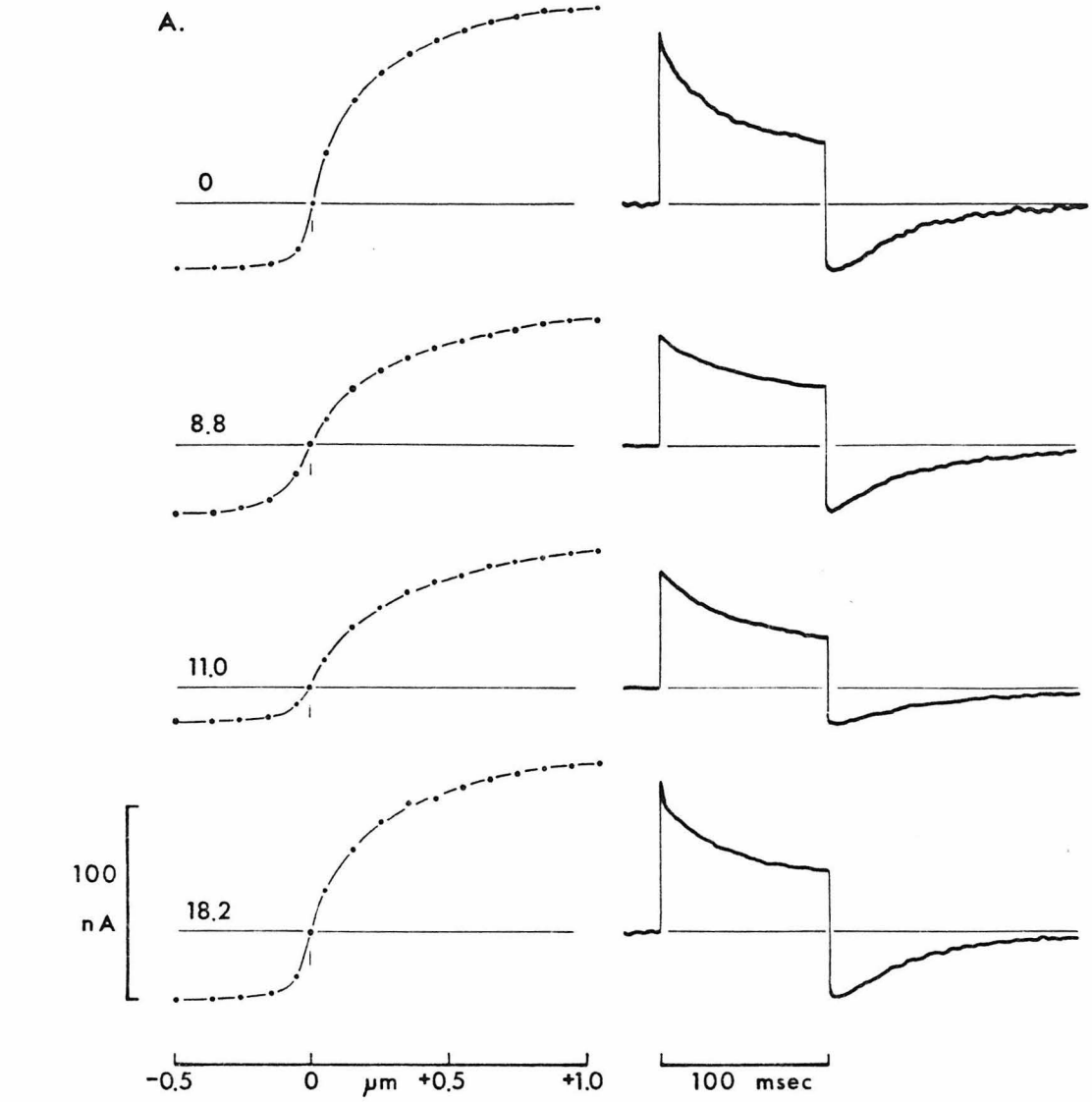
A.
0
8.8
11.0
18.2
100
nA
-0.5
0
μm
+0.5
+1.0
100 msec

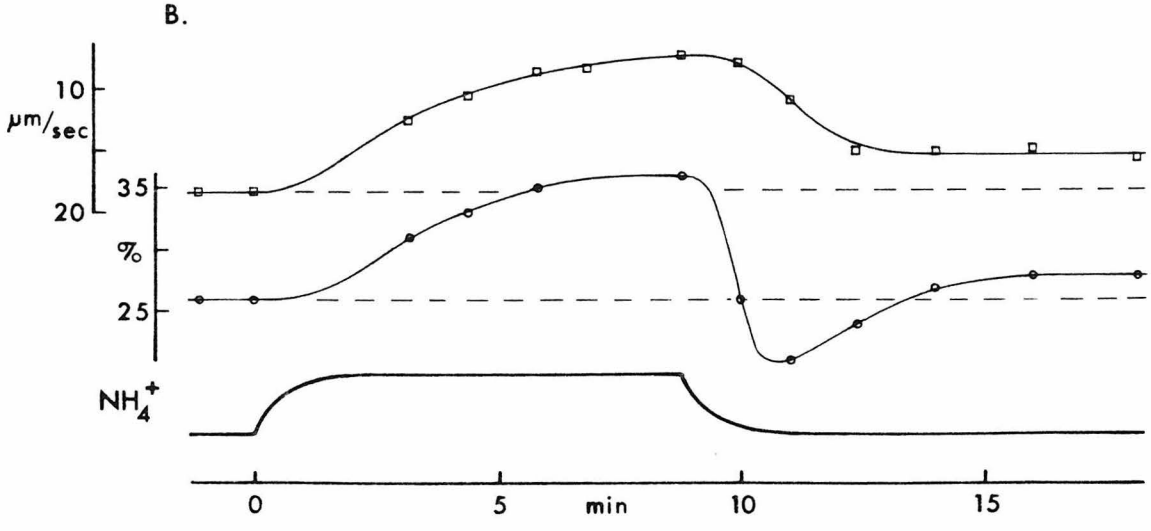
B.
10
μm/sec
20
35
%
25
NH4+
0
5
min
10
15

of an ammonia-rebound acidification. It is not clear, however, whether Ca^{++} or pH is the primary effector. The shift in the resting position of the operating curve could, for instance, result directly from a protonation of some site on the transduction element, and this shift might be effected only indirectly by increased Ca^{++}. Similarly, the increase in the rate of the adaptive shift might be a direct effect of Ca^{++}, also caused indirectly by low pH. In any case, the clear difference in the timecourses of recovery from NH_4^+ endolymph make it difficult to see these two effects as two aspects of the same process.

DISCUSSION

Adaptation processes intrinsic to the transduction mechanism in hair cells have not previously been described, except insofar as phase-lead characteristics of the microphonic have been reported (Jielof et al. 1952; Furukawa & Ishii, 1967b; Kroese et al. 1980). Indeed, the phenomenon was missed in our initial experiments (Hudspeth & Corey, 1977), in part because the stimuli used to test for a slow relaxation were of supersaturating amplitude and not enough time was allowed for the relaxation. Also, the adaptation seems to be a fairly labile phenomenon when studied with intracellular recording (work of Eatock & Hudspeth), and the factors underlying this lability are not understood.

The desirability of an adaptive mechanism clearly varies among organs. Hair cells of the lateral line, sensitive to the velocity of water motion, might not require an additional adaptation. Static pressure differences in the mammalian cochlea are relieved by the helicotrema, so that no static displacements occur. Of the otolithic vestibular organs, those sensitive to gravitational acceleration must not have complete adaptation if balance is to be maintained, while those sensitive to small fluctuations must adapt if large, static accelerations (like gravity) are not to saturate the receptors.

We have argued that the transduction mechanism in bullfrog saccular hair cells is likely to be identical to that in all vertebrate hair cells (Hudspeth & Jacobs, 1979; Corey & Hudspeth, 1979a,b). If so, we must explain an apparent variability in the adaptive shift of the operating curve. As the rate of adaptation depends on the intracellular Ca^{++} concentration, the degree of adaptation might simply be regulated by the control of free intracellular Ca^{++}. This might be controlled for a whole organ by altering the endolymphatic Ca^{++} concentration; here it is interesting to note that mammalian cochlear endolymph is very low in Ca^{++} (30 μM; Bosher & Warren, 1978) and that intracellular recordings from mammalian hair cells show no perceptible

adaptation during a tone burst (Russell & Sellick, 1978). Or it may be controlled within individual cells, by the activity of extrusion and sequestration mechanisms.

The specific properties of the adaptive shift are intriguing, but even collectively are not sufficient to imply a mechanism. The multiple rates of adaptation might suggest a viscoelastic relaxation, as such mechanisms typically produce relaxations with a range of rates. The data of Fig. 4 can be fitted by a simple viscoelastic model (drawn from that of Huxley & Simmons, 1971, and Eyring, 1936), and the model can produce different rates for positive and negative adaptation. But until it is clear that the different rates correspond to a single relaxation mechanism at a single transduction element, such modelling is meaningless. Alternative explanations include population effects, or several entirely different adaptive mechanisms operating simultaneously.

The temperature dependence is similarly inconclusive. The Q_{10} of 2-3 may reflect a direct temperature effect on the adaptive shift, or it might simply reflect the temperature dependence of the intracellular Ca^{++} activity. It probably rules out a multistep mechanism, involving for instance a phosphorylation step. The lack of change in the adaptation rate when the cells are poisoned with DNP also argues against active mechanisms, at least those involving ATP.

The DNP and NH_4 experiments indicate an intracellular site of action for Ca^{++}, but raise the question of whether the dual effects of Ca^{++} are part of the same general mechanism. Our understanding at present is that Ca^{++} actively determines the rate of adaptation, and that it also determines the position of the operating curve, that is, the point on the curve toward which the transducer adapts. These would seem to be two aspects of the same process, and a model supposing that they are would seek to integrate them into a single effect. We believe, instead, that the Ca^{++} effect on the static position of the curve is related to the transduction mechanism <u>per se</u>, and is not directly part of the adaptive shift. More evidence for

this is presented in the next chapter, where we examine the kinetics of the gating mechanism. This is not to say that the Ca^{++} effect on the position of the curve plays no part in the adaptation in general. Ca^{++} entering the cell during strong stimuli must increase the intracellular Ca^{++} at least slightly, and this increase must shift the operating curve, at least slightly. Although separate, we think, from the adaptive shift per se, this effect may confuse studies of the shift.

The data at hand imply no models for the adaptive shift of the operating curve, but they do point in certain directions. One would look towards simple relaxation mechanisms, such as those involving sliding under elastic tension. As the adaptation occurs in both directions, such sliding might involve rigid linkages, or at least tensile linkages with forces directed in both directions. Ca^{++} accelerates the adaptation, and Sr^{++} does not, implying specific biochemical binding and not electrostatic effects. If the adaptation occurred, for instance, as an unbinding and rebinding to sequential sites along a linear linkage, then the temperature dependence and rate of adaptation would suggest a barrier to unbinding of 12-16 kcal/mol. The effect of Ca^{++} could then be seen as a catalysis of the unbinding.

Chapter IV

GATING KINETICS OF THE TRANSDUCTION ELEMENT

PREFACE

Investigation of the kinetics of the response grew very slowly from a concern about the timecourse of the probe motion. The apparent oscillations of the microphonic potential following a step displacement naturally suggested that the bimorph was ringing, and the first of a long line of optical monitors was constructed to measure the motion. Once the motion was easy to record I began casually to measure the latency between the stimulus and the microphonic current response. The investigation became more focused when it became clear that a good determination of the latency could help to indicate a transduction mechanism. After the development of faster probes and optical monitors, and a good method for correcting for epithelial capacitance, a latency of 40 μs at 22° C was measured. This result, along with the temperature dependence, was eventually published in the Biophysical Journal (Corey & Hudspeth, 1979a).

During the last phases of the project, I realized that if all the known delays could be eliminated or accounted for, the remaining latency would be due to the opening of the channels themselves. Though perhaps obvious, this was quite exciting at the time. With much more work, the quasi-exponential approach of the current to equilibrium was determined, as was, even later, the dependence of the rate on the size of the stimulus. The implication of that dependence for a direct connection from hair bundle to membrane channels was immediately appreciated, but the project was put aside in order that we might concentrate on the ionic selectivity of the channel. I returned to the kinetics after a year, and found only recently that a two-state model for the gating was inadequate to explain details of the kinetics, but that a three-state model was satisfactory.

A comprehensive model for the gating of the transduction channel has now been developed, and it can account quantitatively for the fast kinetics of the microphonic current. The model, its implications, and some possible artifacts are presented in this final chapter.

INTRODUCTION

The quantitative description of membrane currents underlying the action potential (Hodgkin & Huxley, 1952) was of monumental importance for neurophysiology, both because of the power of the mathematical formulation, and because of the physical interpretation given to the mathematics. Hodgkin and Huxley supposed that discrete membrane channels were gated by charged "activating particles," which could exist either on the inside or the outside of the membrane, and whose equilibrium distribution was a Boltzmann distribution governed by the electrical energy difference between the two sites. The rate of transitions between these two sites for the activating particle was an instantaneous function of membrane potential, and thus was also a function of the energy difference between the sites.

This notion of a gating mechanism whose transition rates and equilibrium were governed by energy differences between states of the mechanism was drawn upon and extended by Magleby and Stevens (1972) in their quantitative description of end-plate currents. Magleby and Stevens suggested that the "activating particle" was in fact identical with a dipole moment of the channel molecule, the free energy of which changes with different conformations of the molecule. They viewed the binding of the acetylcholine to the receptor molecule as an enzymatic process, whereby the channel molecule undergoes a conformational change to an open state upon binding of the ligand. Perhaps most importantly, they expressed the transition between states as a rate process (Eyring et al. 1949) in which the transition rate depends on an activation energy that is the free energy difference between the molecule in a given conformation and in its transition state. Changing the energy of either conformational or transition states, for instance by applied voltage, changes the transition rates. This voltage sensitivity of the transition rate explained the prolongation of the end-plate current by hyperpolarization.

We present evidence here that the gating of transduction channels in

vertebrate hair cells may also be considered as a redistribution between conformational states; here the energy change is mechanical and is effected by displacement of the hair bundle, rather than by transmembrane potential. A model is proposed that can explain both the equilibrium current and the kinetics of relaxation to an equilibrium as a function of bundle displacement.

The kinetics of the transduction channel is one or more orders of magnitude faster than that of other membrane channels that have been studied (e.g., Nonner, 1980); the fast kinetics underlies the extremely high frequency sensitivity of the auditory system in some animals.

METHODS

Preparation

All experiments used the patch preparation of the saccular macula, in which the otolithic membrane was peeled back to uncouple all but a homogeneous population of hair cells. Care was taken to peel the otolithic membrane well past the region of the macula where the striola was presumed to lie, to prevent contamination of the response by hair cells oriented oppositely to those in the periphery. The thin plastic film that restricted current flow to the stimulated region was arranged particularly closely around that region, to increase the signal-to-noise ratio. This film prevented the otolithic membrane from contacting uncoupled hair bundles outside the stimulated region, and also prevented fluid coupling to those hair bundles by covering them.

Recording

The voltage clamp circuit was typical of those used for clamping squid axons, since squid axons and this preparation have similar impedances and response-time requirements. The head stage of the clamp, placed a few centimeters from the chamber, contained a high-impedance differential amplifier to measure transepithelial potential, and a current-to-voltage converter to measure transepithelial current. Within the clamp circuit, the current signal was multiplied by a passive network of variable resistors and capacitors which could be adjusted to duplicate the passive impedance of the epithelium. A square step of current was passed across the epithelium, and the measured voltage was subtracted from the multiplied current signal at the summing junction of the main clamp amplifier. The variable components were adjusted until the net signal at the output of that amplifier was zero, at which point the impedance of the passive network was equal to that of the epithelium. The portion of the passive network representing the lumped cell capacitance in parallel with the tight junctions (see Chapter I) was then removed from the passive network,

and the voltage clamp feedback connected. This procedure allows the clamp to compensate fully for the series impedance of the chamber and the tissue. The clamp gain was then increased to just below the point of instability.

The response time of the clamp was measured with a passive network that was equal to the equivalent circuit of the epithelium and was placed in the experimental setup at the normal position of the chamber. A photodiode with a 300-ns response time (Hewlett-Packard 5082-4220) was connected in parallel with the impedance representing the apical hair cell surface, and illuminated with a pulsed light-emitting diode (LED). When optimally adjusted, the clamp settled to 95% of the final current value in 3 μs. It was further found that the response time to a step in command voltage equaled that to a step in photocurrent in the equivalent network, so the response time to a voltage step was routinely used as a measure of clamp speed during experiments.

The current signal from the voltage clamp was low-pass filtered with a single-pole filter at 50 kHz and a 6-pole Bessel filter at 100 kHz, then digitized at either 5 or 10 μs per point before averaging. Stimuli of 1-3 msec duration were presented at a rate of 1/60 msec, and 500-1000 responses averaged for each current record.

Stimulation

A glass stimulus probe that was 400 μm in diameter and tapered to 140 μm at the tip was attached to a 4-mm-long piezoelectric bimorph element. The device is shown in Fig. 7b of Corey & Hudspeth, 1980a; it has a resonant frequency of 10 kHz. Oscillation of the probe following step displacements was largely eliminated by using as the driving voltage a step with a ramp onset (Corey & Hudspeth, 1980a). The ramp had either a linear or sigmoidal shape; a linear ramp was used for the majority of the experiments as it provided a slightly faster risetime for the probe (90 μs vs. 110 μs for a sigmoidal ramp).

The short length of bimorph greatly increased the size of the driving voltage needed for reasonable displacements (18 volts for a 2.0 μm step). To prevent electrical pickup of the driving signal by the epithelium, which was positioned just 0.5 cm from the bimorph, the bimorph and associated wiring were enclosed in grounded copper shielding with a small exit hole for the glass stimulus probe. Electrical pickup was measured at the end of an experiment by perfusing the upper bath with a normal endolymph to which was added 4 mM Ni^{++}, a potent blocker of the transduction channel. Any microphonic current signal in response to probe motion under these conditions was considered to be electrical pickup. A simpler method—measuring the current with the probe lifted off the otolithic membrane—was not satisfactory, as there was some fluid coupling to the otolithic membrane even with the probe lifted.

Motion of the probe and of the otolithic membrane was measured optically. Light from a 2-mW He-Ne laser was focused onto a single 60-μm glass fiber at one end of an optic fiber bundle; at the other end, the image of that fiber was focused with a 20X microscope objective to a 10-μm spot. The microscope objective was held by a micromanipulator, in order to position the spot on the object whose motion was of interest. The top and bottom of the experimental chamber were glass coverslips, to provide a continuous light path past the probe and macula that was unperturbed by an air-saline interface. A condenser lens below the experimental chamber collected the transmitted light and focused it onto a photodiode (United Detector Technology PIN-6D). The photocurrent was converted to voltage and amplified; the response time of the circuit, as measured with a pulsed LED, was 1.5 μs. This optical signal was low-pass filtered at 100 kHz with a 6-pole Bessel filter, then digitized at 5 or 10 μs per point before averaging.

To measure probe displacement, the light was focused on the edge of the sitmulus probe near its tip. Lateral displacements changed the amount of light

scattered or absorbed by the probe and so changed the recorded photocurrent. An absolute amplitude calibration was not possible with this arrangement, but the linearity was tested by driving the probe with a slow triangle wave and checking for deviation from linearity in the photocurrent. The amplitude calibration was obtained indirectly by observing the probe tip with a compound microscope at 1000X while driving it with a square wave of known size. The stimulator used for these experiments has a sensitivity of 0.11 μm/V.

The motion of the otolithic membrane was measured during experiments by focusing the spot of light on clumps of otoconia embedded in the membrane. The 50X dissecting microscope that was used did not have sufficient resolution to permit positioning the spot on a selected clump; instead, the spot was moved to a region containing several large clumps and then finely positioned to produce an optical signal when the otolithic membrane was moved. Lifting the probe off the otolithic membrane eliminated the microphonic current and the optical signal simultaneously. In a parallel set of experiments, the preparation was viewed with a compound microscope at 200X, and a similar optical recording system arranged. There it was possible to focus the spot on a single, identifiable clump, and to measure the distance from the stimulus probe to the clump. The propagation of the displacement along the otolithic membrane was measured by focusing on clumps successively further distant from the probe and measuring the delay in arrival of the displacement. The conduction velocity was found to be 6.5 $\pm$ 1.1 μm/μs (SD). It was not possible in the latter experiments to record the microphonic current simultaneously.

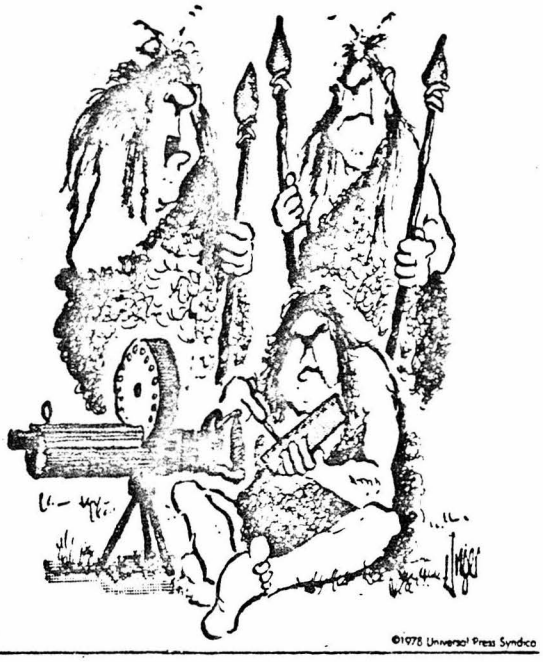

"Are you coming hunting, or are you gonna sit around here all day inventing?"

RESULTS

Latency of the response

If an accurate determination can be made of both the timecourse of hair bundle displacement and the timecourse of the current through the transduction channels, then the delay in onset of the current following a step displacement can be wholly attributed to the transduction process. The magnitude of the delay and its temperature dependence can suggest or rule out possible models for the mechanism of transduction. Any acceptable model must also be able to predict explicitly the magnitude of the current as a function of displacement and time. The mathematics of the modeling is most tractable when the displacements undergo instantaneous step changes, but the validity of the model depends on how well the instantaneous-step condition is met. The motion of the otolithic membrane during a step displacement is consequently of some importance.

The motion of the stimulus probe during a 'step' displacement was measured optically, and is shown in Fig. 1A. The displacement rises sigmoidally over 90 μs and has a slight oscillation following the rise. The motion of the otolithic membrane follows that of the stimulus probe with a delay of ∿30 μs. For this figure, the probe and the measured region of otolithic membrane were on opposite edges of the stimulated patch of macula, so the delay represents the maximum propagation time of the signal. The average delay between probe motion and the motion of the otolithic membrane is thus about 10 μs, when the probe is positioned in the middle of the patch.

Shortly after the otolithic membrane begins to move, the transepithelial current begins to increase. The current was measured with a voltage clamp compensated for the series resistance of the preparation; the response time of the clamp is shown in Fig. 1B. The capacitive-current transient following a voltage step has a time constant of 10-15 μs, which introduces a delay of that amount in the

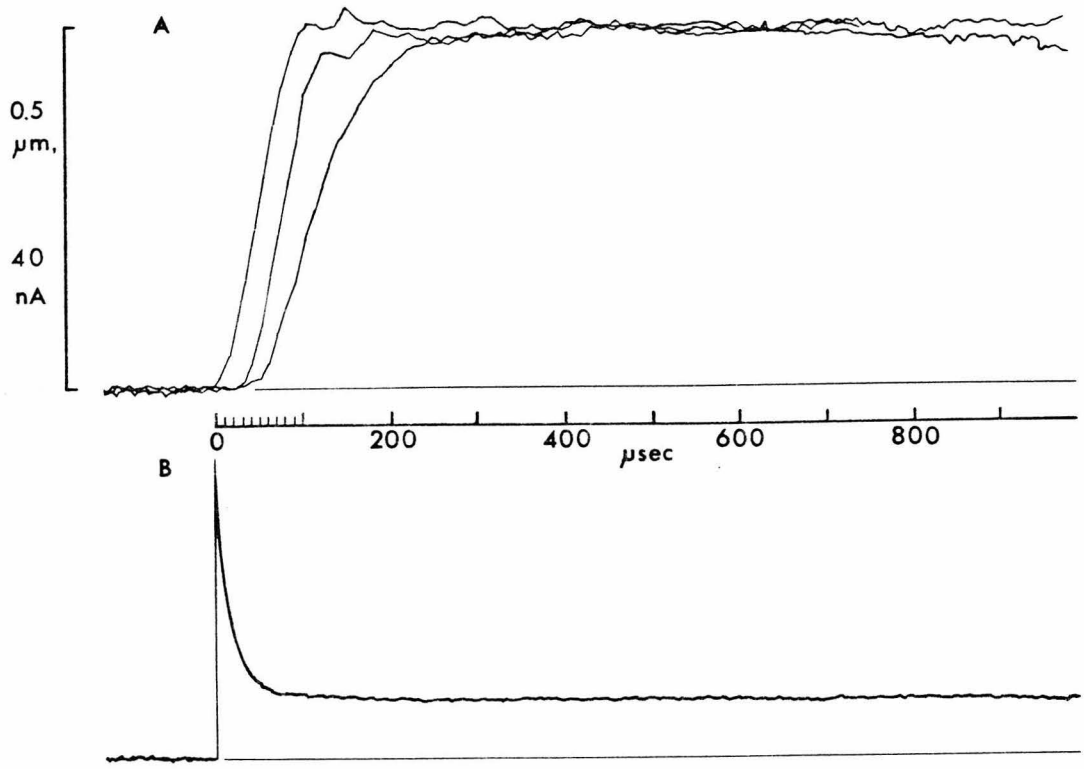

Fig. 1. Determination of the response latency. A, the displacement of the stimulus probe rises over 90 μs to a new position, followed in 30 μs by displacement of the otolithic membrane. The measured portion of membrane was ∿200 μm from the probe, so this delay represents the time required for the signal to propagate across the otolithic membrane. With the probe positioned in the middle of the stimulated patch, the average delay is about 10 μs. The microphonic current follows the otolithic membrane trace by about 30 μs, but shows a more gradual rise to equilibrium. B, the settling time of the voltage clamp in response to a step in command voltage. The capacitive current transient has a time constant of 10 μs. The current signal from the clamp in response to a step change in current rises to the final value with the same time constant (10 μs), or is delayed by that amount if the current changes more slowly. Normal Endolymph and High-K^+ Perilymph, 21.5 °C.

current signal measured by the voltage clamp. With these various delays taken into account, the measured delay in the rise of the microphonic current following a +0.5 μm displacement of the overlying otolithic membrane is between 30 and 40 μs. It remains an assumption that hair bundles follow the otolithic membrane with negligible delay; while we believe the assumption to be reasonable (see **DISCUSSION**), any lag occurring in that step would only decrease the delay attributable to the transduction mechanism.

Kinetics of the response

In Fig. 1A, the microphonic current in response to a +0.5 μm step closely follows the otolithic membrane motion throughout its rise. It is not possible to tell from this experiment whether the delay results from a fixed lag or whether it is a consequence of an opening rate for channels that is finite but short compared to the 90 μs risetime of the otolithic membrane. When smaller steps are presented, however, the rise of the current is slower (Fig. 2). The otolithic membrane is stationary at its new position during most of the rising phase of the current, and during this time the current shows a roughly exponential approach to its new value. The exponential approach suggests a number of mechanisms involving rate processes, whereby the rate of channel opening is proportional at any time to the number of unopened channels.

In addition, the apparent rate decreases with temperature (Fig. 2). The time constant of the relaxation for a step to +0.1 μm increases from 140 μs at 20.4 °C to 420 μs at 3.8°. The calculated Q_{10} for this process is about 2.0. The temperature dependence is consistent with a single transition from a closed to an open state of the channel, with the transition rate apparently a function of bundle position.

The kinetics of the microphonic current following step displacements of the otolithic membrane was consequently measured with a variety of displacement amplitudes. Experiments were done at a low temperature (4°) so that the rise of the

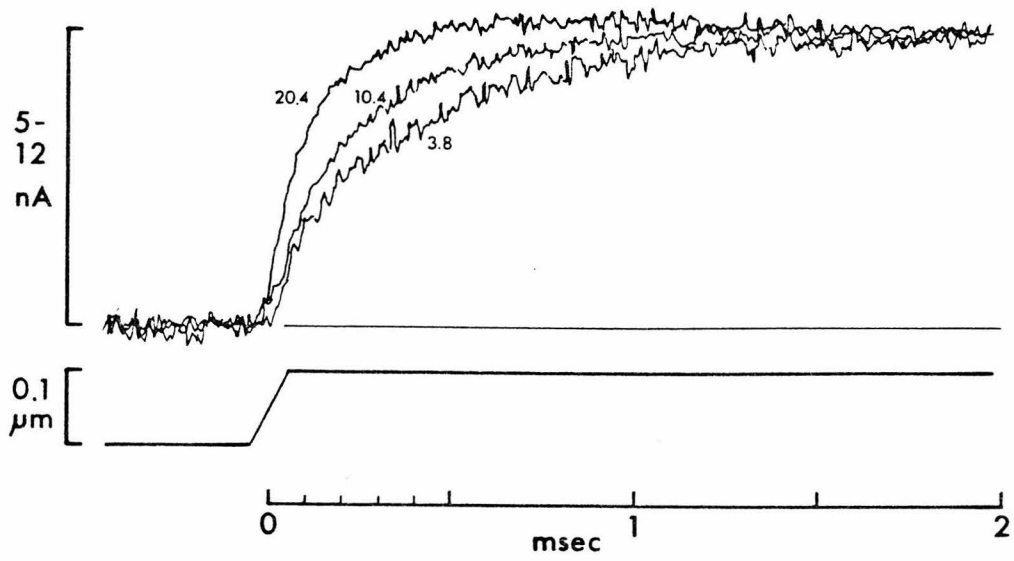

Fig. 2. Temperature dependence of the kinetics. Same conditions as in Fig. 1, but the stimulus was +0.1 μm rather than +0.5 μm. Note the change in time scale. Currents were normalized to the same height. The response at 20.2 °C has an exponential timecourse for the last portion of its rising phase, with a time constant of 140 μs. At 10.8° the response is slower, and at 3.8° is slower still (420 μs). The calculated Q_{10} is 1.9. The motion of the otolithic membrane derived from Fig. 1A is drawn as the stimulus.

current would be slow compared to the motion of the otolithic membrane. The responses to various displacements, from rest or from positively or negatively saturating positions, are shown in Fig. 3. Equilibrium values from Fig. 3A are plotted vs. displacement to construct a displacement-response curve (Fig. 4). The curves of Fig. 3 have several noteworthy features. In Fig. 3A,B the rising phases of currents are clearly dependent on displacement, being faster with more positive displacements. The kinetics is slowest for steps to bundle positions near zero, but is somewhat faster for negative displacements. The falling phases of currents are not as strikingly sensitive to displacement (Fig. 3C, and the negative steps of 3A): the responses to steps from +1.0 μm either to 0 μm or to -0.7 μm, for instance, have nearly equal timecourses.

The kinetics of the current cannot be described in general as a single exponential functions. Rather, the rising phases of Fig. 3B are sigmoidally shaped, especially so for small positive displacements, and the falling phases of Fig. 3C show a two-phase relaxation that is again particularly prominent for steps back to small positive positions. The deviation from a single time constant is shown more clearly in Fig. 5, where single exponential functions fitted to some parts of the curves fail to fit all parts. Fig. 5A also illustrates the variation in sigmoidicity with displacement: the step to 0 μm shows more sigmoidicity than that to +0.4 μm, and the step to +1.0 μm shows little, if any, deviation from an exponential function.

The equilibrium function of displacement (Fig. 4), as noted in Chapter I, is not a simple sigmoid. It has a region of high sensitivity near the resting position and saturates fairly abruptly with negative displacements. The saturation in the positive direction is more gradual: the microphonic current is not fully saturated even for displacements of +1.0 μm. This particular equilibrium curve is somewhat broader (less displacement-sensitive) than most; see for comparison Fig. 4 of Chapter I. Responses of this preparation were chosen for analysis, however, because the

Fig. 3. Kinetics of the microphonic current. In A, the otolithic membrane was moved from rest to various positions and held for 1200 μs, then returned to the rest postion. In B and C, the probe was first moved to the negative (B) or positive (C) extreme of the operating range, and then returned after 800 μs to various positions. The motion of the otolithic membrane derived from Fig. 1A is drawn as the stimulus trace. The voltage clamp was compensated as for Fig. 1B. Normal Endolymph and High-K^+ Perilymph, 3.8 °C.

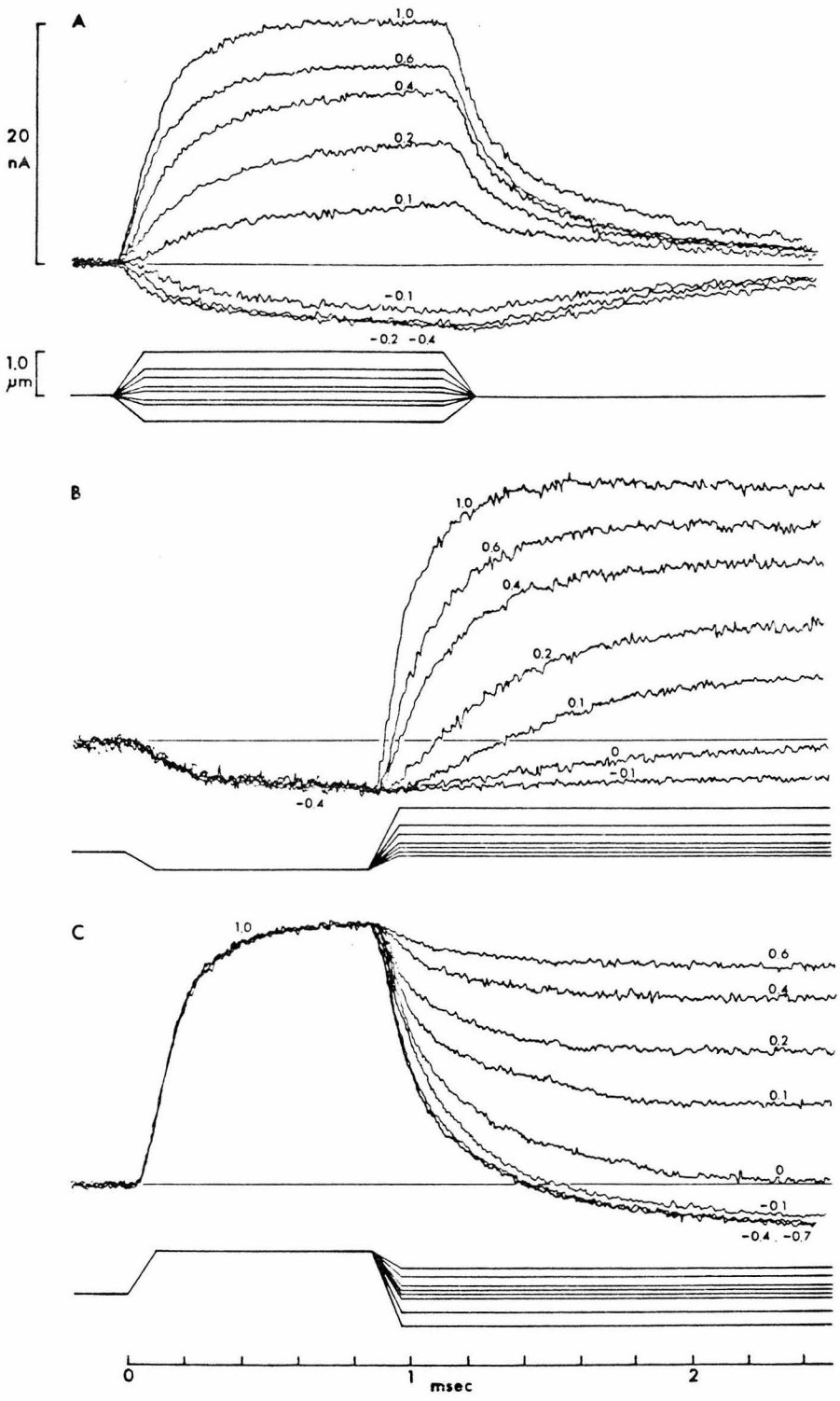
A
1.0
0.6
0.4
0.2
0.1
20
nA
-0.1
-0.2 -0.4
1.0
μm
B
1.0
0.6
0.4
0.2
0.1
0
-0.1
-0.4
C
1.0
0.6
0.4
0.2
0.1
0
-0.1
-0.4 -0.7
0
1
msec
2

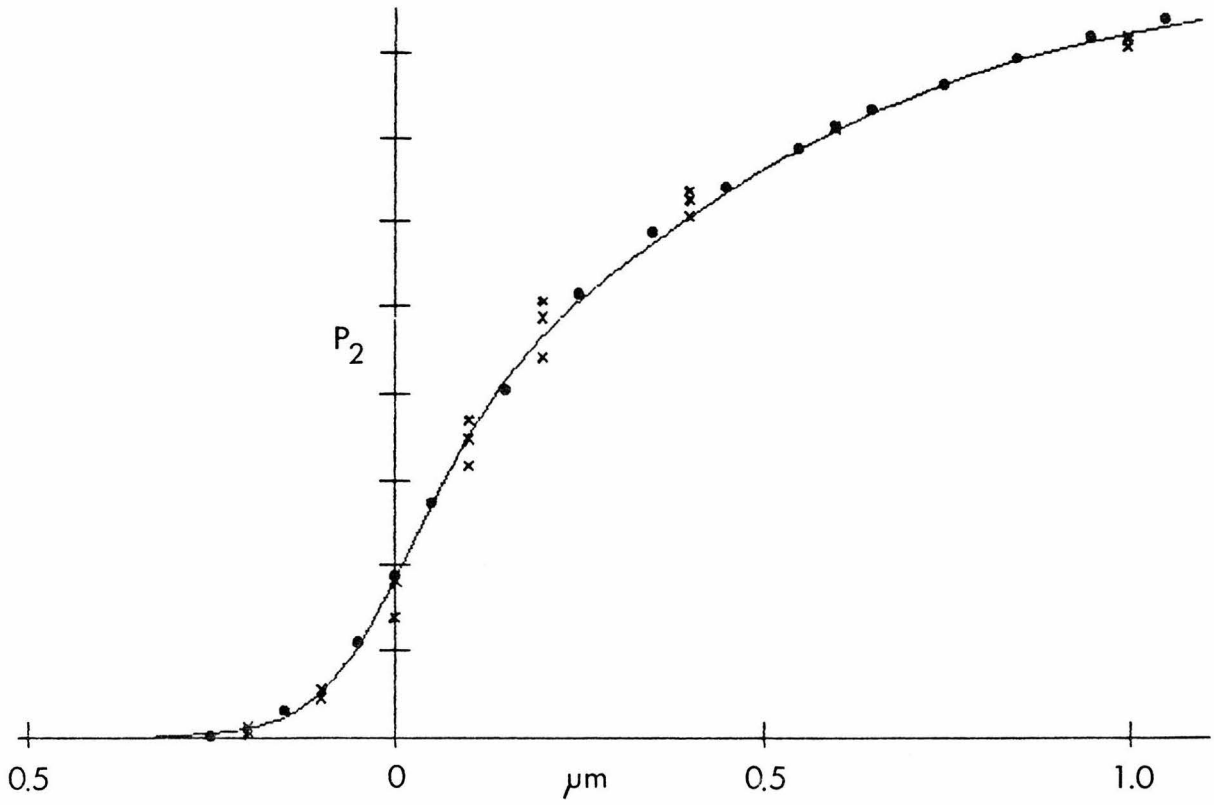

Fig. 4. Displacement-response curve derived from Fig. 3 (x) and from additional displacements to intermediate positions (•). The smooth curve was calculated from the mathematical model presented in the Appendix.

Fig. 5. Deviation from a single exponential function for some parts of the kinetics. A, an 800-μs step to-0.4 μm is followed by steps to +1.0 μm (top), +0.4 μm (middle), or +0.1 μm (bottom). The response to the +1.0 μm step is well-fitted by a single exponential of time constant 101 μs, except for some sag in the response at late times that corresponds to the beginning of the adaptive shift. An exponential fitted to the latter half of the middle trace (+0.4 μm) does not fit the first half, and this deviation is even more apparent for the bottom trace (+0.1 μm). B, an 800-μs step to +1.0 μm is followed by a return to 0 μm. The fast initial drop of the current is fitted with a single exponential curve, but the current diverges from the curve for the remainder of its fall. C and D, displacements for records A and B, respectively. Normal Endolymph and High-K^+ Perilymph, 3.8 °C.

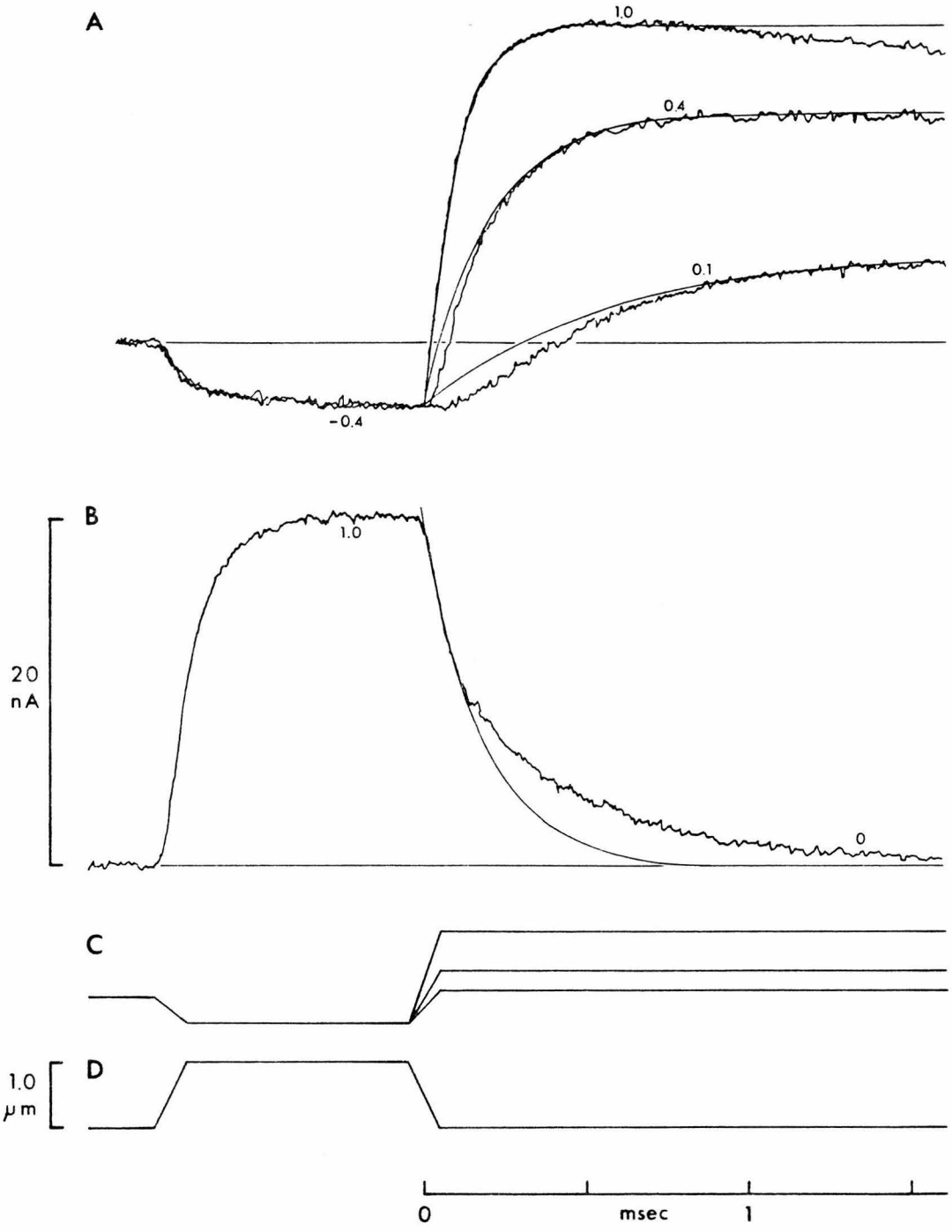
A
1.0
0.4
0.1
-0.4
B
1.0
20
nA
0
C
D
1.0
μm
0
msec
1

preparation was particularly stable over the several hours needed for recording. The responses are at least qualitatively the same among preparations, and a more complete quantitative comparison is underway.

A quantitative description of the microphonic current

An acceptable model for channel gating must be able to explain quantitatively the following features of the kinetics of the microphonic current: 1) the very fast rise of the current following a step displacement, 2) the nearly exponential approach to equilibrium for large displacements and deviation from an exponential timecourse for small displacements, 3) the equilibrium value of the current as a function of displacement, and 4) the temperature dependence of the kinetics. In this section we present a mathematical model that provides a reasonable fit to the observed currents. While the mathematics is developed with a specific model in mind, it should be understood that any model generating similar mathematics is equally plausible.

The model supposes that the transduction channel can exist at any time in one of three states; states 0 and 1 are nonconducting (closed) and state 2 is conducting (open):

$$0 \underset{k_{10}}{\overset{k_{01}}{\rightleftharpoons}} 1 \underset{k_{21}}{\overset{k_{12}}{\rightleftharpoons}} 2$$

There exist energy barriers to transitions that limit the rate of passage between states. The rate constants k_{ij} are of the general form

$$k_{ij} = f \exp(-G/RT)$$

where G is the free energy at the peak of the barrier. R and T are as usual and f is 6×10^{12} sec^{-1}. We assume for simplicity that the free energy G is wholly enthalpic and has no entropic contribution; clarification of this point awaits more extensive experiments over a range of temperatures. The energies of the states are changed by

displacing the hair bundle, and this causes a change in the equilibrium population of the open state. This change in relative energy of the open state underlies the displacement-response curve. Displacing the hair bundle changes the energies of the barriers as well, and thereby changes the rate of approach to equilibrium. The barrier heights and their change with displacement determine the kinetics of the current. As can be seen in the expression for k_{ij}, the temperature-dependence of the rate is also a function of the barrier height.

A more formal description of the model is presented in the Appendix to this chapter, where the equations describing the currents are derived. The expression for the timecourse of the current as a function of time and displacement contains eight free parameters which can be varied to fit the experimental data. Four of the parameters describe the equilibrium population of the open state as a function of displacement, and were chosen first to fit the displacement-response curve. The other four were subsequently varied to fit the kinetics. While the specific parameters chosen are not likely to be exactly correct and vary somewhat among preparations, the approximate value of each of the parameters chosen was critical: if any of the eight was changed significantly, the fit became quite poor.

The energies of all three states were set approximately equal at zero displacement. Thus about a third of the channels are open at the resting bundle position. Positive displacements reduce the energies of states 1 and 2, and so populate those states, but the transition from state 0 to 1 was made very sensitive to displacement while that from 1 to 2 was made less so. The sharp negative saturation of the displacement-response curve is then a consequence of all channels being driven to state 0, and the gradual positive saturation reflects the gradual populating of state 2 from state 1. A fit to the measured data is shown in Fig. 4. The variation in the kinetics is fitted by making the barrier between 0 and 1 rate-limiting for small displacements. As that transition is very displacement-sensitive, the barrier height is

lessened drastically with either negative or positive displacement; the barrier from 1 to 2 then become rate-limiting. The sigmoidal rise observed in Figs. 3C and 5A can now be understood with this model. A negative step drives all the channels to state 0. Following a subsequent positive step, channels must pass through state 1 to reach the open state 2. For small displacements, the transition to state 1 is rate-limiting, causing the lag before onset of the current. For large displacements it is not: the current rises immediately following the step. The sigmoidal rise is not so striking for displacements from rest; state 1 is moderately populated at rest and transitions to the open state begin immediately after positive displacements. The two-phase fall of the current can be understood in similar terms, but will not be elaborated. Note only that making the transition from $2 \rightarrow 1$ not very sensitive to displacement leads to nearly constant rates for the fall.

The predictions of the model for displacements equal to those of Figs. 2 and 3 are shown in Fig. 6. The parameters chosen for this fit are:

G_1	0.35 kcal/mol
G_2	0.3 kcal/mol
z_1	-10.0 kcal/mol·μm
z_2	-1.5 kcal/mol·μm
G_{01}	12.2 kcal/mol
G_{12}	11.9 kcal/mol
δ_{01}	.35
δ_{12}	.50
T	3.8 °C

It is clear that the model predicts the experimentally measured responses with reasonable quantitative agreement. The temperature dependence, at least to the extent that it has been studied, is also predicted by the model. The calculated Q_{10} is 1.95 for steps to +0.1 μm, reflecting the height of barrier G_{01}.

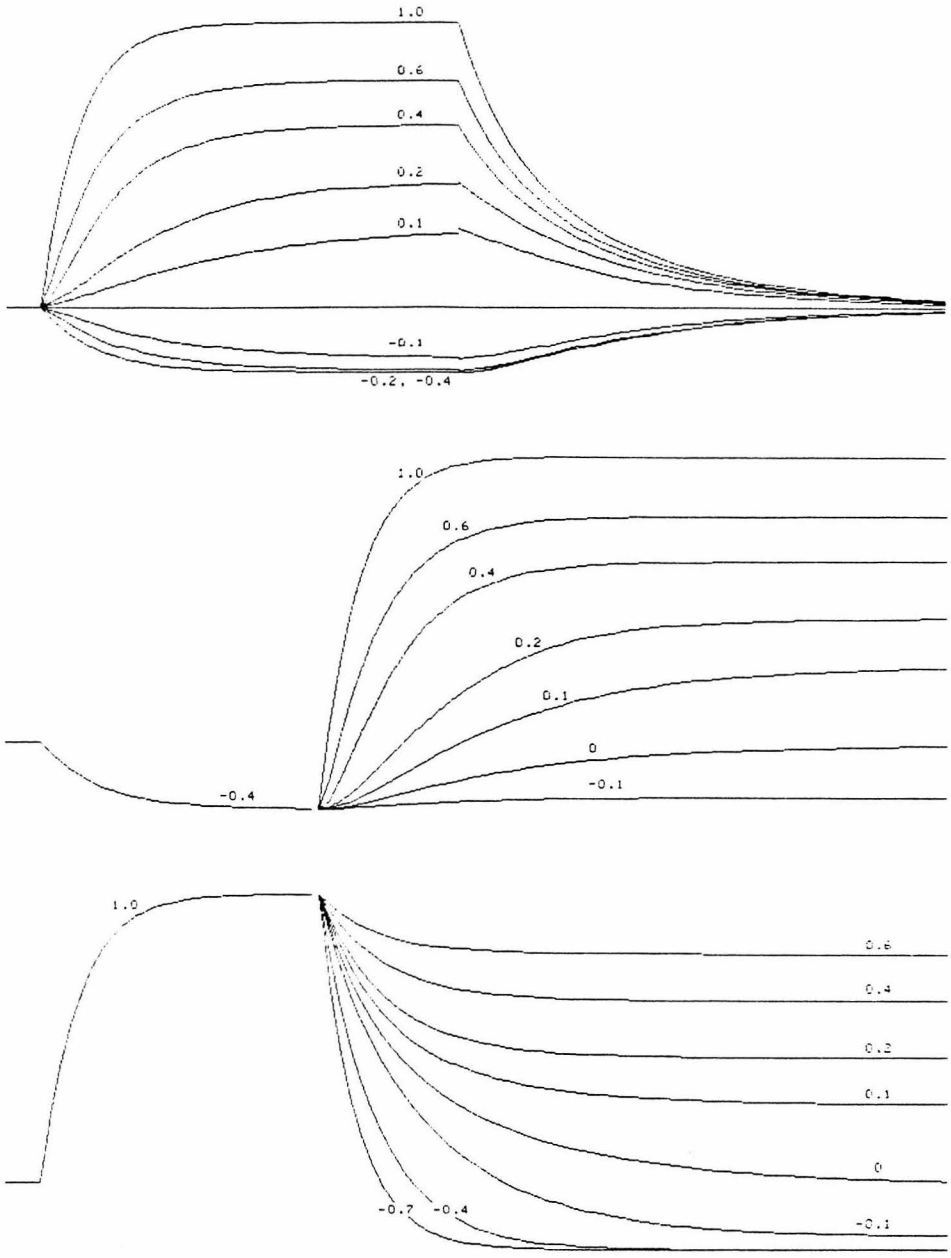

Fig. 6. Currents predicted by the mathematical model. The calculated responses are to displacements and at a temperature equal to those of Fig. 3. The vertical axis was scaled to match the saturated current levels of Fig. 3, but the currents are otherwise determined by the eight parameters of the model. The major deviation from the measured currents occurs in C, for steps from +1.0 μm to -0.4 or -0.7 μm.

DISCUSSION

Latency

The very short latency of the microphonic current in response to a step displacement by itself places some constraints on possible models for the transduction process. Forty microseconds, for instance, permits ionic diffusion of no more than 0.5 μm, assuming three-dimensional diffusion of an ion with diffusion constant $D = 1.3 \times 10^{-5}$ cm^2/s, as for K^+ in squid axoplasm (Hodgkin & Keynes, 1953). If a second messenger is involved in hair cell transduction, the last mechanical stage must be physically close to the ionic conductance element. The temperature dependence argues against a diffusion-limited second messenger, as the Q_{10} for diffusion ranges from 1.05 for a neutral species to about 1.3 for an electrolyte, both much lower than the measured Q_{10} of 2.0.

We favor instead the model developed above, in which the energies of states of the channel are directly and continuously changed by bundle position. Before acceptance of the model, however, a number of possible artifacts must be considered.

Sources of artifact

Hair bundles might not follow directly the motion of the overlying otolithic membrane: the exponential rise of the current could in fact reflect a relaxation of the bundle to the new position. This is unlikely, because the Reynolds number for otolithic membrane motion is much less than 1 with the displacement velocities presented here. Mechanical motions of a hair bundle are dominated by viscous forces, and the inertia of the bundle is negligible. Viscous forces are applied by the fluid between the apical surface of the epithelium and the lower surface of the otolithic membrane; if these are considered as infinite planar surfaces moving relative to each other, then the shear profile is linear with height above the apical surface. Even if stereocilia were completely flexible elements and not attached at their tips to the otolithic membrane, they would move over short times as rigid elements bending at

their bases. As it is likely that the adequate stimulus for stereocilia is bending at their bases, it seems improbable that relaxation of the bundle is a source of artifact.

Individual hair bundles might have different resting biases, or the stimulus probe might drift in position during an experiment. Records would then be distorted by a smear of apparent displacements. The existence of the adaptation mechanism probably mitigates the latter difficulty, as the effective bias on transduction elements within each hair cell relaxes to a rest position within seconds. Intracellular recording reveals a reasonable homogeneity in resting biases of hair cells in the peripheral macula (A. J. Hudspeth, unpublished observations), arguing against the former objection.

A similar smear in displacement sensitivities might occur among cells, or even among transduction elements of a single cell. However, the variation among cells is probably small. Bundle orientations are spread over no more than 80° in the peripheral patch; as the stimulus direction bisects the orientation, the effective stimulus—proportional to the cosine of orientations—varies by 20%. The variation within a cell is harder to estimate and might be significant, since the lengths of stereocilia vary by more than two-fold within a bundle. The angular displacement of different stereocilia can be calculated from the geometry of the bundle for a given displacement at the tip of the kinocilium. In fact, the geometry is such that the variation in angular displacement for all stereocilia of a bundle is no more than a few percent (calculation of A. J. Hudspeth). Some variation in displacement sensitivity is unavoidable, and in this respect the gating stimulus is much less well-defined than that for voltage-dependent channels. It is probably not severe enough to upset the validity of the model.

We have assumed that the energy change associated with displacement of the hair bundle is a linear function of displacement, and we set z_1 and z_2 as the coefficients of proportionality in the equations. The energy change might instead be

considerably nonlinear with displacement. The displacement-response curve, for instance, might result from a simple distribution between just two states; its failure to fit a simple sigmoid of the form

$$P = \frac{1}{1 + \exp(-G)}$$

would reflect instead the nonlinearity of the energy change. There is no way of knowing whether this possibility is reasonable. We can say at least that it is not sufficient to explain all of the observed phenomena; specifically, it cannot produce the observed two-phase kinetics of the microphonic current. A model involving transitions between just two states generates relaxation kinetics that are single exponential functions, no matter what may be the relation between displacement and equilibrium values.

A two-state model might explain the kinetics of the current if the smear in displacement sensitivities produced a smear in time constants. The current in response to a step displacement would then be a sum of single exponentials with a range of time constants. This possibility could explain the fall in microphonic current following a step displacement, but it cannot explain the sigmoidal rise in currents. For all step responses, it would predict a fast change followed by a slower relaxation, but never a sigmoidal onset to the current.

The sigmoidicity of the kinetics for some steps argues as well against improper series-resistance compensation in the voltage clamp. Undercompensation adds a second, slow phase to a single exponential, overcompensation gives a single exponential an overshooot, but neither can generate sigmoids and both have a consistent effect on currents, whether rising or falling.

Although the latency of the response argues against a diffusion process, it does not rule it out. If channel gating were arbitrarily fast, and distances small, then diffusion of an activating substance from a nearby site of production could explain

the delay. With more complicated schemes it could also explain a two-phase kinetics: multiple sequential compartments with restricted access between them would produce the same effects as the sequential states of the channel in our model. The temperature dependence is still a strong argument, however, against any model in which diffusion is the rate-limiting process.

We conclude that the model remains at least qualitatively valid, although some sources of artifact—in particular the smear of sensitivities and the questionable linearity of the energy as a function of displacement—may produce small quantitative errors.

Further tests of the model

A more confident acceptance of the model requires a number of additional experiments. The displacement-response curve, for instance, is a function of Ca^{++} (or H^{+}) concentration in both its position and shape. The change induced by the ion should be interpretable as a modification of the transduction element in terms of this model, and the modification would predict specific changes in the kinetics. The temperature dependence of the kinetics should also be studied in detail, both to see whether the model holds for a range of temperatures and to check for entropic contributions to the energies. Models for voltage-dependent channels have been confirmed (or eliminated) by measuring the power spectrum of current fluctuations (Anderson & Stevens, 1973; Sigworth, 1980) or by recording gating currents corresponding to the motion of charged portions of channel molecules (Armstrong & Bezanilla, 1976; Nonner, 1980). Spectral analysis is conceivable for this preparation: the model predicts a spectrum with two Lorentzian components, whose characteristic frequencies depend on the bundle position. The test is technically formidible, however, as the expected fluctuations are of very high frequency. The recording system must have intrinsic current noise of < 0.2 nA rms at a bandwidth of 20 kHz. Mechanical noise introduced by a stimulus probe or by Brownian motion of the hair

bundle would introduce artifactual fluctuations in the equilibrium current; the mechanical noise of the probe used here, 0.003 μm rms, is probably inadequate. Gating currents, on the other hand, are not expected to be a useful test, as they are not predicted by the model. No voltage sensitivity of the gating mechanism has been found (Chapter II, Fig. 7), implying that there is no net displacement of charged groups through the membrane field that is associated with the mechanical gating.

Implications for a model of transduction

The simplest and most basic interpretation of this study is that transduction in vertebrate hair cells involves a direct mechanical link between displacement of stereocilia and the element that produces a membrane conductance change. We suspect but certainly have not demonstrated that this element is a membrane protein, that it can exist in states that correspond to different conformations of the protein, one of which forms a transmembrane channel, and that the free energies of the conformations are changed by a mechanically applied stress consequent upon stereociliary bend. Two general observations support this interpretation. The latency of the response and the temperature dependence of the latency are not consistent with a link involving a chemical messenger, unless that messenger is created and liberated near enough to the conductance element so its diffusion is not rate-limiting. The transition rate of the channel to an open state must then be rate-limiting; the scheme is of the following general form:

$$M + C \rightleftharpoons CM \rightleftharpoons CM^*$$

where M is the messenger, C is the channel, and CM^* is the conducting state of the complex. This scheme is inconsistent with the observed variation in kinetics of the current with bundle position, as it separates the conductance element from positional information. Models that suppose that creation of a chemical messenger is both dependent on bundle position and rate-limiting, and that neither diffusion of the

messenger nor subsequent opening of the channel are rate-limiting, could possibly be made to fit the data, but seem unnecessarily baroque. The simplest interpretation of the involves invovles a direct link to the transduction channel.

APPENDIX TO CHAPTER IV

The transduction channel is assumed to exist at any time in one of three states. Two are nonconducting states (closed) and one is conducting (open); the states differ in their free energies at rest and in the change in free energy occurring with hair bundle displacement. The channel must surmount large energy barriers to move between states; the two barriers (between states 0 and 1, and 1 and 2) differ in their peak energies, and in the change in peak energy with displacement. The model is completely described with 8 parameters, shown schematically below.

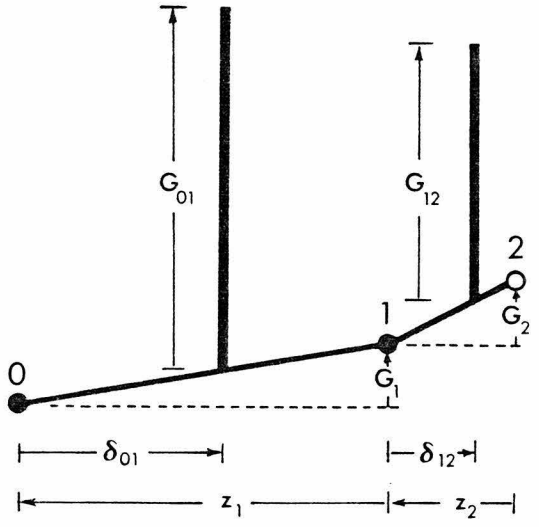

State 1 (closed) has a higher free energy than state 0 (closed) by an amount G_1 kcal/mol, and state 2 (open) is higher than state 1 by G_2. The change in G_1 with displacement is $z_1 D$, where z_1 is in kcal/mol·μm, and D is hair bundle displacement in μm. A greater displacement sensitivity is shown schematically as a longer distance z. (Both z's are negative, to reduce the energies of states 1 and 2 with positive displacements.) The height of the barrier to transitions between states 0 and 1 is G_{01}, measured above a linear baseline. The barrier "feels" some proportion δ_{01} of the energy of state 1; δ_{01} ranges from 0 to 1.0 and is shown schematically as a

proportion of the distance z_1. The free parameters are thus:

parameters		units
G_1	G_2	kcal/mol
Z_1	Z_2	kcal/mol·μm
G_{01}	G_{12}	kcal/mol
δ_{01}	δ_{12}	-

The rate of transition over a barrier is determined by the difference in energy between the state and the peak of the barrier. The rate constant k_i is:

$$k_i = f \exp(-\Delta G/RT)$$

where $f = kT/h = 6 \times 10^{12}$ sec^{-1} and k, T, h and R have their usual thermodynamic meanings. There are then four rate constants (transitions directly between states 0 and 2 are forbidden):

$$k_{01} = f \exp(-[G_{01} + \delta_{01}(G_1 + z_1 D)]/RT)$$

$$k_{10} = f \exp(-[G_{01} + (\delta_{01} - 1)(G_1 + z_1 D)]/RT)$$

$$k_{12} = f \exp(-[G_{12} + \delta_{12}(G_2 + z_2 D)]/RT)$$

$$k_{21} = f \exp(-[G_{12} + (\delta_{12} - 1)(G_2 + z_2 D)]/RT$$

The derivation to this point is obviously intended to be similar to that for charged species moving under the influence of an electric field. The displacement sensitivity z is equivalent to valence, and the displacement D is equivalent to membrane potential. See Appendix to Chapter II. The derivation differs from some other descriptions of three-state models for channel gating (e.g., Chiu, 1977), in that it gives the rate constants in terms of explicit energies of states, rather than using the general form:

$$k_i = \exp(A + B \cdot D).$$

Both approaches have the same number of free parameters (8), but in this derivation the parameters represent physical characteristics of the channel rather than unitless free parameters.

With the rate constants, we can solve for the distribution of channels among the three states. Let P_0 be the proportion of channels that are in state 0 (or alternatively, the probability that a channel is in state 0). The change in P_0 with time is then

$$\frac{dP_0}{dt} = -k_{01}P_0 + k_{10}P_1.$$

Similarly,

$$\frac{dP_1}{dt} = -k_{10}P_1 + k_{01}P_0 - k_{12}P_1 + k_{21}P_2$$

and

$$\frac{dP_2}{dt} = -k_{21}P_2 + k_{12}P_1.$$

At equilibrium

$$\frac{dP_0}{dt} = \frac{dP_1}{dt} = \frac{dP_2}{dt} = 0$$

and at any time

$$P_0 + P_1 + P_2 = 1.$$

These five expressions may be solved to find the equilibrium values of the probabilities:

$$P_1 = \frac{1}{1 + \frac{k_{12}}{k_{21}} + \frac{k_{10}}{k_{01}}}, \quad P_0 = \frac{k_{10}}{k_{01}} P_1 \quad \text{and} \quad P_2 = \frac{k_{12}}{k_{21}} P_1$$

The equilibrium probability of the channel being in the open state (P_2) can be expressed in terms of the energies of the states, by substituting the defined expressions for the rate constants k_{ij}:

$$P_2 = \frac{1}{1 + \exp([G_2 + z_2 D]/RT)(1 + \exp([G_1 + z_1 D]/RT))}$$

Note that, as might be expected, the heights and positions of the barriers drop out: the equilibrium probability is determined by the energies and displacement sensitivities of the states.

If the displacement is jumped to a new value, the probability of being in the open state relaxes to a new equilibrium value. The time course of the relaxation is described by a second-order differential equation

$$\frac{d^2P_2}{dt^2} + C_2 \frac{dP_2}{dt} + C_1 P_2 + C_0 = 0$$

where the coefficients are $C_0 = -k_{01}k_{12}$

$$C_1 = k_{12}k_{01} + k_{21}k_{01} + k_{21}k_{10}$$

and $$C_2 = k_{12} + k_{21} + k_{10} + k_{01}.$$

This has the general solution

$$P_2(t) = P_{0e} + K_1 \exp(-L_1 t) + K_2 \exp(-L_2 t)$$

where $$L_1 = \tfrac{1}{2}[C_2 + (C_2{}^2 - 4C_1)^{\frac{1}{2}}]$$

$$L_2 = \tfrac{1}{2}[C_2 - (C_2{}^2 - 4C_1)^{\frac{1}{2}}]$$

$$K_1 = [(k_{12} + k_{21} - L_2)P_{2i} + k_{12}P_{0i} - k_{12} + L_2 P_{2e}]/[L_1 - L_2]$$

and $$K_2 = P_{2i} - P_{2e} - K_1.$$

P_{0i} and P_{2i} are probabilities immediately before the step, and P_{0e} and P_{2e} are equilibrium values after the step, defined as above.

The relaxation is thus the sum of two exponential functions of time, with time constants $1/L_1$ and $1/L_2$. The time constants are not simple expressions: each has fourteen terms that are combinations of rate contants, and each rate constant is an exponential function of four parameters as defined above. At the extremes of

displacement, of course, the time constants will usually be dominated by a single rate constant. The plot below gives values for the four rate constants, and for the lumped rate constants L_1 and L_2, as a function of displacement. The parameters chosen for this plot are close to those that fit the experimental data.

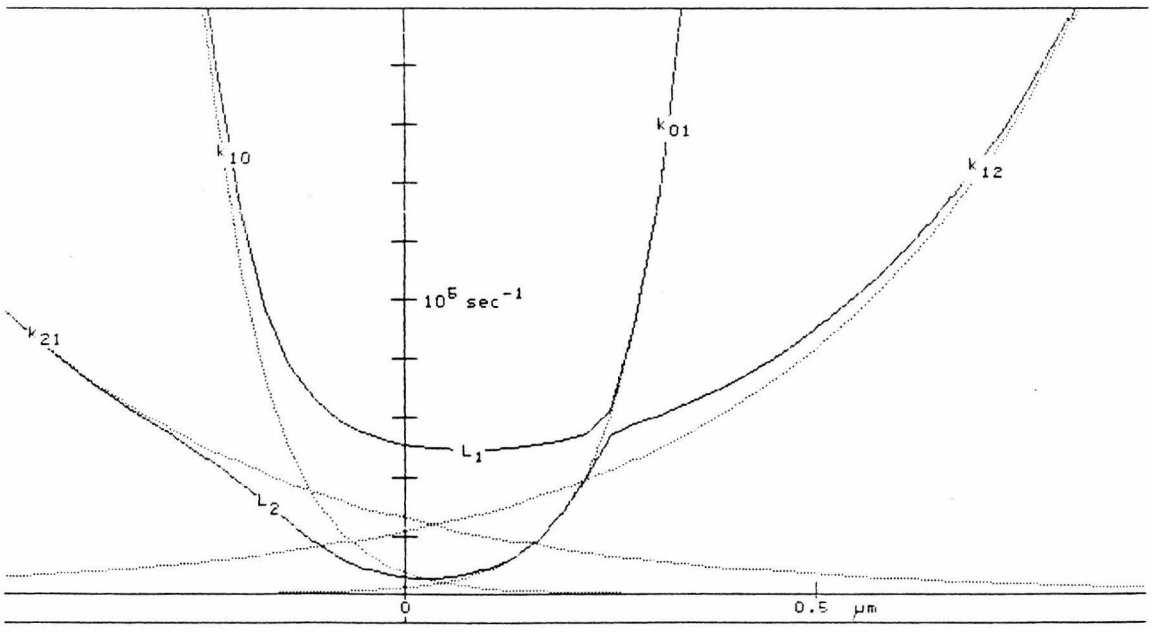

REFERENCES

Adams, D. J. & Gage, P. W. (1979). Sodium and calcium gating currents in an Aplysia neurone. J. Physiol. **291**, 467-481.

Adrian, E. D. (1931). The microphonic action of the cochlea: an interpretation of Wever and Bray's experiments. J. Physiol. **71**, xxvii-xxix.

Adrian, E. D. (1928). The Basis of Sensation. London: Christophers.

Aickin, C. C. & Thomas, R. C. (1977). An investigation of the ionic mechanism of intracellular pH regulation in mouse soleus muscle fibers. J. Physiol. **273**, 295-316.

Anderson, C. R. & Stevens, C. F. (1973). Voltage clamp analysis of acetylcholine produced end-plate current fluctuations at frog neuromuscular junction. J. Physiol. **235**, 655-691.

Armstrong, C. M. & Bezanilla, F. (1977). Inactivation of the sodium channel. II. Gating current experiments. J. gen. Physiol. **70**, 567-590.

Baker, P. F. & Honerjäger, P. (1978). Influence of carbon dioxide on level of ionized calcium in squid axons. Nature, Lond. **273**, 160.

Bastian, B. L. & Fain, G. L. (1979). Light adaptation in toad rods: requirement for an internal messenger which is not calcium. J. Physiol. **297**, 493-520.

Baylor, D. A. & Fettiplace, R. (1977). Transmission from photoreceptors to ganglion cells in turtle retina. J. Physiol. **271**, 391-424.

Baylor, D. A., Lamb, T. D. & Yau, K.-W. (1979). Responses of retinal rods to single photons. J. Physiol. **288**, 613-634.

von Békésy, G. (1950). D-C potentials and energy balance of the cochlear partition. J. acoust. Soc. Am. **22**, 576-582.

von Békésy, G. (1951). Microphonics produced by touching the cochlear partition with a vibrating electrode. J. acoust. Soc. Am. **23**, 29-35.

von Békésy, G. (1952a). D-C resting potentials inside the cochlear partition. J. acoust. Soc. Am. **24**, 72-76.

von Békésy, G. (1952b). Gross localization of the place of origin of the cochlear microphonics. J. acoust. Soc. Am. **24**, 399-409.

von Békésy, G. (1962). The gap between the hearing of external and internal sounds. Symp. Soc. exp. Biol. **16**, 267-288.

Bezanilla, F. & Armstrong, C. M. (1972). Negative conductance caused by entry of sodium and cesium ions into the potassium channels of squid axons. J. Gen. Physiol. **60**, 588-608.

Boron, W. F. & De Weer, P. (1976). Intracellular pH transients in squid giant axons caused by CO_2, NH_3, and metabolic inhibitors. J. gen. Physiol. **67**, 91-112.

Bosher, S. K. & Warren, R. L. (1978). Very low calcium content of cochlear endolymph, an extracellular fluid. Nature, Lond. **273**, 377-378.

Brown, J. E., Brown, P. K. & Pinto, L. H. (1977). Detection of light-induced changes of intracellular ionized calcium concentration in Limulus ventral photoreceptors using arsenazo III. J. Physiol. **267**, 299-320.

Chiu, S. Y. (1977). Inactivation of sodium channels: second order kinetics in myelinated nerve. J. Physiol. **273**, 573-596.

Claude, P. & Goodenough, D. A. (1973). Fracture faces of zonulae occludentes from "tight" and "leaky" epithelia. J. Cell Biol. **58**, 390-400.

Clausen, C., Lewis, S. A. & Diamond, J. M. (1979). Impedance analysis of a tight epithelium using a distributed resistance model. Biophys. J. **26**, 291-318.

Corey, D. P. (1979). Notes on the single barrier model. (Unpublished.)

Corey, D. P. & Hudspeth, A. J. (1979a). Response latency of vertebrate hair cells. Biophys. J. **26**, 499-506.

Corey, D. P. & Hudspeth, A. J. (1979b). Ionic basis of the receptor potential in a vertebrate hair cell. Nature, Lond. **281**, 675-677.

Corey, D. P. & Hudspeth, A. J. (1979c). Ionic basis of the receptor current in a vertebrate hair cell. Soc. Neurosci. Abstr. **5**, 18 (abstract).

Corey, D. P. & Hudspeth, A. J. (1980a). Mechanical stimulation and micromanipulation with piezoelectric bimorph elements. Am. J. Physiol. (submitted).

Dallos, P. (1973). The Auditory Periphery. New York: Academic.

Davis, H. (1953). Energy into nerve impulses: hearing. Med. Bull. St. Louis Univ. **5**, 43-48.

Davis, H. (1965). A model for transducer action in the cochlea. Cold Spring Harb. Symp. quant. Biol. **30**, 181-190.

Dodge, F. A., Knight, B. W. & Toyoda, J. (1968). Voltage noise in Limulus visual cells. Science, N.Y. **160**,88-90.

Dowling, J. E. (1963). Neural and photochemical mechanisms of visual adaptation in the rat. J. gen. Physiol. **46**, 1287-1301.

Dwyer, T. M., Adams, D. J. & Hille, B. (1979). Ionic selectivity of end-plate channels. Biophys. J. **25**, 671 (abstract).

Eatock, R. A., Corey, D. P. & Hudspeth, A. J. (1979). Adaptation in a vertebrate hair cell: stimulus-induced shift of the operating range. Soc. Neurosci. Abstr. **5**, 19.

Eaton, D. C. (1972). Potassium ion accumulation near a pace-making cell of Aplysia. J. Physiol. **224**, 421-440.

Eyring, H. (1936). Viscosity, plasticity, and diffusion as examples of absolute reaction rates. J. Chem. Phys. **4**, 283-291.

Eyring, H., Lumry, R. & Woodbury, J. W. (1949). Some applications of modern rate theory to physiological systems. Record Chem. Prog. **10**, 100-114.

Flock, Å. (1965). Electron microscopic and electrophysiological studies on the lateral line canal organ. Acta oto-lar (suppl.) **199**, 1-90.

Flock, Å. & Russell, I. (1976). Inhibition by efferent nerve fibers: action on hair cells and afferent synaptic transmission in the lateral line canal organ of the burbot Lota lota. J. Physiol. **257**, 45-62.

Flock, Å. & Wersäll, J. (1962). A study of the orientation of the sensory hairs of the receptor cells in the lateral line organ of fish, with special reference to the function of the receptors. J. Cell Biol. **15**, 19-27.

Frankenhauser, B. & Hodgkin, A. L. (1957). The action of Ca^{++} on the electrical properties of squid axons. J. Physiol. **137**, 218-244.

Fukami, Y. & Hunt, C. C. (1977). Structures in sensory region of snake spindles and their displacement during stretch. J. Neurophysiol. **40**, 1121-1131.

Furukawa, T. & Ishii, Y. (1967a). Effects of static bending of sensory hairs on sound reception in the goldfish. Jap. J. Physiol. **17**, 572-588.

Furukawa, T. & Ishii, Y. (1967b). Neurophysiological studies on hearing in goldfish. J. Neurophysiol. **30**, 1377-1403.

Furukawa, T., Ishii, Y. & Matsuura, S. (1972). An analysis of microphonic potentials of the sacculus of goldfish. Jap. J. Physiol. **22**, 603-616.

Geisler, C. D., Mountain, D. C., Hubbard, A. E., Adrian, H. O. & Ravindran, A. (1977). Alternating electrical-resistance changes in the guinea-pig cochlea caused by acoustic stimuli. J. acoust. Soc. Am. **61**, 1557-1566.

Getchell, T. V. & Shepherd, G. M. (1978). Adaptive properties of olfactory receptors analyzed with odour pulses of varying durations. J. Physiol. **282**, 541-560.

Goldman, D. E. (1943). Potential, impendance and rectification in membranes. J. gen. Physiol. **27**, 37-60.

Hagiwara, S. & Yoshii, M. (1979). Effects of internal potassium and sodium on the anomalous rectification of the starfish egg as examined by internal perfusion. J. Physiol. **292**, 251-265.

Harris, G. G., Frishkopf, L. S. & Flock, Å. (1970). Receptor potentials from hair cells of the lateral line. Science, N.Y. **167**, 76-79.

Hille, B. (1971). Voltage clamp studies on myelinated nerve fibers. In Biophysics and Physiology of Excitable Membranes, ed. Adelman, W. J. New York: Van Nostrand Reinhold.

Hille, B. (1973). Potassium channels in myelinated nerve: selective permeability to small cations. J. gen. Physiol. **61**, 669-686.

Hille, B. (1975). Ionic selectivity of Na and K channels of nerve membranes. In sodium channels of nerve: divalent ions, monovalent ions, and pH. Phil. Trans. R. Soc. B **270**, 301-318.

Hodgkin, A. L. & Huxley, A. F. (1952). A quantitative description of membrane current and its application to conduction and excitation in nerve. J. Physiol. **117**, 500-544.

Hodgkin, A. L. & Katz, B. (1949). The effect of sodium ions on the electrical activity of the giant axon of the squid. J. Physiol. **108**, 37-77.

Hodgkin, A. L. & Keynes, R. D. (1953). The mobility and diffusion constant of potassium in giant axons from Sepia. J. Physiol. **119**, 513-528.

Honrubia, V. & Ward, P. H. (1969). Dependence of the cochlear microphonics and the summating potential on the endocochlear potential. J. acoust. Soc. Am. **46**, 388-392.

Hubbard, A. E., Geisler, C. D. & Mountain, D. C. (1977). Comparisons between CM and apparent resistance changes in scala media. J. acoust. Soc. Am. **61**, S95.

Hubbard, A. E., Mountain, D. C. & Geisler, C. D. (1979). The spectral content of the cochlear microphonic measured in scala media of the guinea pig cochlea. J. acoust. Soc. Am. **66**, 415-430.

Hubbell, W. L. & Bownds, M. D. (1979). Visual transduction in vertebrate photoreceptors. A. Rev. Neurosci. **2**, 17-34.

Hudspeth, A. J. (1980). Fine structure of hair cells and supporting cells in bullfrog saccular epithelium. (In preparation.)

Hudspeth, A. J. & Corey, D. P. (1977). Sensitivity, polarity, and conductance change in the response of vertebrate hair cells to controlled mechanical stimuli. Proc. natn. Acad. Sci. U.S.A. **74**, 2407-2411.

Hudspeth, A. J. & Jacobs, R. (1979). Stereocilia mediate transduction in vertebrate hair cells. Proc. natn. Acad. Sci. U.S.A. **76**, 1506-1509.

Huxley, A. F. & Simmons, R. M. (1971). Proposed mechanism of force generation in striated muscle. Nature, Lond. **233**, 533-538.

Jielof, R., Spoor, A. & de Vries, H. L. (1952). The microphonic activity of the lateral line. J. Physiol. **116**, 137-157.

Kilbride, P. & Ebrey, T. G. (1979). Light-initiated changes of cyclic guanosine monophosphate levels in the frog retina measured with quick-freezing techniques. J. gen. Physiol. **74**, 415-426.

Kirsch, G. E. & Narahashi, T. (1978). 3,4-diaminopyridine: a potent new potassium channel blocker. Biophys. J. **22**, 507-512.

Konishi, T., Kelsey, E. & Singleton, G. T. (1966). Effects of chemical alteration in the endolymph on the cochlear potentials. Acta Otolaryngol. **62**, 393-404.

Kroese, A. B. A. & van den Bercken, J. (1980). Dual action of ototoxic antibiotics on sensory hair cells. Nature, Lond. **283**, 395-397.

Kroese, A. B. A., van der Zalm, J. M. & van den Berken, J. (1980). Extracellular receptor potentials from the lateral-line organ of Xenopus laevis. J. exp. Biol. (In the press.)

Lauger, P. & Neumcke, B. (1975). Theoretical analysis of ion conductance in lipid bilayer membranes. In Membranes, vol. 3, ed. Eisenman, G., pp. 1-58. New York: Marcel Dekker.

Lea, T. J. & Ashley, C. C. (1978). Increase in free Ca^{2+} in muscle after exposure to CO_2. Nature, Lond. **275**, 236.

Lewis, C. A. & Stevens, C. F. (1979). Mechanism of ion permeation through channels in a postsynaptic membrane. In Membrane Transport Processes, vol. 3, ed. Stevens, C. F. & Tsien, R. W. New York: Raven.

Lisman, J. E. & Brown, J. E. (1972). The effects of intracellular iontophoretic injection of calcium and sodium ions on the light response of Limulus ventral photoreceptors. J. gen. Physiol. **59**, 701-719.

Lowenstein, O. & Wersäll, J. (1959). A functional interpretation of the electron-microscopic structure of the sensory hairs in the cristae of the elasmobranch Raja clavata in terms of directional sensitivity. Nature, Lond. **184**, 1807-1808.

Magleby, K. L. & Stevens, C. F. (1972). A quantitative description of end-plate currents. J. Physiol. **223**, 173-197.

Matsuura, M., Ikeda, K. & Furukawa, T. (1971). Effects of Na^+, K^+, and ouabain on microphonic potentials of the goldfish inner ear. Jap. J. Physiol. **21**, 563-578.

McLaughlin, S. G. A., Szabo, G. & Eisenman, G. (1971). Divalent ions and the surface potential of charged phospholipid membranes. J. gen. Physiol. **58**, 667-687.

Meech, R. W. (1978). Calcium-dependent potassium activation in nervous tissues. Ann. Rev. Biophys. Bioeng.**7**, 1-18.

Meech, R. W. & Thomas, R. C. (1977). The effect of calcium injection on the intracellular sodium and pH of snail neurons. J. Physiol. **265**, 867-879.

Mendelson, M. & Lowenstein, W. R. (1964). Mechanisms of receptor adaptation. Science, N.Y. **144**, 554-555.

Moreno, J. H. & Diamond, J. M. (1975). Cation permeation mechanisms and cation selectivity in "tight junctions" of gallbladder epithelium. In Membranes, vol. 3, ed. Eisenman, G., pp. 383-517. New York: Marcel Dekker.

Muller, R. V. & Finkelstein, A. (1972). The effect of surface charge on the voltage-dependent conductance induced in thin lipid membranes by monazomycin. J. gen. Physiol. **60**, 285-306.

Nakajima, S. & Onodera, K. (1969). Adaptation of the generator potential in the crayfish stretch receptors under constant length and constant tension. J. Physiol. **200**, 187-204.

Newman, E. B., Stevens, S. S. & Davis, H. (1937). Factors in the production of aural harmonics and combination tones. J. acoust. Soc. Am. **9**, 107-118.

Nonner, W. (1980). Relations between the inactivation of sodium channels and the immobilization of gating charge in frog myelinated nerve. J. Physiol. **299**, 573-603.

Peterson, S. K., Frishkopf, L. S., Lechène, C., Oman, C. M. & Weiss, T. F. (1978). Element composition of inner ear lymphs in cats, lizards, and skates determined by electron probe microanalysis of liquid samples. J. comp. Physiol. **126**, 1-14.

Pinto, L. H. & Brown, J. E. (1977). Intracellular recordings from photoreceptors of the squid (Loligo peali). J. comp. Physiol. **122**, 241-250.

Russell, I. J. & Sellick, P. M. (1976). Measurement of potassium and chloride ion concentrations in the cupulae of the lateral lines of Xenopus laevis. J. Physiol. **257**, 245-255.

Russell, I. J. & Sellick, P. M. (1978). Intracellular studies of hair cells in the mammalian cochlea. J. Physiol. **284**, 261-290.

Sand, O. (1975). Effects of different ionic environmetns on the mechano-sensitivity of lateral line organs in the mudpuppy. J. comp. Physiol. **102**, 27-42.

Sand, O., Ozawa, S. & Hagiwara, S. (1975). Electrical and mechanical stimulation of hair cells in the mudpuppy. J. comp. Physiol. **102**, 13-26.

Sellick, P. M. & Johnstone, B. M. (1975). Production and role of inner ear fluid. Prog. Neurbiol. **5**, 337-362.

Shotwell, S. L. & Hudspeth, A. J. (1980). Two-dimensional sensitivity of hair bundles of single cells from the bullfrog sacculus. (In preparation.)

Sigworth, F. J. (1980). The variance of sodium current fluctuations at the node of Ranvier. J. Physiol. (in the press).

Smith, C. A., Lowry, O. H., & Wu, M. L. (1954). The electrolytes of the labyrinthine fluids. Laryngoscope, St. Louis **64**, 141-153.

Standen, N. B. & Stanfield, P. R. (1979). Potassium depletion and sodium block of potassium currents under hyperpolarization in frog sartorius muscle. J. Physiol. **294**, 497-520.

Sushi,D. F. F. (1980). Response to an hypothesis regarding the site of transduction in vertebrate hair cells. J. comp. Cuis. **51**, 5-9.

Tasaki, I., Davis, H. & Leqouix, J.-P. (1952). The space-time pattern of the cochlear microphonics (guinea pig) as recorded by differential electrodes. J. acoust. Soc. Am. **24**, 502-519.

Tasaki, I., Davis, H. & Eldredge, D. H. (1954). Exploration of cochlear potentials in guinea pig with a microelectrode. J. acoust. Soc. Am. **26**, 765-773.

Taylor, R. E., Bezanilla, F. & Rojas, E. (1980). Diffusion models for the squid axon Schwann cell layer. Biophys. J. **29**, 95-117.

Umbach, J. A. (1979). Effects of lowered intracellular pH on excitability in Paramecium. Soc. Neurosci. Abstr. **5**, 297 (abstract).

de Vries, H. & Bleeker, J. D. J. W. (1949). The microphonic activity of the labyrinth of the pigeon. II. The response of the cristae in the semicircular canals. Acta oto-lar. **37**, 298-306.

Weiss, T. F., Mulroy, M. J. & Altmann, D. W. (1974). Intracellular responses to acoustic clicks in the inner ear of the alligator lizard. J. acoust. Soc. Am. **55**, 606-619.

Wever, E. G. & Bray, C. W. (1930). Action currents in the auditory nerve in response to acoustical stimulation. Proc. natl. Acad. Sci. U.S.A. **16**, 344-350.

Woodhull, A. M. (1973). Ionic blockage of sodium channels in nerve. J. gen. Physiol. **61**, 687-708.